# Cruise Report

## NBP07-02

03 February - 26 March 2007

McMurdo to Punta Arenas

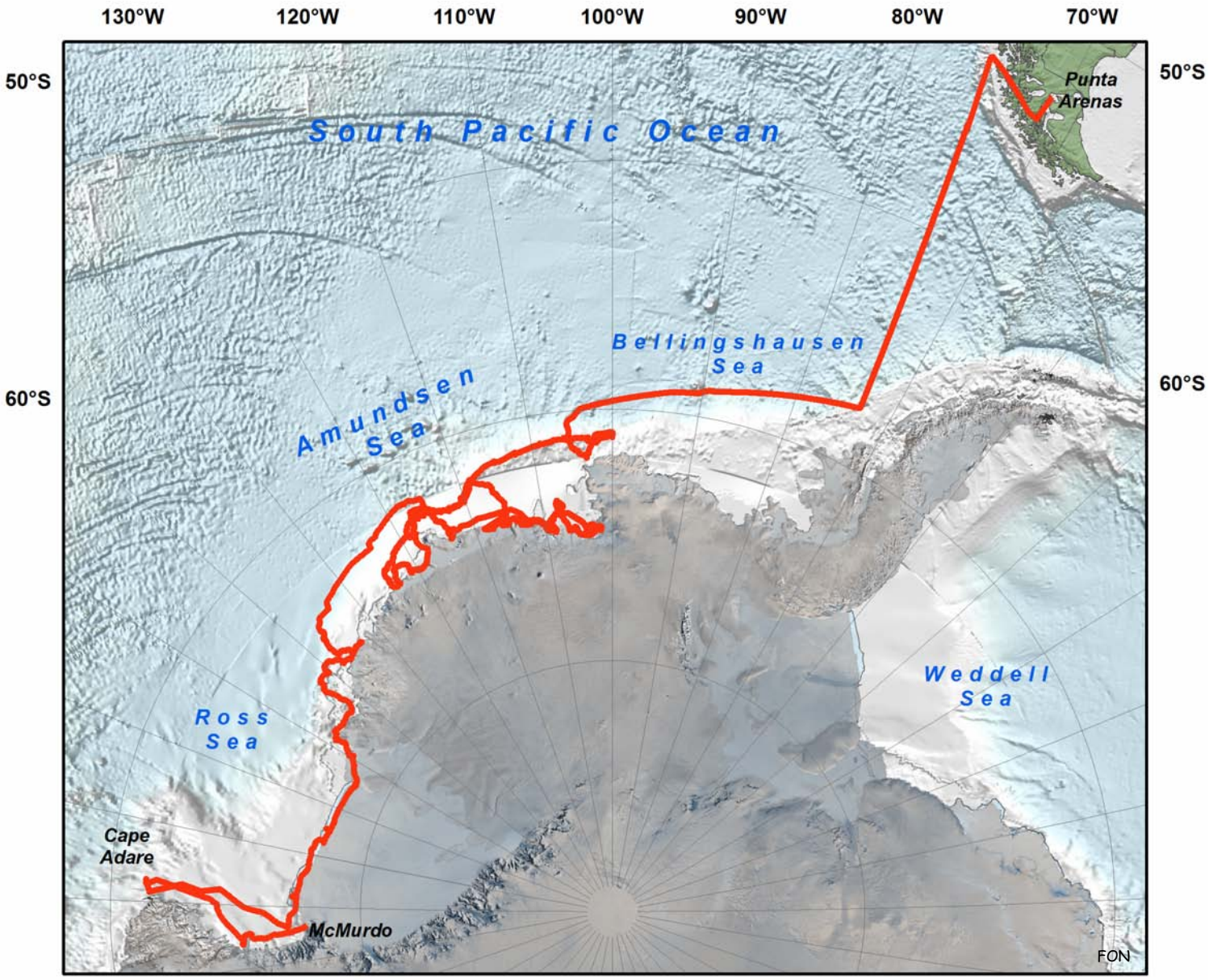

NBP07-02: The Amundsen Continental Shelf and the Antarctic Ice Sheet

List of Figures

# 1 Background

The morphology of Antarctica's continental shelf influences and is influenced by the evolution of the Antarctic Ice Sheet. Seawater that invades this region plays an important role in driving that evolution, which in turn modulates the properties of abyssal and surface waters formed in the Southern Ocean. The objectives of this project are to investigate aspects of the complex interplay between the sea floor, ocean and ice sheet in the context of climate change in the SE Pacific sector. The proposed study focused on the intrusion of upper Circumpolar Deep Water (uCDW) onto the continental shelf and its subsequent modifications in the glacial troughs and under the floating ice shelves. It anticipated utilizing ship-based CTD/rosette casts, acoustic doppler current profiler (ADCP) measurements, swath mapping of the sea floor, and the U.K. AUV 'Autosub,' to extend shipboard observations beneath the ice shelves and the perennial or land-fast sea ice.

Antarctica's continental shelf seas experience two contrasting oceanic regimes. In most regions the water column is mostly occupied by near-freezing waters formed in situ by intense cooling, sea ice formation and convective overturning during winter. In the Amundsen & Bellingshausen (A&B) Seas, however, seawater as much as 4°C warmer than the in situ melting point intrudes onto the continental shelf at depth. This 'warm' uCDW derives from the dominant, mid-depth water mass in the deep basins of the Southern Ocean. Where it extends onto the continental shelf, little or no Antarctic Bottom Water is produced; where it has access to an ice shelf base, average melting can rise two orders of magnitude above that under the cold-regime Ross and Filchner-Ronne Ice Shelves. This melting drives upwelling that modifies the near-surface layers, which are then advected westward by easterly and offshore winds. Recent changes in the volume or properties of uCDW on the shelf may help to account for reported ice shelf thinning in this sector.

Initial ice shelf studies in the A&B Seas focused on George VI Ice Shelf, which could be accessed from research stations sited on the Antarctic Peninsula (AP). Early work suggested a high and spatially variable melt rate and later studies demonstrated the link between rapid melting and the presence of uCDW beneath that ice shelf. More recently, oceanographic and remote sensing studies have led to estimates of even higher melting at the base of ice shelves fed by the Pine Island Glacier (PIG) and other glaciers in the Amundsen Sea. The PIG and neighboring Thwaites Glacier catchment basins are now known to be the sites of the most rapid ongoing change in the ice sheet, with enough mass loss to make a significant contribution to global sea level rise. Ice sheet deflation in this area, which theory has suggested is the most likely region for the initiation of West Antarctic Ice Sheet collapse, is qualitatively consistent with high rates of ice shelf melting, high glacier velocities, receding ice fronts and large numbers of grounded and drifting icebergs.

The observational record of ocean temperatures on the Bellingshausen continental shelf is now longer than a century, but relatively sparse. No ocean stations had been taken on the Amundsen shelf prior to NBP94-02, and its northern limits were not defined until NBP00-01. Deep temperatures on the A&B continental shelves were found to be typically above +1°C, increasing toward the east in the southern Amundsen, where the highest values were near the seabed in Pine Island Bay (PIB). Swath mapping of the sea floor of the Amundsen shelf showed spectacular deep troughs on the inner shelf seaward of the ice shelf fronts. Oceanographic measurements revealed evidence for rapid ice shelf melting, upwelling uCDW and temporal variability in ocean properties. Since 1994 four attempts to make more detailed ocean measurements near the calving front of the PIG had been unsuccessful due to extensive fast ice, equipment problems and fieldwork scheduled when an early freezeup threatened besetment.

The A&B Seas are important in several other ways, for reasons that are also not yet fully understood. For example, their apparent strong link to the tropical Pacific and an increasingly positive Southern Oscillation Index may be related to the pronounced warming that has occurred on the AP over recent

decades. This region appears to be the source of a multidecadal freshening downstream in the Ross Sea, perhaps resulting from increased melting, decreased sea ice formation and changes in wind strength. And observations suggest that the PIG grounding line position is sensitive to basal melting of its floating terminus and dynamical changes in the glacier flow, with evidence for recent retreat, thinning and acceleration. With the highest balance flux of any glacier in West Antarctica, and deeply incised crystalline bedrock near the ice front, this PIG may not flow over a deforming till, the current paradigm for enabling fast glacier flow.

## 2 Initial Objectives

The primary objective of the proposed work was to study the floating ends of the Pine Island, Thwaites and Smith Glaciers in the Amundsen Sea, focusing in particular on the provenance of uCDW in PIB and its impact on these features. Secondary objectives, given difficult ice conditions, were similar studies in the vicinity of the Dotson/Getz, Abbot or George VI Ice Shelves.

Specific questions to be addressed included:

What is the distribution of water masses seaward of the floating ice, how is this related to the continental shelf topography, and has it changed since earlier surveys?

How do upwelling and vertical mixing over the continental shelf influence water column structure and heat transport into sub-ice shelf cavities?

What processes control the vertical transport of heat to an ice shelf base and the spatial pattern of basal melting?

How much meltwater is produced beneath the ice shelves and what is its fate?

What is the shape and nature of the sea floor on the 'open' continental shelf and beneath the floating ice tongues?

To address such questions requires measurements of the properties and motion of waters over the open continental shelf and under the ice shelves, along with configurations of the shelf troughs & ridges, and of the sub-ice cavities. Our overall aim has been to construct as complete a picture as possible of the spatial distribution of melting and mixing, with the longer-term goal of using the oceanographic data to validate numerical models of the cavity and shelf circulations.

Since the *NB Palmer* was scheduled to make two transit cruises, from the Ross Sea to NZ and from NZ to Chile, in early 2006, at a time when the NERC Autosub was not otherwise committed, that appeared to be a good opportunity to utilize the NBP and Autosub on a 45-day McMurdo to Punta Arenas leg from ~15 Jan-28 Feb, 2006. This is what was proposed, in May 2004, coincident with a proposal by co-PI A. Jenkins to NERC to support the Autosub operations.

Contingency plans noted the possibility that the Autosub might be unavailable, damaged, lost or fail to perform as expected, in which case the standard CTD/LADCP/rosette and multibeam

work would be carried out. This would allow detail to be added to the emerging picture of a long-neglected sector of the Southern Ocean that appears sensitive to recent climate variability, and a possible analogue for larger-scale, longer-term climate change. Since our measurements near the front of PIG in 1994, several studies have revealed short-term changes in the adjacent ice sheet. Repeat ocean observations were considered essential to determine whether concurrent change was occurring deep on the Amundsen shelf that might be triggering the inland change. Related work included geochemical sampling under the direction of P. Schlosser, parallel modeling efforts at NYU and BAS, and the compilation and merging of all available bathymetry data in the Amundsen Sea from several US, UK and German expeditions. In addition, we expressed interest in accommodating synergistic projects that might acquire time series data, study the sea ice cover, and/or not in need of significant ship time.

## 3 Revised Objectives

In the time that passed between proposing this work and NBP07-02, several important events occurred. The primary Autosub was lost beneath the Fimbul Ice Shelf in early 2005, after completing one sortie there. The field work on this project was scheduled for early 2007 rather than 2006, its term extended by one year and its budget enhanced by ~$50K. The enhancement was used to acquire instruments for six low-cost, low-profile 'bottom landers,' supplemented by instruments borrowed from the RPSC 'pool.' The resulting arrays were deployed during a geophysical cruise of the Polarstern in the SE Pacific sector in Feb-Mar 2006. On the same cruise an Automatic Weather Station provided by the Univ of Wisconsin was deployed on Peter 1 Island. The CALM (Cape Adare Long-term Mooring) project was funded, and coupled to the front end of NBP07-02, adding 5-6 days to the length of the cruise. Word filtered down that the ship's OS-38 ADCP was inoperable, and several attempts to right that problem eventually led to the conclusion that repair could not be done until the next drydock. The backup Autosub required extensive sea trials, and during the last N. Hemisphere summer NERC decided it was not yet ready for Antarctic work. That eliminated a large fraction of the science complement from the cruise roster, so a few additional projects and personnel, including several students, were entrained into 0702. As a nearly simultaneous oceanographic cruise on the JC Ross into the Bellingshausen Sea this year appeared to have that sector covered, we decided to repeat a time-series section along the front of the Ross Ice Shelf, last occupied by us in 2000 and in part by an Italian group last year. In the Amundsen Sea, we refocused on repeating measurements along the ice fronts and outer continental shelf, in an attempt to 'close the box' with regard to inflows and outflows.

## 4 Results

In light of the altered plans, we have been reasonably successful in achieving most of the cruise objectives. Sufficient time and fuel were available to cover much of the anticipated track, including a return to the Ross Island area to start the Ross Ice Shelf transect. The weather cooperated, except for a few days of adverse weather off Cape Adare and a very cold period near

the end of the Amundsen work, at which time we could have done without the wished-for southerlies. The sea ice cover was heavier than experienced previously west of Siple Island, and sometimes appeared where the satellite passive microwave data suggested otherwise. However, a tongue of fast ice extending north of the Thwaites/B-22 iceberg complex disintegrated at the right time, allowing work in PIB. The calving front of the PIG was blocked by fast ice and icebergs, and work on the important shelf region north of PIB was limited by deteriorating ice conditions late in the cruise. A new CALM mooring was set off Cape Adare, but an existing mooring there could not be recovered. Five of six bottom landers set a year ago were retrieved, one in the Bellingshausen Sea, and all instruments returned complete records.

A total of 190 CTD stations were occupied, thousands of water samples taken and processed, or packed for later analyses, and 13,400 km of ship's track swath mapped. Key areas of the Amundsen continental shelf were charted for the first time, and some findings made that will no doubt lead to further investigations. Related ship-of-opportunity projects collected numerous underway and on-station surface and bottom samples. The diverse science and support complements represented oceanography, geophysics, geochemistry, modeling, meteorology and cryology, along with foreign collaborators, graduate and undergraduate students, and highly qualified technicians of several stripes. Some observations were made for the first time in the SE Pacific sector, sampling gear was fabricated, a simple mooring array design validated, and equipment failures were few and far between. Veni vidi vici.

Several preliminary results were noted in our weekly progress reports (q.v., below). Much data reduction and sample processing remains to be done before we will know to what extent the questions above can be resolved by the NBP07-02 datasets. For the time being, then, we will briefly note only the following:

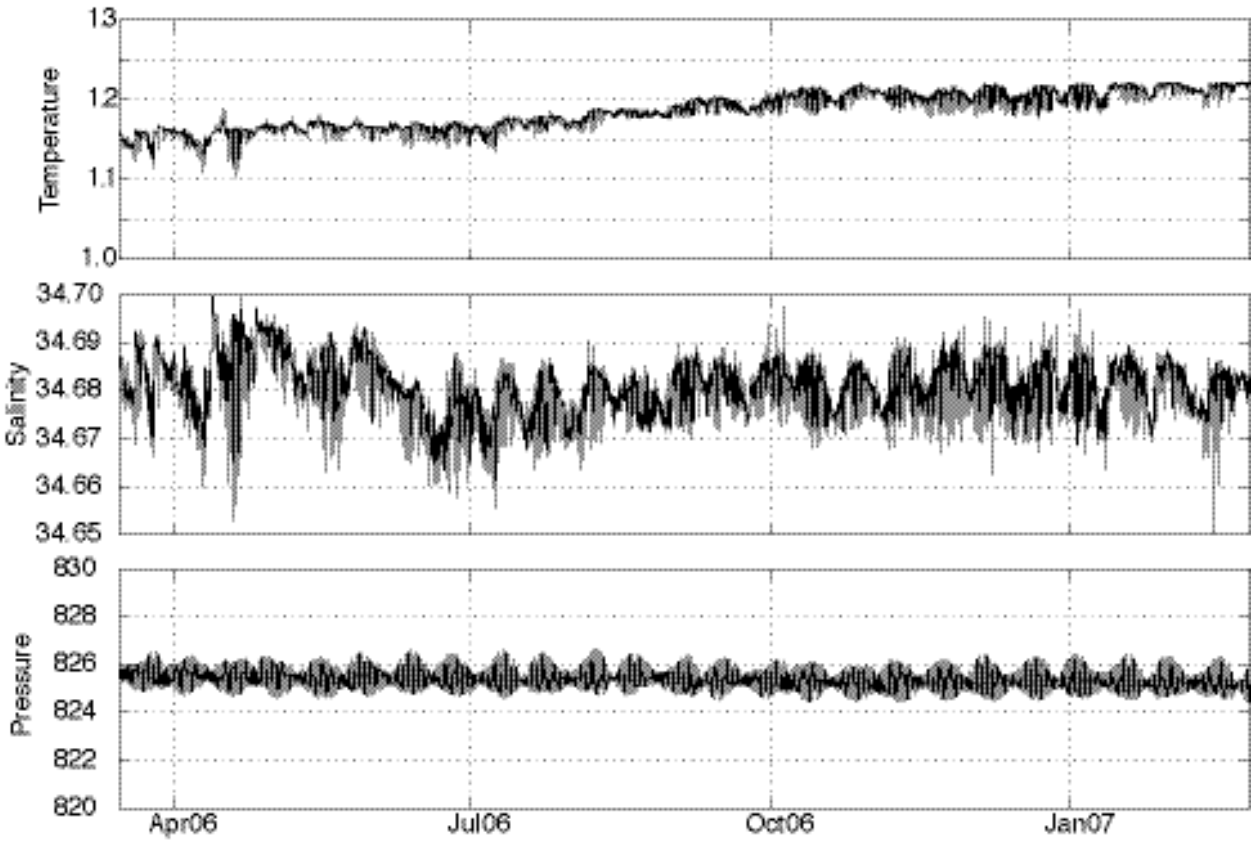


Figure 1. Uncorrected temperature, salinity and pressure from a 'bottom lander' moored in Pine Island Bay (~74 37S, 103 52W) at a depth of 825 m, 2m above bottom, and recording from 14 Mar 2006 through 26 Feb 2007.

The first lengthy time series record in the 'warm,' salty CDW that inhabits the deep troughs in PIB and melts its fringing ice shelves is shown in Figure 1. While the data remain to be edited and the Microcat that acquired it must be recalibrated, several preliminary comments can be made. First, there is no obvious seasonal signal in the temperature record, which shows gradual increases followed by plateaus, ending in February 2007 about 0.07°C warmer than in March 2006. The salinity record is ambiguous in this respect, displaying more variability in autumn, but little net change over the longer term. Both temperature and salinity respond to the fortnightly tidal cycle, rising when tidal amplitudes are high and falling when they are low. These changes suggest lateral gradients in the CDW, but there is also a tendency toward diurnal peaks in the opposite direction. The recorded temperatures are warmer than measured in PIB in 1994 and 2000, consistent with 2006 measurements. While the subsurface Amundsen appeared relatively warmer this year in several areas, more analysis will be needed to determine if the apparent changes exceed the large scale interannual variability previously observed. Nonetheless, ongoing work suggests a PIG sensitivity to temperature of ~7m/°C, in which case the rising temperature from this mooring corresponds to an increased melt rate of ~0.5m/yr.

The second set of observations we will note here resulted from a planned experiment that went awry, but yielded some interesting results. In brief, we put off until late in the cruise a projected time series station involving repeated CTD casts to assess the diurnal tidal cycle. The plan was to occupy for 24 hours a fixed location several km south of the shelf break, near bottom lander #5. That proved impossible when we arrived on site, even within an iceberg-infested polynya, as strong southerly winds were moving the entire ensemble northward at ~0.5 kts. We thus opted for a drift experiment, setting up on one edge of the polynya and lowering the CTD at half-hour intervals as the NBP was advected across the shelf break.

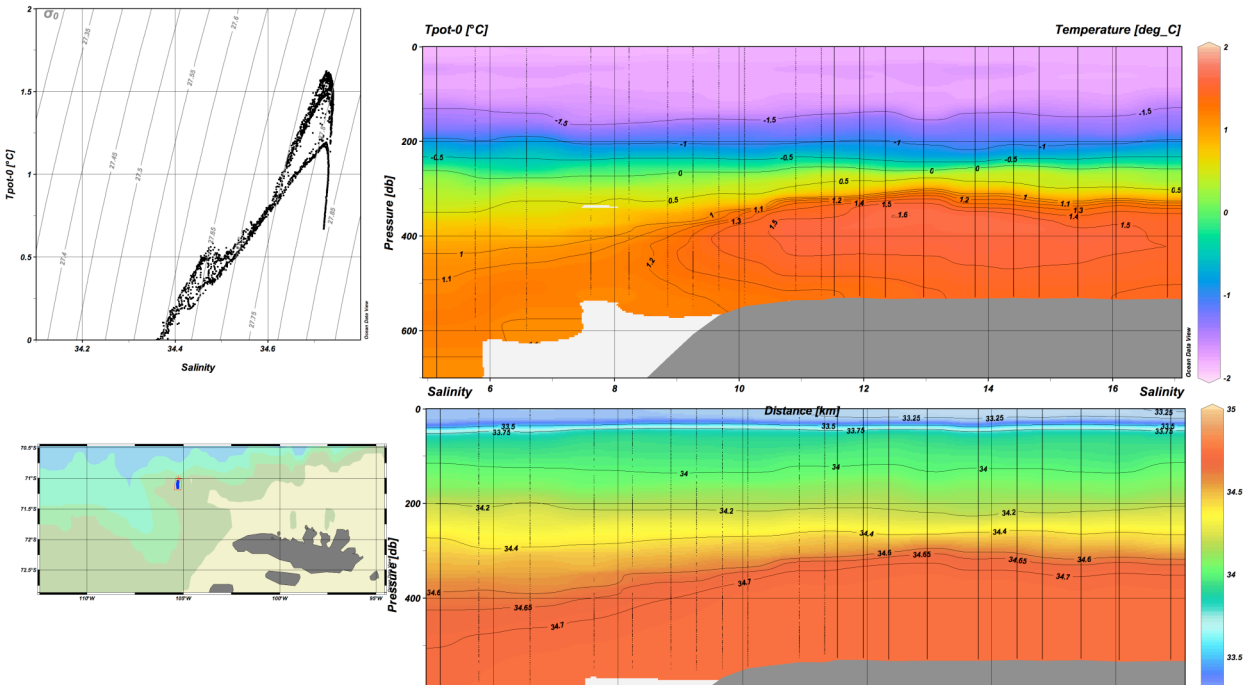


Figure 2 Temperature and salinity sections, and an accompanying T/S diagram for CTD casts made during a 9.5 hour period when the NBP drifted northward across the continental shelf break near 105°W on 17/18 March 2007.

Preliminary temperature and salinity measurements during that drift are shown in Figure 2. Note that the deeper isohalines (therefore isopycnals) rise southward, 34.7 by >150m to ~350m, an indication that troughs or depressions at the shelf break (near km 10 in the figure) are not essential to the transport of CDW onto this part of the continental shelf, contrary to what might be inferred from Walker et al (2007). However, an isolated region of warmer water on the outer shelf with a N-S dimension > 8km appears to have gained access to the shelf at some other location/time, and may be tracking along-shelf. Thermohaline properties on- vs off-shelf also show a substantial gap in T/S space, similar to that reported across the Antarctic Slope Front in the Ross Sea by Stover et al (2005). Furthermore, the lateral temperature gradient exceeding 0.3°C in 2 km near the shelf break indicates that we must be cautious in comparing 'repeat' stations for signs of temporal change.

# 5 Acknowledgments

We would like to thank all who made cruise NBP07-02 possible, productive and enjoyable. These include the National Science Foundation, OPP, the RPSC support group, steady as always, the reliable ECO ship operators, and families and friends ashore.

# 6 Cruise Component Summaries

## 6.1 CTD Operations

### 6.1.1 Overview

All casts were carried out with a Sea-Bird 911plus CTD system and SBE 24-place carousel mounted on a Sea-Bird rosette frame. Bullister-type rosette bottles were used, with specially treated buna-N O-rings provided by the LDEO tracer team. Commonly referred to as 10 liter bottles, the deliverable volume of the bottles was measured to be just over 8 liters.

No major repairs or replacements were required for any electronic components. Some bottles required routine maintenance or replacement to correct for leaks. Data was acquired on Windows XP Professional PC running Seasave 5.37d. The system crashed twice during stations, but no other problems occurred. Preliminary data processing was carried out immediately following each cast using Seabird processing software (scripts, configuration files and batch files used are on the data distribution DVD).

The sensor suite comprised two sets of ducted TC sensors with two SBE 43 oxygen sensors, each set with its own pump and plumbing (see photos below). Full ocean depth rated fluorometer and transmissometer completed the sensor suite. A 12kHz pinger and bottom contact switch aided in monitoring proximity to the bottom. A digital camera was mounted on the frame for some stations in an effort to obtain bottom photographs. Small bottom samples were obtained beginning part way through the cruise with a mini-corer designed and built on board, suspended from the bottom contact lanyard. Continuous profiles of ocean currents were obtained on all stations with a Lamont-provided Lowered Acoustic Doppler Current Profiler (LADCP).

A total of 190 casts were made, summarized in tabular form in Appendix 1.

#### 6.1.1.1 CTD Salinity and Oxygen Procedures

(R. Cullather)

Each CTD cast was equipped with primary and secondary sensors for measuring oxygen, conductivity and temperature at a rate of 24 scans per second (Figure 3, Figure 4). These sensors are connected to a pump system on the CTD that circulates the water to the sensors, allowing for continuous measurements to be taken despite variable winch speeds and current flow. The pump was found to engage within a minute or so of entering the water, after which a short period of time was allowed for the primary and secondary sensors to come into stable agreement. This “soaking” of the unit is largely for the benefit of the unit’s primary and secondary oxygen sensors, and usually occurred either just below the surface or at the 10m level, depending on the sea state. When the soaking was completed, data recording commenced at the level just below the water surface, and the unit was sent on its way. The sensors provided a full vertical profile of temperature, oxygen content, and salinity in the ocean water column in real-time during each cast. These data were used to identify water column levels that were of interest for sampling on the way back up to the surface using the 24-bottle rosette which sits atop the CTD. Together, the CTD and the rosette are informally referred to as the “package” or the “fish”. Typically, rosette bottles (hereafter

referred to as niskins) were fired in pairs for redundancy and for more rapid sampling on deck. The number of unique levels sampled by the rosette normally ranged from 4 to 12. The cast depth ranged from 300m to almost 3000m, with a median depth around 800m.

When the unit returned to the deck, the pump system was flushed with DI water for several minutes while water sampling occurred. Samples for measuring salinity and oxygen content were specifically taken from niskins where tracers were taken. In some cases, a level was rejected for salinity sampling if it was reasonably concluded that the sample would not provide a stable reading, such as in the presence of a strong gradient or if CTD measurements taken during the descent of the unit differed greatly from those taken during the subsequent ascent. Level rejection occurred to a smaller degree for oxygen sampling. On the pecking order, oxygen was sampled first or second depending on whether Helium tracer water was taken; salinity was typically sampled third or fourth from a given 10-litre niskin. One person was responsible for oxygen sampling during each shift. Two scientists were responsible for sampling salinity during each 12-hour shift, however their duties also covered the preparation of the rosette and preserving the water sampling hierarchy, otherwise known as the "bottle cop".

Salinity sampling used 250mL glass bottles and plastic caps, which were thoroughly rinsed 3 times in water from the niskin and were then filled. One hundred twenty glass bottles were rotated through the salinity sampling and analysis process. More than 980 salinity samples were taken at 190 stations, for an average of 6 samples per cast. An early problem with salinity sampling was a chipping of the open rim of the glass bottles on the metal pin of the niskin spigot. As the salinity measuring device requires a tight seal on the glass bottle for sampling through suction, any deformation of the top rim renders the bottle useless. Twelve bottles were lost in this manner, and the NBP should carry a larger supply on future 'CTD cruises.'

After a few days of sampling, salinity measurements were taken on the accumulated inventory of samples. In the time between measurement sessions, the samples were allowed to equilibrate to room temperature. The measuring device was the onboard Autosal salinometer, which measures salinity through conductivity. The salinometer is located in a central, temperature-controlled room of the ship. After standardizing the salinometer with control samples, each glass bottle was measured by first flushing the device three times with the sample and then measuring three times. If the sample measurements were not stable, additional measurements were taken. The session was then completed with a second measure of a control sample, followed by flushing with DI water.

Water samples for oxygen content were collected from niskins using flexible tubing to rinse a 250mL glass sampling flask. The flask was rinsed by overflowing its volume three times using the niskin water before filling (Figure 3). The sample was then immediately "pickled" with MnCl2 and Nal/NaOH which, when combined with dissolved oxygen, forms a precipitate. Approximately 30 oxygen sampling flasks were rotated through the sampling and analysis process. For additional information on the O2 program, see that section in the report.

For bottle-CTD comparisons, corresponding CTD instrument values were obtained by averaging the CTD telemetry over the time that each niskin was closed. Two notable difficulties with the CTD-rosette fish were identified during the cruise. The first was a pathological problem associated with niskin 20. Analysis of oxygen data indicated an outlier with the primary CTD sensor, while the rosette value and the secondary CTD sensor showed reasonable agreement. Niskin 20 is located directly over the Y-tube for the primary sensor pump (**Figure 5**). Apparently the bottom cap of the niskin, when fired, would occasionally make contact with the tubing and briefly disturb water flow to the sensors. This problem showed up more prominently in the oxygen sensor data. To deal with it, the Y-tube was tied to the CTD frame (see the green string in **Figure 5**). This remedy appears to have been applied somewhere between CTD-75 and CTD-85. A second problem occurred when a jellyfish was ingested into the secondary sensor tubing during CTD-140, and affected that station as well as 141 and 142 (**Figure 5**). Results of the CTD vs bottle salinity and O2 analyses appear in their respective sections of this report.

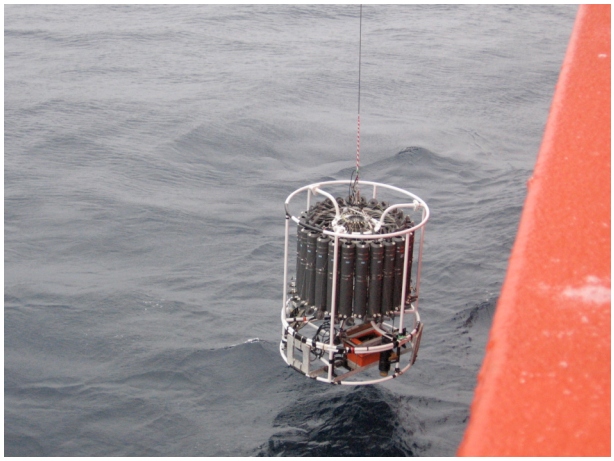

Figure 3  The CTD and niskin rosette fish. Left: on deck in Baltic Room.  Right: during deployment.

Figure 4  . Left: CTD primary and secondary sensor arrays and Y-tube water pump system. Right: sampling for oxygen content.

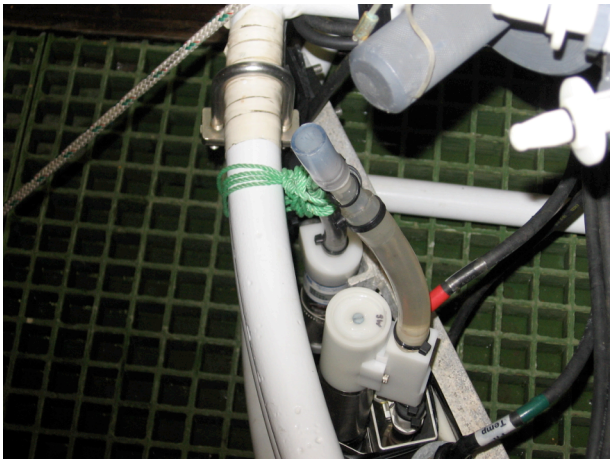


Figure 5 Left: proximity of Y-tubing for primary sensors and lower cap of niskin 20. Right: Jellyfish tentacle on niskin.

### 6.1.2 Salinity analysis

Salinity Determination (Autosal) and Temperature/Conductivity Sensor Behavior

Raul Guerrero and Richard Cullather

In order to monitor the performance of the CTD conductivity sensors, 978 salinity samples were analyzed during the cruise using one of the onboard Autosal salinometers. Autosal NSF-SN 01555 was used for all the stations as Autosal NSF-SN 04504 malfunctioned during the standardization procedure. Autosal 01555 performed within factory specifications. Laboratory room temperature control was excellent, remaining 0.5 to 1.5°C below the Autosal temperature setting of 21°C. A fan located on top of one of the salinometers kept the air temperature vertically homogeneous. Data from the Autosal were captured using the ACI 2000 hardware/software package. The connection failed on 3 occasions when the suppression knob was on the "read" position, probably as a result of a poor connection on the 50-pin ribbon cable.

On each "run", an average of two boxes (48 samples collected over 7 to 8 stations) were measured by Richard Cullather and Raul Guerrero. The standardization was performed at the beginning of each "run" using a recently dated vial, and a control of drift was done at the end of the run, using an older, but stable, vial. The standards for calibration came from batch P147 (OSI) from June 2006 (approximately 28 vials used), while P143-2003 (11 vials), P140-2000 (15 vials) and P138-2000 (2 vials) were used for closure. On runs 1, 2, 4 and 21, these vials were used consecutively for comparisons, resulting in no significant differences between them. Autosal 01555 was stable throughout the whole cruise. As may be seen in Table 1, little or no re-standardization was required between the runs. The extreme "standby" values were 5988 on Run 6 and 6007 on Run 3, but the values were between 5994 and 6002 on 22 of the 24 runs. For reference, 10 units change in the "standby" reading is equivalent to 0.00008 CR units or about 0.0015 units in salinity.

| Run | 0 | 1 | 2 | 3 | 4 | 5 | 6 | 7 | 8 | 9 | 10 | 11 |
|---|---|---|---|---|---|---|---|---|---|---|---|---|

| 01555 | 5998 | 5996 | 5999 | 6007 | 6001 | 6002 | 5988 | 6001 | 6001 | 6000 | 6000 | 6000 |
|---|---|---|---|---|---|---|---|---|---|---|---|---|
| Run | 12 | 13 | 14 | 15 | 16 | 17 | 18 | 19 | 20 | 21 | 22 | 23 |
| | 5999 | 6001 | 5994 | 5994 | 5999 | 5999 | 6000 | 5997 | 5995 | 5999 | 5999 | 6000 |

Table 1. Salinometer "standby" reading throughout the cruise. Good stability was observed between runs as little or no re-standardizing was needed.

Twenty duplicates samples were randomly drawn for controlling the repeatability of the salinity measurements (see the "duplicates spreadsheet" in SalBot.xls). The extreme differences were +0.006 and –0.0009 with an overall standard deviation of 0.0023.

Errors in salinity resulting from the primary and secondary conductivity sensors were tracked throughout the 190 stations (Fig. 1). Salinity errors, denoted as DeltaS, are reported as the rosette salinity minus the CTD sensor salinity. Primary and secondary CTD salinity sensor values showed a pressure dependency error when compared against the rosette salinities. This effect could be absent when the error estimation is performed on the conductivity variable derived from the rosette salinities, so errors reported here should be considered preliminary and with the only objectives being the evaluation of the behavior of the sensors throughout the cruise, the identification of niskin leakage and/or contamination, and to recognize unstable layers no suitable for calibration. DeltaS for primary and secondary sensors Sal00 and Sal11, respectively, are plotted versus the CTD pressure values (hereafter PrDM) in Fig. 2. The upper 500m shows a clear slope, so linear regression versus PrDM was independently applied above and below 500m. Rosette salinities with an absolute DeltaS larger than 0.03 were not considered for the error analysis. Two iterations were allowed to identify and flag outliers that were two standard deviations away from the mean. A final regression versus station number was applied to compensate for the drift throughout the cruise, which is particularly obvious on the primary sensor (Fig. 1). A final fitting with the statistically accepted DeltaS was performed– first versus PrDM, and then versus the station number– to come up with the final corrected CTD salinities. The fitting coefficients and the residual standard deviation for both sensors are presented in Table 2.

| Sensor | Error for 0-500db (PrDM) | | Error for 500-3000db (PrDM) | |
|---|---|---|---|---|
| | Slope | Bias | Slope | Bias |
| Primary | –1.3802E–5 | +0.0020 | –3.8322E–7 | –0.0031 |
| Secondary | –1.1809E–5 | +0.0036 | –9.2266E–7 | +0.0035 |

| Sensor | Error Statistic | | | Std Dev of Resid. | Percent of Points Used |
|---|---|---|---|---|---|
| | Second Order | First Order | Bias | | |

| | | | | | |
|---|---|---|---|---|---|
| Primary | 2.4919E-7 | +1.386E–5 | +0.00118 | 0.0028 | 82.1 % |
| Secondary | --- | 5.5594E–6 | –0.00062 | 0.0024 | 75.5 % |
| Flagged in Upper 500m | | | | | Primary:15.8%<br>Second: 19.3% |
| Flagged below 500m | | | | | Primary:1.5%<br>Second: 2.5% |

Table 2. Fitting of DeltaS values as a function of PrDM and Stat# and standard deviation of residual are presented for primary and secondary sensor. Also the percentage of point used for the fittings.

Of the 978 niskin samples, 661 samples, or roughly two-thirds were taken from the upper 500m of the water column, while 317 were taken from deeper levels. The final regression analysis for the primary and secondary CTD sensors used 804 and 760 points, representing a usage of 82.2 percent and 77.7 percent, respectively. More data points from the upper 500m of the water column were rejected from the analysis than from the deeper levels. Of the 661 samples taken at 500m or above, 16 percent were rejected from the primary sensor analysis while 23 percent were rejected from the secondary sensor analysis. Of the 317 points taken from deeper levels, 2 percent in average were rejected from the analysis of both sensors (see table 2).

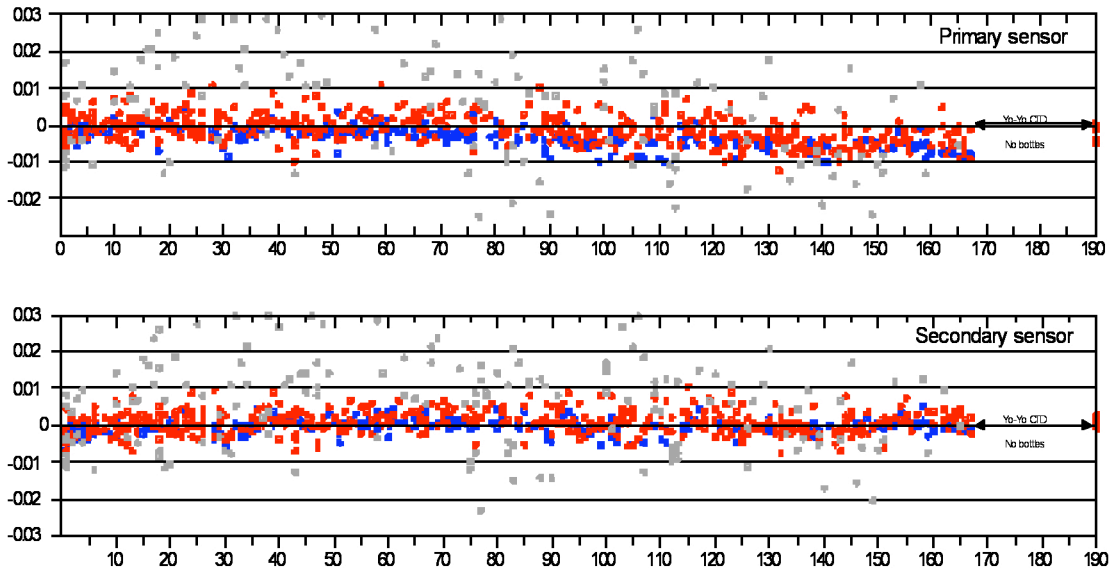


Figure 6 Salinity difference, DeltaS (rosette minus CTD), versus Station # for primary and secondary conductivity sensors. Red points denote values taken above 500m in the water column, while blue points are deeper than 500m. Grey points were discarded for the final fitting.

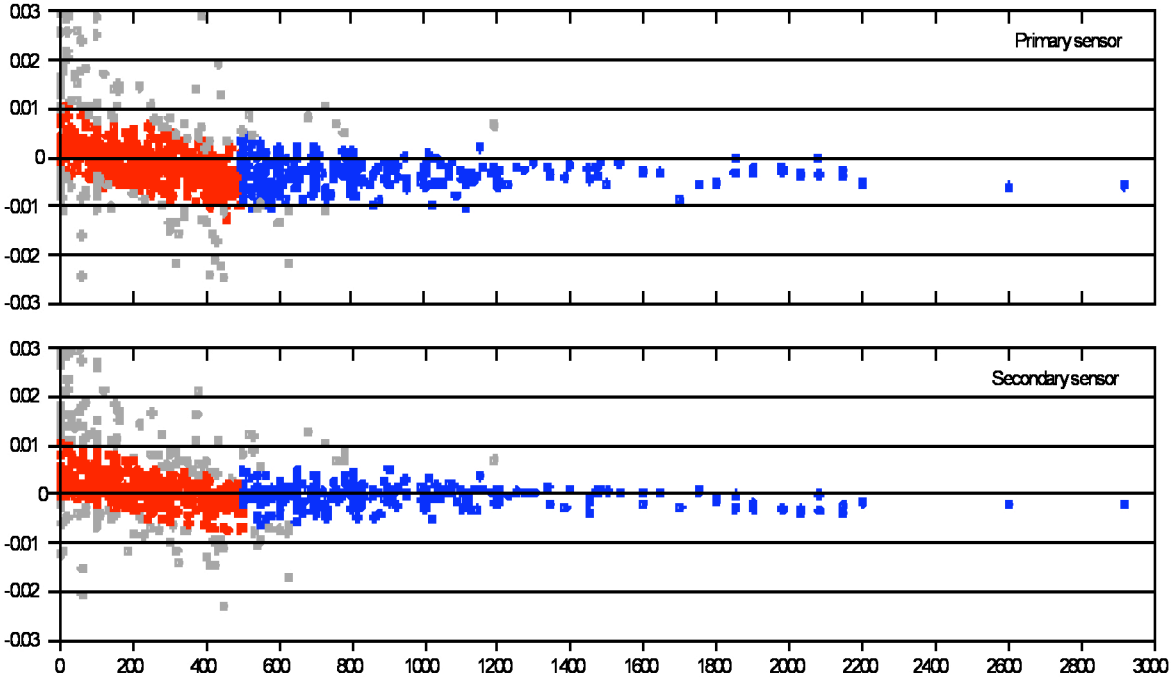


**Figure 7** DeltaS versus PrDM, for primary and secondary sensors showing the pressure dependency. Regression was independently applied above (red points) and below (blue points) 500m. Grey color points were flagged and discarded for the final fitting.

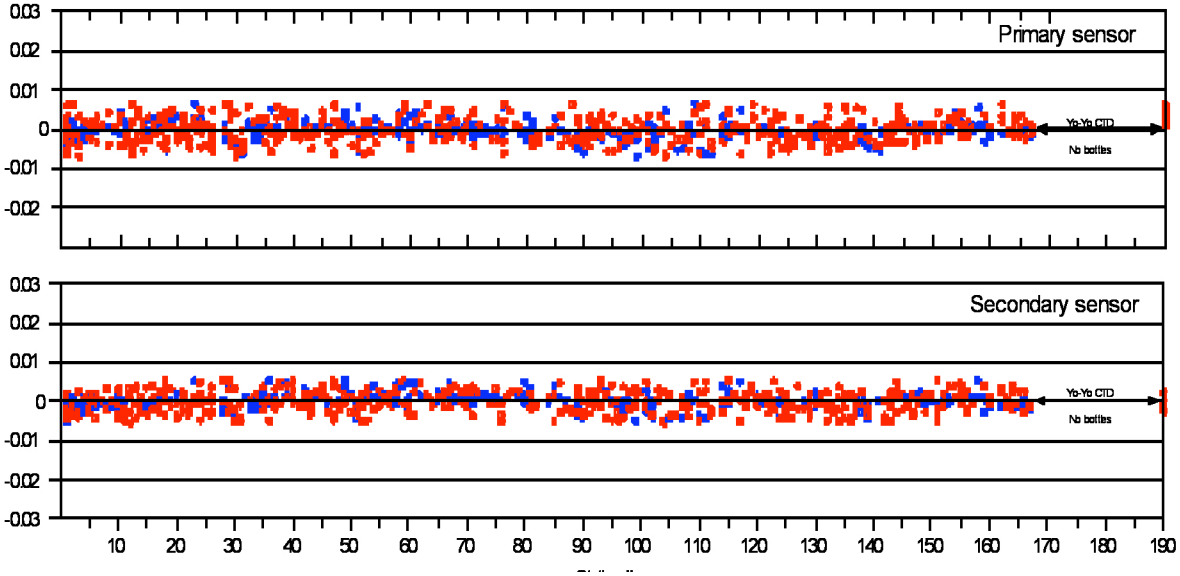


Figure 8 Residual for Delta-Sal00 and Delta-Sal11 vs. station number, after applying calibration coefficients( from table 2) on Sal00 and Sal11. Red points denote values above 500m and blue points are values below 500m.

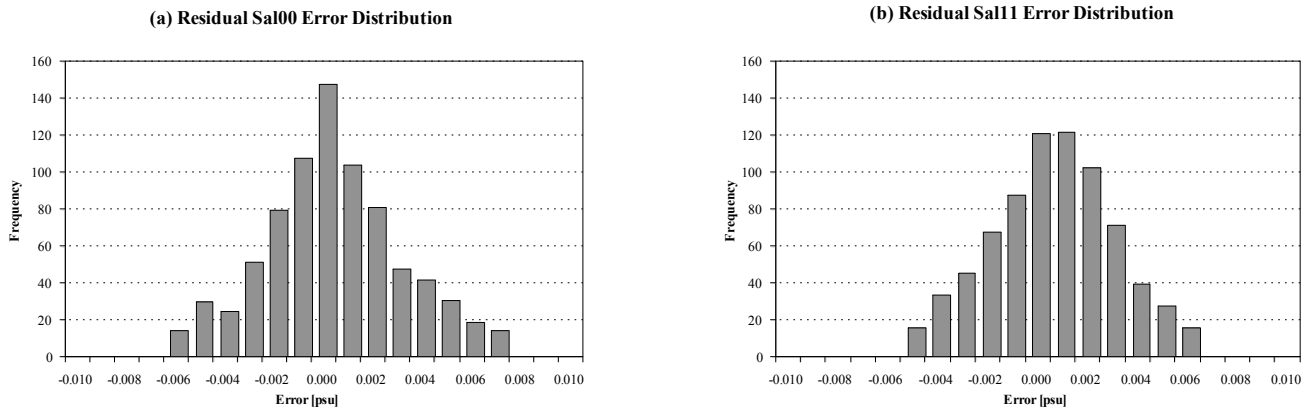


Figure 9 Residual histograms for: (a) primary sensor and (b) secondary sensor. The standard deviations are reported in Table 2. Standard deviation for Sal00 and Sal11 residuals were 0.0028 and 0.0024 respectively.

On station 140 some jellyfish entered the secondary plumbing and affected Co and Ox measurements through stations 142. A thorough back flush on the sensor tubing was performed after station 141. On station 143 Sal11 and Ox1 reading reestablished to expected values.

Recommendations

A final and more thorough evaluation should be performed on the relation between rosette salinity observations and CTD sensor values, particularly using Co from RosSal and factory corrected CTD pressure and temperature. Nevertheless, some recommendations already arise from this analysis.

The secondary sensors were less noisy (lower StdDev in their residual) and were more stable in the time lapse of the cruise. The residual histogram for the secondary sensor has a more normal distribution than for the primary. A reason for the large difference in the number of discarded points between the sensors was not immediately apparent. The post-cruise analysis may show why this is true, or correct it if there was a mistake in this analysis. This preliminary report suggests that the secondary temperature and conductivity sensors– after corrections– are to be used for the final data set. Over 20 percent of the points were discarded for not showing a consistent difference with the CTD. This occurred when a salinity sample was taken from an unstable layer, or possibly when the sample and/or the bottle were contaminated. As a consequence, many rosette salinity values are not suitable for use in quality control for other bottle parameters (like, oxygen, nutrients or tracers). On the other hand, the corrected CTD_Sal, using the coefficients in Table 2, is adequate for any quality control.

Bottle Data Files

A Microsoft Excel spreadsheet file was generated with bottle information coming from the rosette niskin measurements performed onboard and from CTD instruments at the corresponding niskin firing

levels. Rosette bottle parameters measured were: salinity, oxygen and nutrients. The corresponding CTD instrument values are extracted by the CTD software (modules "datcnv" and "rossum"), which averages over 2 seconds or 48 scans around the tripping of the niskin. Bottle files are Bottle_CTD001-CTD050.xls; Bottle_CTD051-CTD100.xls and Bottle_CTD101-CTD150.xls, and Bottle_CTD151-200.xls. Variables for each station are contained on an individual spread sheet. The file Bottle_Stats.xls contains an individual spreadsheet for each variable.

All rosette salinities (Ros_sal) have been included in the bottle files. Values flagged as doubtful or bad on both Delta-Sal00 and Delta-Sal11 have been "painted" yellow and light yellow when only one delta was flagged.

Two new columns have been added to bottle files, CTD Sal00c and CTD Sal11c, which are the preliminary corrected CTD salinities after applying the coefficients from Table 2.

Associated files to this analysis:

SalBot.xls: Contains, in one spreadsheet all the station bottle files,
corresponding regression for Pr and Sta#,
corresponding residual histograms
and percentage of usage.

Autosals.xls: Contains rosette salinities measured on the autosal by run.

NBP0702_000 to NBP0702_023.raw (output files form ACI 2000 software)

NBP0702_000 to NBP0702_023.hdr (output files form ACI 2000 software)

NBP0702_000 to NBP0702_023.dat (output files form ACI 2000 software)

NBP0702_000 to NBP0702_023.xl (converted, to one line per sample, from ".dat" files)

- Richard Cullather wrote two routines:

readbottle.f: Re-arrange CTD ".btl" files into "bottle….xls" files.

readrosette2.f: Re-arrange ACI 200 ".dat" files into ".xl" files.

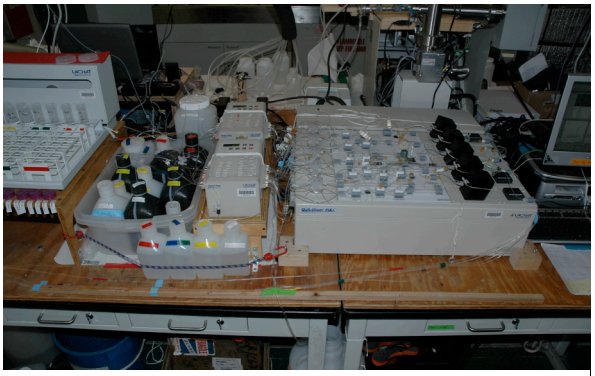

***Figure 10. The Lachat, as seen on NBP0702***

### 6.1.3 Nutrient analysis

Cruise Report – Nutrient Section

Authors: C. Little/B. Loose

#### 6.1.3.1 Overview

Nutrient analysis on NBP0702 was conducted to support biological analyses in the upper water column and to investigate the use of nutrients as independent and/or complementary water mass tracers in the Amundsen Sea. Seawater samples were

analyzed using RPSC's Lachat QC8000 nutrient analyzer, coupled to a Lachat XYZ autosampler, two Lachat pumps, and the Omnion software analysis package (figure 1).

The Lachat uses a colorimetric analysis technique to determine the concentration of each analyte; phosphate ($PO_4$), nitrate ($NO_3$), ammonium ($NH_4$), nitrite ($NO_2$), and silicate ($SiO_2$) were analyzed on this cruise.

Samples were injected into five channels (one per analyte) using a Low Nutrient Seawater (LNSW) carrier. In each channel, reagents are introduced to generate suitable absorbing species. Products from these reactions then pass into a detector, in which absorbance at a specified wavelength is measured. For nitrate, which is reduced to nitrite in a copper activated-cadmium column before detection, the measured analyte is "N+N", the sum of nitrite and nitrate concentrations.

Chris Little and Brice Loose were responsible for managing the sample collection, processing, and data entry/correction. Bettina Sohst (Raytheon) provided invaluable guidance, operational support and troubleshooting guidance throughout the cruise. Amy Leventer, Rose Vail, and Stephanie McClellan assisted greatly by collecting samples.

***Figure 10. Nuthouse inmates (Bettina, Chris, Brice)***

6.1.3.2 Sampling Methodology

For samples from the rosette after CTD casts, nutrient samples were taken after other time-sensitive gases were sampled. 1106 nutrient samples were collected at depths ranging from the surface to 2700 m on over 160 CTD casts. Sample depths were chosen based on review of water column temperature, salinity, $O_2$, and transmissivity (or flourometry) measurements on the CTD downcast. In general, the upper water column (>100m) was sampled more densely than the deeper sections. Underway surface samples were also collected, in conjunction with $TCO_2$ samples (to be analyzed at Lamont-Doherty), from the NBP's uncontaminated seawater system at 12 hour intervals (12 am and 12 pm ship time). Additional samples were collected if the underway $pCO_2$ or fluorometer showed evidence of upwelling and/or increased productivity at the surface. Over the course of the cruise, 88 underway samples were collected and analyzed using the techniques described below.

Both rosette and underway samples were collected according to the sampling protocol. A 60 ml syringe with a 5 μm membrane filter was rinsed 3 times with the seawater to be sampled, then injected into a rinsed 50 ml sample vial. After sampling, the vials were capped and refrigerated until they were placed on the Lachat for analysis. Samples were processed no later than 48 hours after sampling. Despite the known sensitivity of ammonium to contamination (in storage or when sampling), samples left up to 2 days showed little evidence of contamination, often revealing a sub-surface ammonium maximum in the mixed layer and minimal concentrations elsewhere in the water column. All equipment was washed with hydrochloric acid before use.

6.1.3.3 Method

Standard Preparation

Stock standards were prepared before the cruise with pre-weighed solids from Oregon State University. Calibration standards were prepared from the stock standards before each day's run(s). The concentrations of standards used in the calibration for each analyte are shown in the table below.

| Std # | $PO_4$ | $NO_2$ | N+N | $NH_4$ | $SiO_2$ |
|---|---|---|---|---|---|
| 0 | 0 | 0 | 0 | 0 | 0 |
| 1 | 0.501 | 0.201 | 7.704 | 0.3844 | 25.04 |
| 2 | 1.002 | 0.402 | 15.403 | 0.7687 | 50.07 |
| 3 | 1.503 | 0.603 | 23.108 | 1.1533 | 75.12 |
| 4 | 2.010 | 0.807 | 30.908 | 1.5426 | 100.48 |
| 5 | 2.507 | 1.005 | 38.530 | 1.9229 | 125.26 |

Table 1. Standard concentrations (μM)

These standards, along with a dummy sample, a LNSW (carrier) sample from the North Pacific subtropical gyre near Hawaii, an OSIL (Ocean Sciences Industries, Ltd.) LNSW sample, a mid-range standard check, and a column efficiency check, were used to calibrate the Lachat before each run. For the first run of the day, duplicates of each standard were used. Calibrations of each run were reviewed for errors and contamination, occasionally resulting in the use of a subset of the standards.

Samples were analyzed with concentrations in excess of the standard concentrations. These include phosphate (35 samples, with a maximum value of 2.6 μM), silicate (8, 136 μM), and ammonium (37, 8.5 μM)

QA/QC

Runs typically consisted of 30-40 samples along with calibration standards and replicates. Mid-range standards were analyzed as unknowns, on average, every 12 samples. These measurements were used to examine the replicability of results and/or drift throughout the runs. Additionally, replicates of water samples were run back-to-back between each standard check. Generally, silicate demonstrated the largest sample-to-sample variation, on the order of 1%.

Blank correction

"Blanks", obtained by analyzing OSIL LNSW with known concentrations, were used to correct for nutrient concentrations in the carrier. In addition to this correction, the OSIL LNSW contained 0.56 uM $SiO_2$, and 0.01 uM $PO_4$, which was added to the blank and/or drift-corrected values.

6.1.3.4 Performance and Error

In addition to the replicates and standard checks employed throughout the individual runs, a series of standards were analyzed at the beginning of the cruise. The mean detection limit at the lowest standard concentration and variance of a mid-range standard were determined. These results are presented, along with a recovery analysis performed on an OSIL standard solution, below.

| | PO4 | | NO2 | | N+N | | NH4 | | SiO2 | |
|---|---|---|---|---|---|---|---|---|---|---|
| Standard 1 | | | | | | | | | | |
| MDL (3*STDEV)= | 0.03 | | 0.01 | | 0.03 | | 0.03 | | 0.63 | |
| Standard 3 | | | | | | | | | | |
| Variance= | 0.92 | % | 0.48 | % | 0.27 | % | 1.15 | % | 0.18 | % |
| OSIL Standard | | | | | | | | | | |
| Recovery= | 101.7 | % | 108.2 | % | 103.5 | % | 93.1 | % | 101.2 | % |

Table 2. Error/Recovery analysis

Bubbles

Air bubbles occasionally distorted sample peaks. If possible, samples were re-run. Otherwise, if the bubble's impact was not near the center of the peak, it was possible to manually integrate the peak. If it was impossible to correct the automatic integration, the data point was not used.

Data Processing

All runs were post-processed to review calibration curves, examine the peak shape and timing, and to review any drift in the run. Phosphate was particularly susceptible to drift in the first run of the day, a 1.50 μM standard generally experiencing a linear drift to concentrations near 1.70 μM over the course of the run. Later in the cruise, silicate showed higher variability.

Ammonium channel

The ammonium channel clogged during a run containing CTD 71-74. No ammonium data was collected for this run.

6.1.3.5 Preliminary Analysis

In general, high values of all nutrients are found across the Ross and Amundsen continental shelves, with moderate, spatially variable locations of drawdown in the surface layers. Cumulative data for all analytes except $NO_2$ (which was found in low concentrations and showed little variability) are shown against depth in Figure 11.

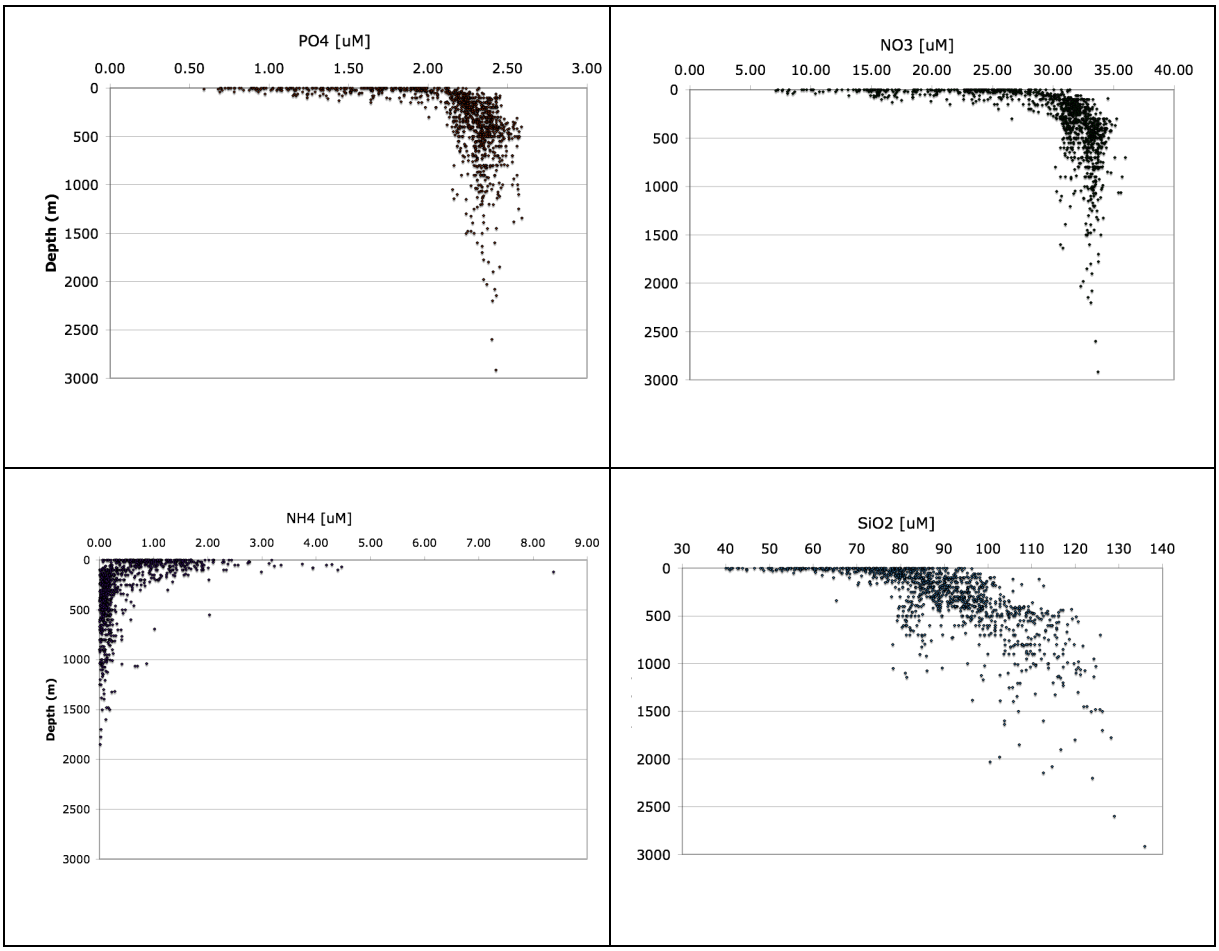


Figure 11 Nutrient concentrations vs. Depth (cumulative over cruise)

$PO_4$ and $NO_3$ generally co-vary, however, $PO_4$ showed higher spatial variability than $NO_3$. Ammonium concentrations are, in general, low. However, several subsurface NH4 spikes (>4 μM, with a maximum value of >8 μM) with associated higher near-surface concentrations were observed, often coincident with drawdown of $NO_3$ and $PO_4$.

The Amundsen continental shelf shows particularly high values of $PO_4$, $NO_3$ and $SiO_2$ below the eutrophic zone, consistent with other tracers that indicate relatively unmodified CDW on the continental shelf. A preliminary analysis indicates that silicate tracks intrusion of upper CDW onto the continental shelf. Concentrations as high as ~120 μM were found in Pine Island Bay and in the CDW core near the shelf break, areas shown to be characterized by high temperature and salinity on this and other cruises. Smaller scale variability of the silicate concentration may indicate localized upwelling (such as that occurring on the western side of the PIG transect), however, given the spatial resolution of these measurements, robust conclusions about the origin and modification of high silicate values may be difficult to achieve. How productivity and/or mixing of surface water on the shelf, or sub ice shelf processes, modify nutrient concentrations will invoke advective, remineralization, and mixing timescales, and possibly more dense sampling.

Ice Shelf Fronts

A transect of the Ross Ice Shelf was completed (see Figure 12). High $PO_4$ and $NO_3$ concentrations are present in the western Ross Sea. Silicate distribution is patchier, with a maximum ([Si] ~ 92μM) near 174E.

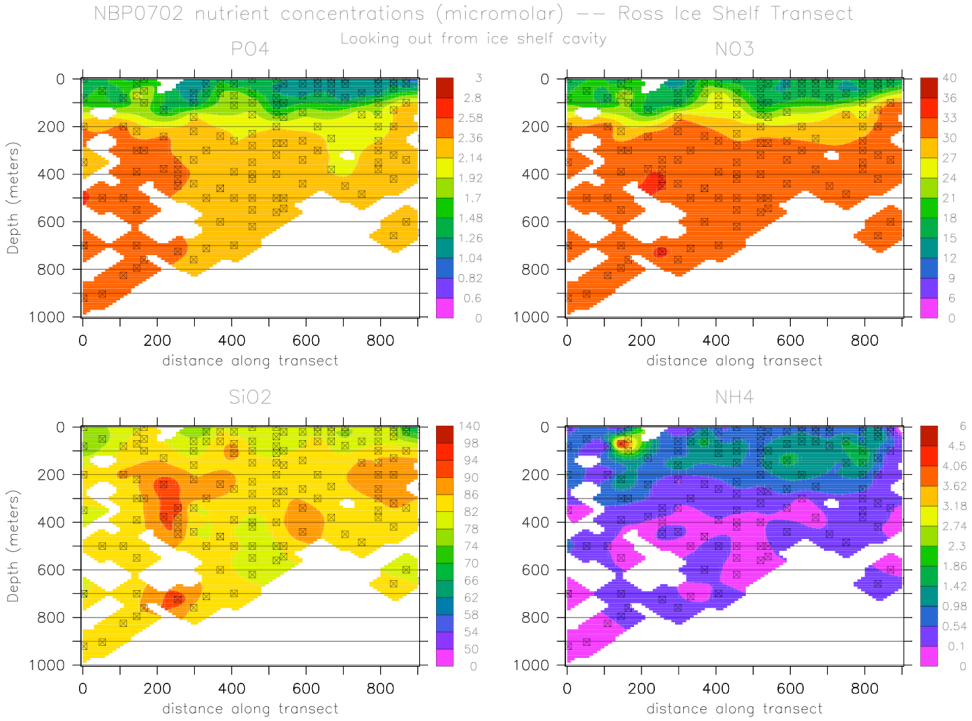


**Figure 12** Ross Ice Shelf front nutrient concentrations

Nutrients were collected and analyzed across eight distinct ice shelf fronts in the Amundsen – four separate shelves comprising the western Getz ice shelf (G1-G4), the Central and East Getz ice shelves (G5, G6), Dotson (DOT), and PIG (see Figure 13). Two stations were occupied between the Dotson and PIG ice shelf transects near the Crosson Ice Shelf and Thwaites Glacier Tongue.

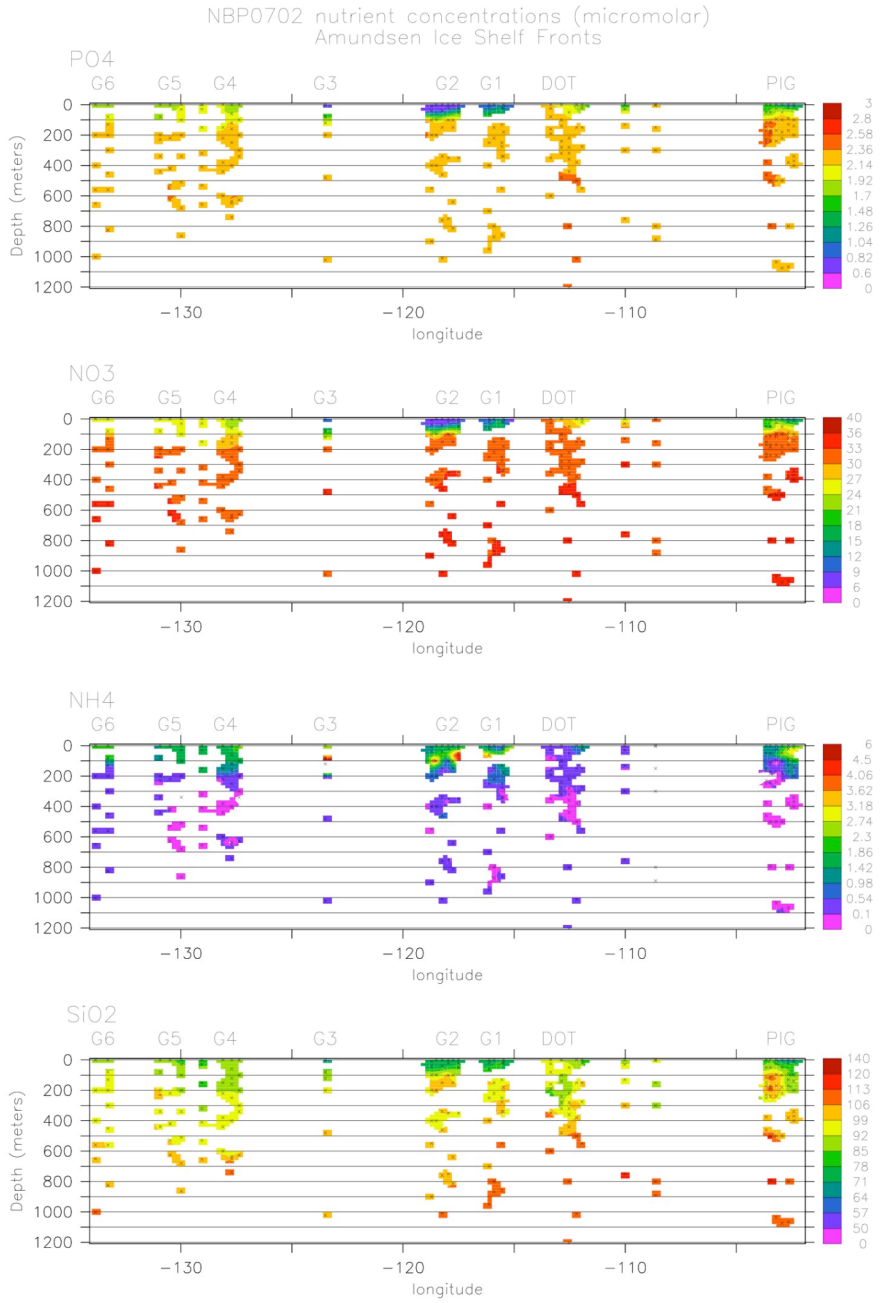


Figure 13 Amundsen Sea Ice Shelf front nutrient concentrations

As expected, nutrient concentrations in the Amundsen reflect the presence of CDW near ice shelves in this sector. Significant contrasts were found across the ice shelves. In the Amundsen, there was a zonal gradient in surface and deep nutrients, especially silicate, with the highest values occurring in easternmost Pine Island Bay. Particularly sharp nutrient drawdown and low pCO2 was found in front of the East and Central Getz ice shelves. Possible interpretations of this anomaly include increased light due to late summer sea ice melt, or advection of formerly productive surface water masses to the ice shelf front. In contrast, high nutrient concentrations were found coincident with high pCO2 near the Dotson ice shelf. Whether this is a signal of local glacially-driven upwelling or simply a lack of biological productivity is

an open question. Quantitative analysis of the phytoplankton communities conducted later on surface water samples may help determine the underlying causes of this prominent near-surface variability.

Open Ocean/Continental Shelf Break

Activity later in the cruise focused on a CTD transect along the Amundsen Sea continental shelf break from ~135°W to ~100°W. Nutrients were collected at stations on the shelf and slope sides of the shelf break (see Figure 14, only shelf stations shown). General trends include a decrease toward the east in $SiO_2$ concentrations at the surface. This surface trend is accompanied by weaker increase in $SiO_2$ at depth (in contrast to the stronger variability the ice shelf fronts). A drawdown in surface nutrients is apparent between 117°W and 121°W.

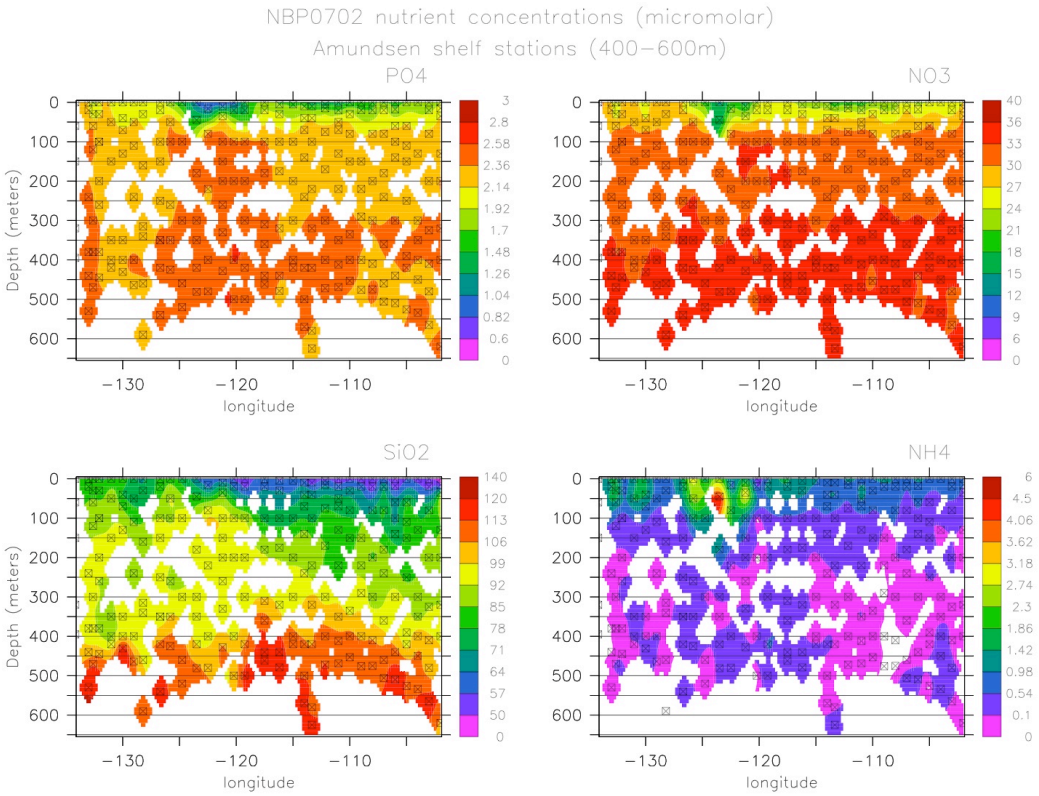


**Figure 14** Amundsen Sea shelf break nutrient concentrations

Previous Datasets

In 1994, ps94 visited the Ross Ice Shelf, while np9402 collected nutrients in the Amundsen and Bellingshausen Seas. Only the np9402 dataset was available aboard the NBP. A cursory comparison shows agreement in high concentrations of $SiO_2$ both on and off the continental shelf, the presence of surface $NO_3$ and $PO_4$ drawdowns, and high variability in $PO_4$ values (compared to $NO_3$). Nutrient data from np9402 are, in the words of the cruise report, "noisy", and consist of more deep (>1000 m) measurements. To provide an adequate comparison to the measurements taken on NBP0702, the data from np9402 has been limited to those stations taken in the Amundsen Sea (west of 100°W). Two different subsets of data are compared in table 3 – samples taken at depths greater than 1000m, and stations from np9402 at a depth less than 2000m (in an attempt to capture both slope and shelf stations, but eliminate deep stations).

| NBP0702 (1.0285kg/L conversion) | | | | NP9402 | | | |
|---|---|---|---|---|---|---|---|
| 71 samples > 1000m | | | | 300 samples > 1000m | | | |
| | PO4 | NO3 | SiO2 | | PO4 | NO3 | SiO2 |
| MEAN | 2.30 | 32.09 | 108.34 | MEAN | 2.18 | 32.20 | 124.60 |
| MAX | 2.52 | 34.63 | 132.16 | MAX | 2.42 | 33.90 | 148.10 |
| MIN | 2.09 | 29.46 | 76.12 | MIN | 1.88 | 30.40 | 87.10 |
| STDEV | 0.09 | 0.93 | 11.45 | STDEV | 0.08 | 0.50 | 13.09 |

| NBP0702 (1.0285kg/L conversion) | | | | NP9402 | | | |
|---|---|---|---|---|---|---|---|
| 903 samples from stations <2000m | | | | 444 samples from stations <2000m | | | |
| | PO4 | NO3 | SiO2 | | PO4 | NO3 | SiO2 |
| MEAN | 2.06 | 28.51 | 87.03 | MEAN | 2.03 | 29.25 | 86.90 |
| MAX | 2.52 | 34.73 | 132.16 | MAX | 2.47 | 35.00 | 130.60 |
| MIN | 0.57 | 6.91 | 37.43 | MIN | 0.75 | 12.20 | 40.90 |
| STDEV | 0.40 | 5.72 | 17.69 | STDEV | 0.27 | 4.15 | 16.54 |

Table 3. NBP0702 and np9402 nutrient data comparison (μmols/kg)

Phosphate shows a systematic bias towards higher values on NBP0702 (see Figure 15), while concentrations of nitrate are somewhat lower that seen on np9402. However, higher $PO_4$/lower $NO_3$ concentrations are also evident in a nearby WOCE transect used in the np9402 report. For shelf/slope stations, the mean silicate concentration and its variability are similar across the datasets.

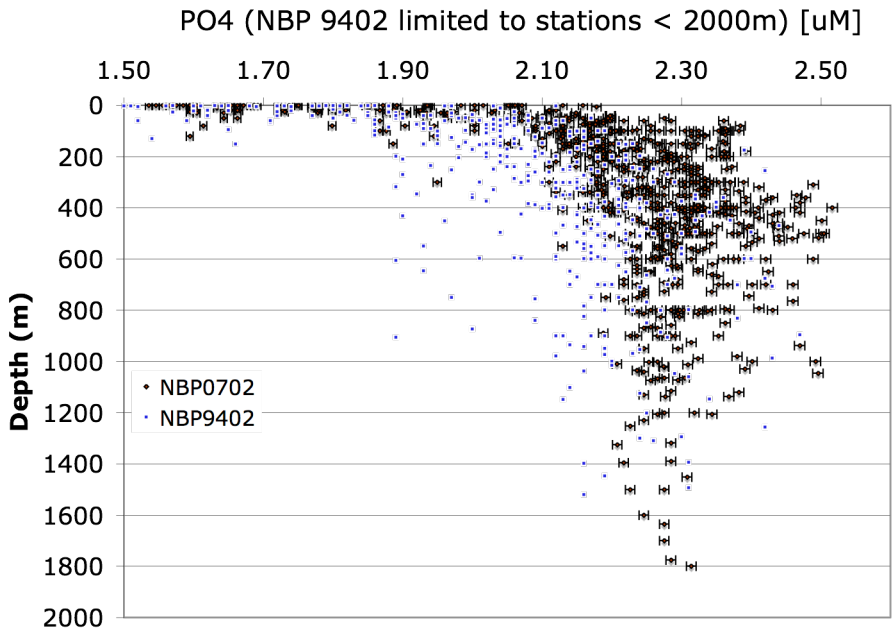


Figure 15 Phosphate concentrations – NBP0702 and np9402

Because of the differing distributions of stations among shelf, slope, and deep ocean locations, care must be exercised in the comparison of these datasets; more thorough comparison of available coastal and deep ocean data is required to validate these measurements.

#### 6.1.3.6 Suggestions and Further Thoughts

It may be worthwhile to reevaluate the protocol for and utility of ammonium in future cruises. Error due to delayed ammonium analysis can arise from contamination or degradation of the signal. The former can be seen in standard check values that increase between runs; the latter is seen in the decreased concentration of uncontaminated standards over the course of a day. This time-sensitivity is not seen in the other analytes, and ammonium often drives the timing of runs. Depending on staffing, this may not be a concern, but it is useful to consider in advance of a cruise in which nutrients may play a relatively minor role.

Using macronutrients in this region as water mass tracers poses some challenges. There may not be enough variability in source water masses to compensate for their biologically active nature and local-scale variability on the continental shelf. Silicate's increase with depth in CDW may be useful as a complement to traditional CDW tracers on the continental shelf. Both tracers indicate the potential to distinguish between warm CDW, cold Winter Water and fresh Surface Water, however, the signal to noise ratio is in general larger than what is found with the geochemical tracers (He, Ne, O-18). In the Amundsen Sea, cold, fresh inputs at mid depth from Winter Water and glacial melt are relatively indistinguishable. In Figure 16, both water masses exhibit a positive oxygen concentration, and a relatively depleted macronutrient concentration. Given the short time scale of cavity circulation in the Amundsen, CFC's may prove the most effective parameter in distinguishing between glacial melt and Winter Water, to the degree that their source functions can be considered steady-state.

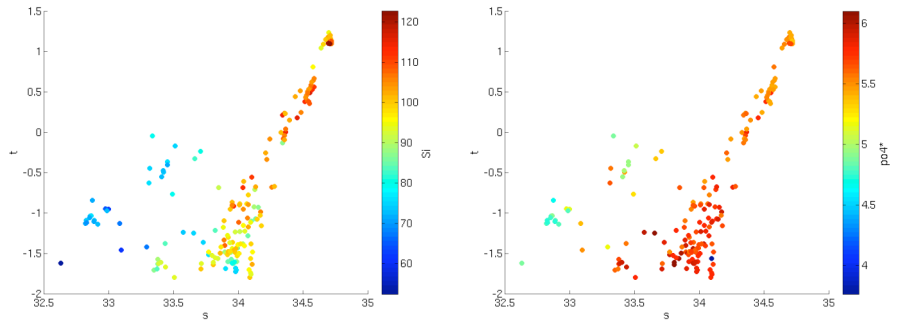


Figure 16 Si* (Si*=[Si]-[NO3]) and $PO_4$* (PO4*=[PO4]+[O2]/175+1.95) from stations 51-95 in the Amundsen Sea.

The use of nutrients to understand variability cause by continental shelf processes such as biological productivity, ice melt, or sub-ice shelf processes will require finer ice shelf front measurements, possibly with a complementary micronutrient (i.e. iron) analysis.

Practicalities

All raw "Omnion" files and runs (with calibration information) are kept in folders named with the date of the run within the NBP-0702/Nutrients/NBP-0702 Nutrients/ directory. Peak heights, peak areas, and concentrations based on the calibration are exported as .csv files in each folder. The summary workbook, NBP0702_nutrients.xls, contains a cumulative spreadsheet, a blank correction worksheet, some cumulative plots, and the .csv spreadsheets, with any applied drift correction and with formatting changed for incorporation into the cumulative spreadsheet.

### 6.1.4 Dissolved Oxygen

(A. Criscitiello, K. Leonard and R. Cullather)

Dissolved oxygen measurements were made in conjunction with geochemical tracer sampling to help determine water mass source, formation, residence time and mixing, along with saturation level, surface equilibration, biological productivity and meltwater content. Titrated values by the Winkler method are also necessary to 'calibrate' the CTD oxygen sensors, i.e., to correct for sensor bias, drift and potential offsets.

Two SBE 43 oxygen sensors are now a standard part of the CTD sensor array. SBE 43 sensors are reported by the vendor to be accurate within 2% of saturation, with a stability of 2% per 1000 hours. On NBP07-02, 1,030 oxygen samples were collected for Winkler titration on 165 stations. The Langdon amperometric titrator was used to determine dissolved oxygen concentrations in whole bottle samples. Titrations proceeded smoothly, with several exceptions when the stir bar did not remain centered in the sample flask for the entire titration due to ship movement. Bubbles in the micro burette or bubbles injected into samples by pickling dispensers occurred occasionally. Stable blank determinations took many runs to achieve, and may be due to inconsistent dispensing of the standard by the 1 ml dispenser. Standard determinations showed normal variation and expected values.

The results show minimal sensor drift, but considerable bias, higher at high oxygen concentrations (near-surface samples). Titration values consistently fell between the primary and secondary oxygen sensor values. After outliers were removed, 915 data points were available for comparison with $O_2$ sensor values. This high rejection rate is partly explained by Figure 17 and Figure 18. Niskin #20 displayed an unusually high rosette-CTD delta for most stations. The primary reason for excluding Niskin #20 from analysis is that the lower Niskin cap would occasionally hit the Y-tubing connecting the pump to the

primary sensors when tripped, resulting in bad readings from the primary CTD oxygen sensor. Additionally, Niskin #20 was generally fired at a high gradient depth which can produce large sensor errors. All Niskin #20 data were removed from the titration vs sensor analysis because of errors introduced by these two factors. Secondary oxygen sensor data from stations 140 through 142 are unusable, thanks to a jellyfish brought up on CTD 140. Tentacles wrapped around the Y-tubing connection to the secondary sensors apparently interfered with that sensor performance through CTD 142. The remaining 19 outliers not used for CTD sensor correction probably resulted from sampling or titrating errors. Outliers that have been removed are not presently noted in the master spreadsheet.

A possible pressure dependence can be seen in the nonlinear relationship between Ox1 minus Ox2 sensor values and rosette oxygen (Figure 19). The non-linearity is likely the result of different slopes of the two regression curves. In multiple linear regressions using both sensors and pressure, the pressure term received an insignificant coefficient and dropped out. The lowest standard error is achieved by using Ox1, Ox2 and pressure to rosette oxygen (RMS=0.0625). Linear regressions applied to rosette oxygen versus Ox1 and Ox2 sensor values are shown in Fig. 4, with RMS errors of 0.0655 and 0.0736.

Two oxygen sampling experiments were conducted. On the first, 23 same-Niskin replicates were taken over the course of the cruise due to air bubbles introduced to the sample flask during the pickling process. The average difference between those replicates was 0.02 ml/L, with all <0.08 ml/L, which suggests this is not a significant source of error. At (test) station 1, two same-Niskin replicates were taken by the two $O_2$ samplers (K. Leonard and A. Criscitiello) each sampling the same bottle. The differences (<0.02 ml/L) also suggest that significant errors were not introduced by sampling technique.

The second experiment tried to determine if errors were introduced by sampling a Niskin for dissolved oxygen first, versus sampling an adjacent Niskin triggered at the same station and depth, but after the helium sample was drawn. Fourteen such pairs were sampled, showing an average difference of 0.02 ml/L and a maximum <0.06 ml/L. This suggests that errors introduced by sampling for oxygen after helium and sampling from different Niskins triggered at the same depth does not introduce significant errors. For both experiments, linear regressions show that errors decreased over time. In the future, oxygen techs should continue sampling two Niskins tripped at the same station and depth to make this dataset of duplicates more robust. A similar result could lead to reduced CTD sampling time.

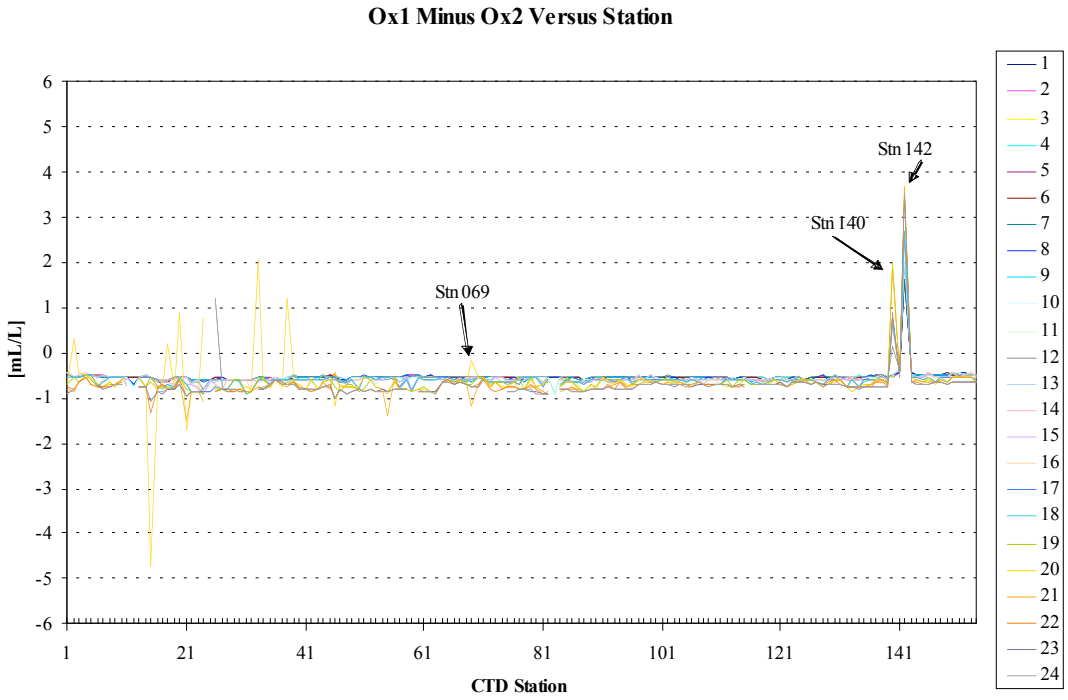


Figure 17 Ox1 minus Ox2 sensor values versus CTD station. Note significant errors at CTD stations 140 to 142, and on Niskin 20.

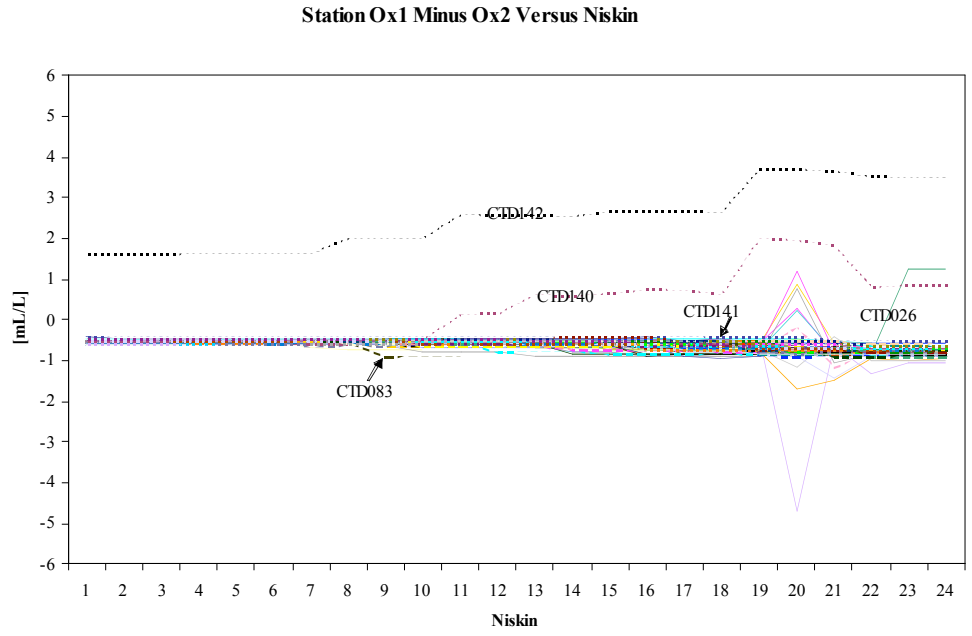


Figure 18 Ox1 minus Ox2 sensor values versus Niskin bottle. CTD 140 to 142 jelly errors are noted in the text.

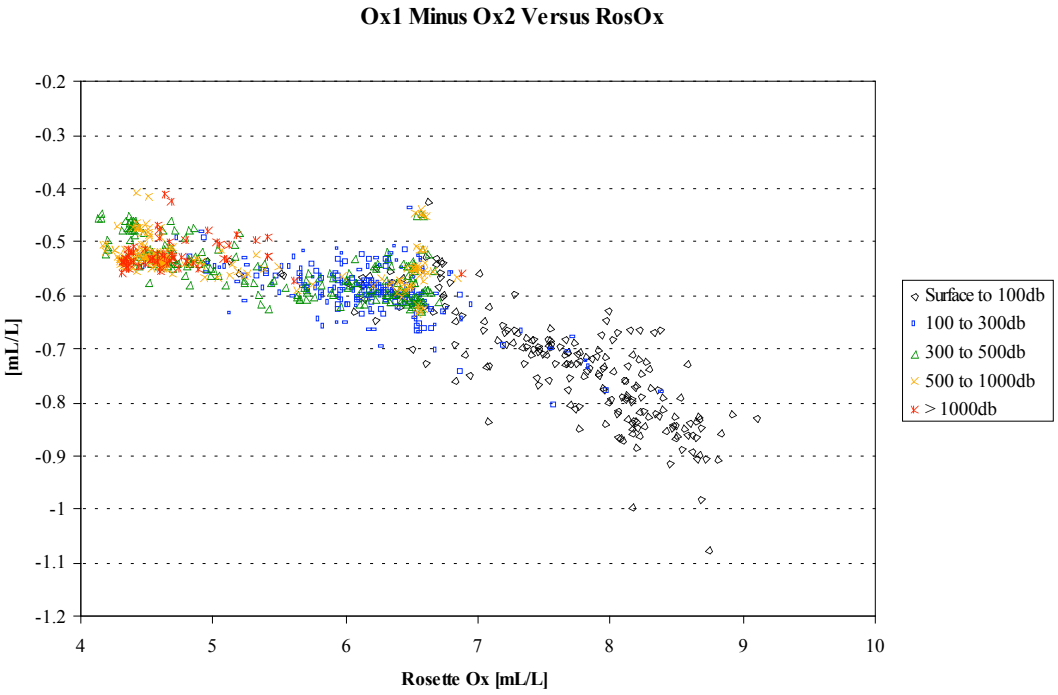


Figure 19 Ox1 minus Ox2 sensor values versus rosette (Niskin) oxygen values.

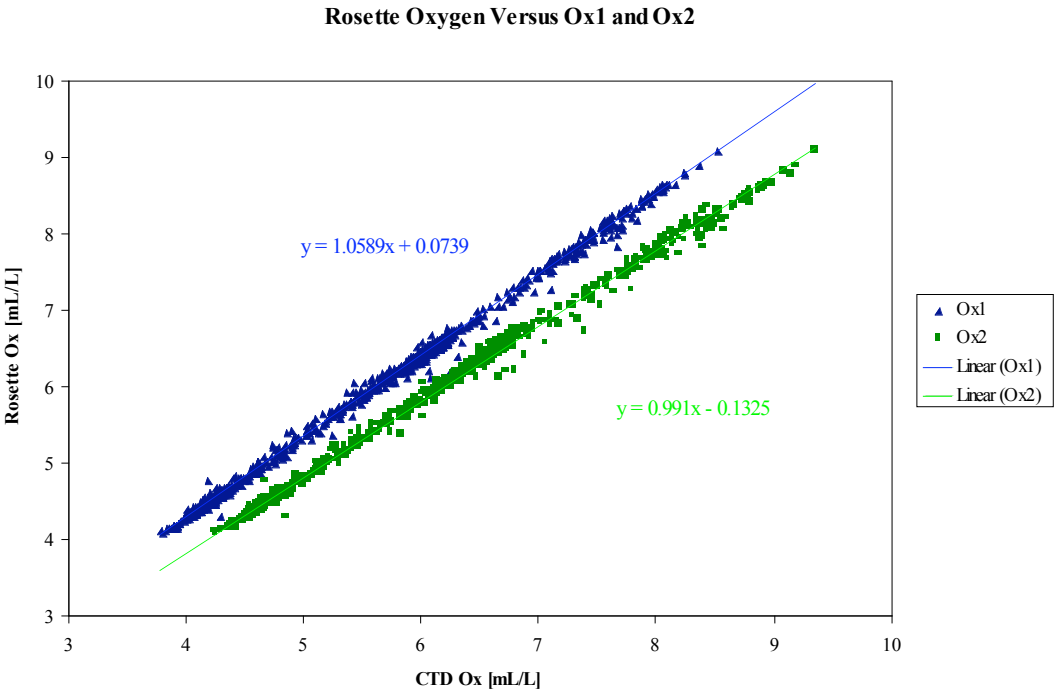


**Figure 20** Rosette oxygen versus Ox1 and Ox2 sensor values. Outliers have been removed and linear regressions applied.

### 6.1.5 Tracers

Noble gas and stable isotope tracers (helium, neon, tritium, oxygen 18)

(Brice Loose, Chris Little)

Noble gas tracers were collected from the Niskin rosette at 122 of the 167 stations sampled during the cruise, 22 in the Ross Sea, and 100 in the Amundsen Sea (Figure 21). In total 591 He, 593 oxygen-18, and 300 tritium samples were collected, with an average of 4.8 He and oxygen-18 samples per station; most tracer stations were 600 m or shallower, resulting close to 100 m vertical sampling resolution, on average.

Sample collection

Helium samples were collected in copper tubes, sealed with a stainless steel pinch clamp on both ends, to create a water and gas-tight seal; the stored volume is approximately 40 ml. Helium channels are flushed with approximately 1L of water, while the sample is repeatedly impacted with a hammer to dislodge bubbles, which can collect on the side walls of the tubing and compromise sample integrity.

Oxygen-18 samples were collected in 110 ml glass bottles with a conical polyethylene stopper. The sample is introduced to the bottle using a Tygon tube, which is placed at the bottom of the bottle, and the sample volume is replaced three times before closing the top. Tritium samples were collected in 1L amber bottles.

Application

Helium 4, neon and oxygen 18, all strong proxies of glacial melt, and helium 3 which is high in Circumpolar Deep Water (CDW). The combination should be ideal for this region, where the warm CDW signal is relatively unmodified before it sinks beneath the ice shelves. The tracer measurements will be used to constrain cross-shelf fluxes of heat and freshwater, and provide an additional dataset for the validation of numerical models of the continental shelf and sub-ice shelf circulations.

Transient Tracers (SF6, CFC-11, 12, and 113)

SF6 and CFC's were collected at 79 of the 167 CTD stations; this includes 3 stations offshore of Cape Adare, 16 stations in the Ross Sea; the remainder were in the Amundsen Sea (see Figure 1).. A total of 352 SF6 samples were collected from the niskin rosette. Samples were stored in 250 ml glass bottles with a ground glass stopper. These bottles were immersed in plastic jars, filled with water from the same depth. The objective of this sample collection style is to isolate the sample from the surrounding air with a water buffer. The low solubility of the gas ensures much smaller sample contamination. Water samples were kept cool in a freezer whose mean temperature was -1 C, to avoid thermal expansion and degassing.

Brice Loose and Chris Little conducted noble gas and transient tracer sampling. Samples were packed and stored for shipment to Lamont-Doherty Earth Observatory for analysis. SF6 and CFC samples will be analyzed at LDEO during June and July of 2007.

Application

SF6 has a constant monotonic increase of 6-7 % per year in the atmosphere. This makes it an ideal tracer for estimates of transport time scales in recently ventilated waters (~20 years). While much of the water column in the Amundsen Sea is expected to have little or no SF6 concentration, this deficit as compared to what would be expected in a stagnant water column can be used to estimate the rate of replenishment or residence time of CDW on the continental shelf.

CFC-11, 12, and 113 are all decreasing in the atmosphere. Over the past 10 years, their inputs have been relatively constant. It may be possible to use CFC's as a water mass tracer to separate recently formed

winter water, which has penetrated below the mixed layer, from the cold, fresh input of glacial meltwater which will have no CFC content.

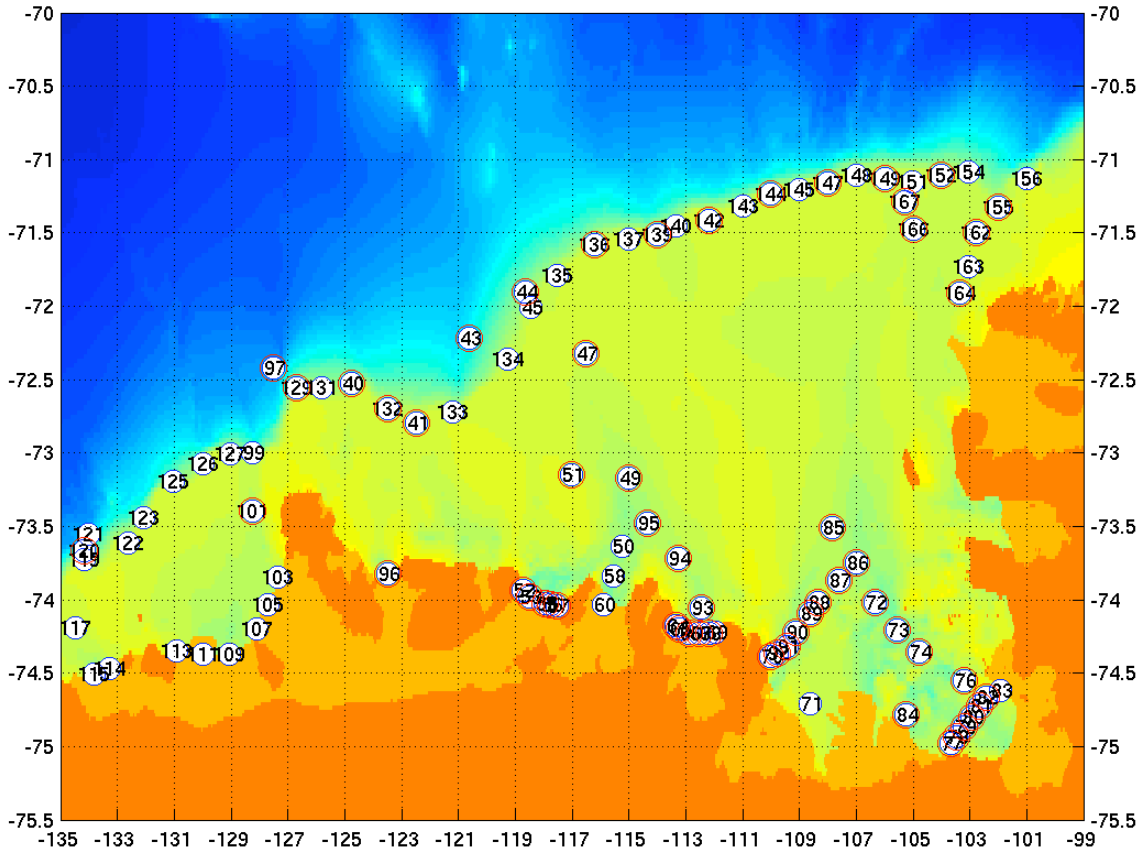


**Figure 21 :** Geochemical tracer stations in the Amundsen Sea during NBP07-02. Stations with a red halo indicate stations where SF6 and CFC's were collected, as well as helium, tritium, and oxygen-18.

### 6.1.6 Lowered Acoustic Doppler Current Profiler (LADCP)

#### 6.1.6.1 Overview

Profiles of ocean currents were provided with each CTD cast by the LDEO LADCP system mounted on the CTD/Rosette frame. The system comprises two RDI/Teledyne WH300 acoustic Doppler current profilers (300 kHz ADCP heads) mounted on the rosette frame, one pointed up and the other down, and a rechargeable lead-acid battery in a deep sea housing (DeepSea Power and Light). The two heads are operated in master/slave mode, with the downlooking head serving as master. The synchronization signal, communications lines, and power lines are served to the heads and battery via a breakout cable designed at LDEO and manufactured by Impulse. For this program, the master was a custom-built high power WH300 which was expected to provide improved range over the standard WH300 units.

Setup of the instruments and post-cast data download were managed by software designed by Andreas Thurnherr of LDEO (version as of Jan 2007), running on a linux-based notebook computer. The lead-acid battery was recharged between casts using a battery charger provided by DeepSea Power and Light. Downloaded data were processed on B. Huber's MacBook Pro running Matlab R2006b and version IX_4 of the LDEO processing software (Visbeck, Krahmann, and Thurnherr).

#### 6.1.6.2 Installation

Mechanical -

The ADCP heads and battery were installed on the CTD/Rosette frame by RPSC personnel prior to the port call at McMurdo, using materials provided by LDEO and a battery mount frame fabricated on board by RPSC staff. The installation required only very minor adjustments.

The LADCP system is internally recording and draws power exclusively from the DSPL battery pack, so there are no cables between the LADCP and CTD systems. However, the LADCP must be connected between casts to the data management and the battery charger computer (set up in the aft dry lab). The LADCP cable system has two free ends for this purpose, both of which are terminated in high pressure dummy plugs during deployment. The ends of the cable are color coded but the same gender. Two cables were run from the aft dry lab to the Baltic room: a two-conductor neoprene jacketed cable for battery charging, and a 7-conductor cable provided by RDI for communications and data download. The ends of the lab cables were left coiled in the Baltic room and were also protected by dummy plugs during a cast.

Cabling has always been a weak link in the LADCP system, owing in large part to the repeated mating/unmating of the connectors for data download and battery charging, the concomitant strain placed on the cables, and corrosion of the connector pins. To alleviate at least some of these problems, short extension cables were used on those ends of the breakout cable normally subjected to frequent handling. In the event of damage to the mating end of the cable, the extension could be easily replaced. The cable ends were secured to the frame with Velcro straps to serve as strain relief during connection to the deck cables. The connectors were rinsed in fresh water immediately before unmating and mating, to remove any traces of salt water. The connectors are wet-mateable, but are nonetheless a bit fragile and susceptible to corrosion if not rinsed. It is particularly important that the dummy plugs be replaced before a cast. The plugs were secured to the cabling with string so they would not wander off, and the RPSC Baltic room staff were asked to make sure there were no dangling dummies as the CTD was being deployed. They did a fine job, and we had no mishaps. No cables required replacement. This is probably a record.

Computer –

All communications and data logging were performed on a Dell Latitude C610 notebook computer running linux (Fedora Core 6). Simultaneous connections to the two ADCP heads is made via a PCMCIA 4-port USB2 card and two Keyspan (model #19HS) RS232-USB converters. The communications cable system is set up to use a USB extender and up to 90 m of CAT5 ethernet cable if needed to deal with electrical noise. We found though that this was not necessary, and the RDI communications cable was run directly from the Baltic room to the computer, where connection was made via a Y cable to the two Keyspan converters.

The Dell was connected to the ship's network so that downloaded data could be backed up to the ship's network . In addition, the network connection was used to synchronize the Dell's clock to the network time server using ntpd. This is very convenient, since it is essential that the ADCP clocks be synchronized with the CTD times for proper post-cast processing. The ADCP clocks are updated as part of the pre-cast initialization scripts.

Software setup consisted mainly of modifying the DEFAULTS.expect file in the software suite to reflect cruise-specific data (such as backup data paths, file name conventions, and so on). The software and documentation are included in the LADCP data distribution. The interested reader is referred to these and to the extensive documentation available on the LDEO LADCP website for details.

In principle, the post processing can be carried out immediately after data download on the Dell (or whatever computer is used for system control). It was found more convenient however to have B Huber do the processing on his computer, for several reasons. The Matlab license server on the Dell had some problems adjusting to host name changes, so it always took some fiddling to start Matlab (required to run to the processing software). We are using version IX_4 of the processing suite. This is a new release, and it took some time to become familiar with the setup. It turned out to be easiest to just run all the processing on the MacBook Pro. Since the computers were all networked, this was never a real bottleneck.

System parameters –

Data were recorded in beam coordinates, with a bin size of 8 m.

See appendix for command files used and more details of the system parameters.

Master (downlooking) instrument: sn 7280. Firmware rev. 16.28

Slave (uplooking) instrument: sn 754. Firmware rev. 16.28

Processed data – Post cast processing consists of converting the beam-coordinate, relative LADCP velocities into earth-referenced absolute velocity profiles adjusted to CTD pressure as a vertical coordinate. The data are reduced to a bin size of 20 dbar. GPS data recorded with CTD scans (but see note below) is used as one of the constraints in estimating the velocity profile. Ship's hull-mounted ADCP (SADCP) data are also used during processing as a constraint for the near surface (16 – approximately 150 m). Details of the processing procedures, discussion of the various plots produced and error considerations can be found in the documents on the LDEO website and stored with the LADCP data distribution.

#### 6.1.6.3 Performance evaluation

Overall, the system performed well, with minimal intervention required on the part of watchstanders. The currents observed were relatively weak (Figure 22), so it is difficult to assess the performance of the LADCP system at the preliminary processing stage. The data will be reprocessed once the ship ADCP data have been through final processing at U of Hawaii.

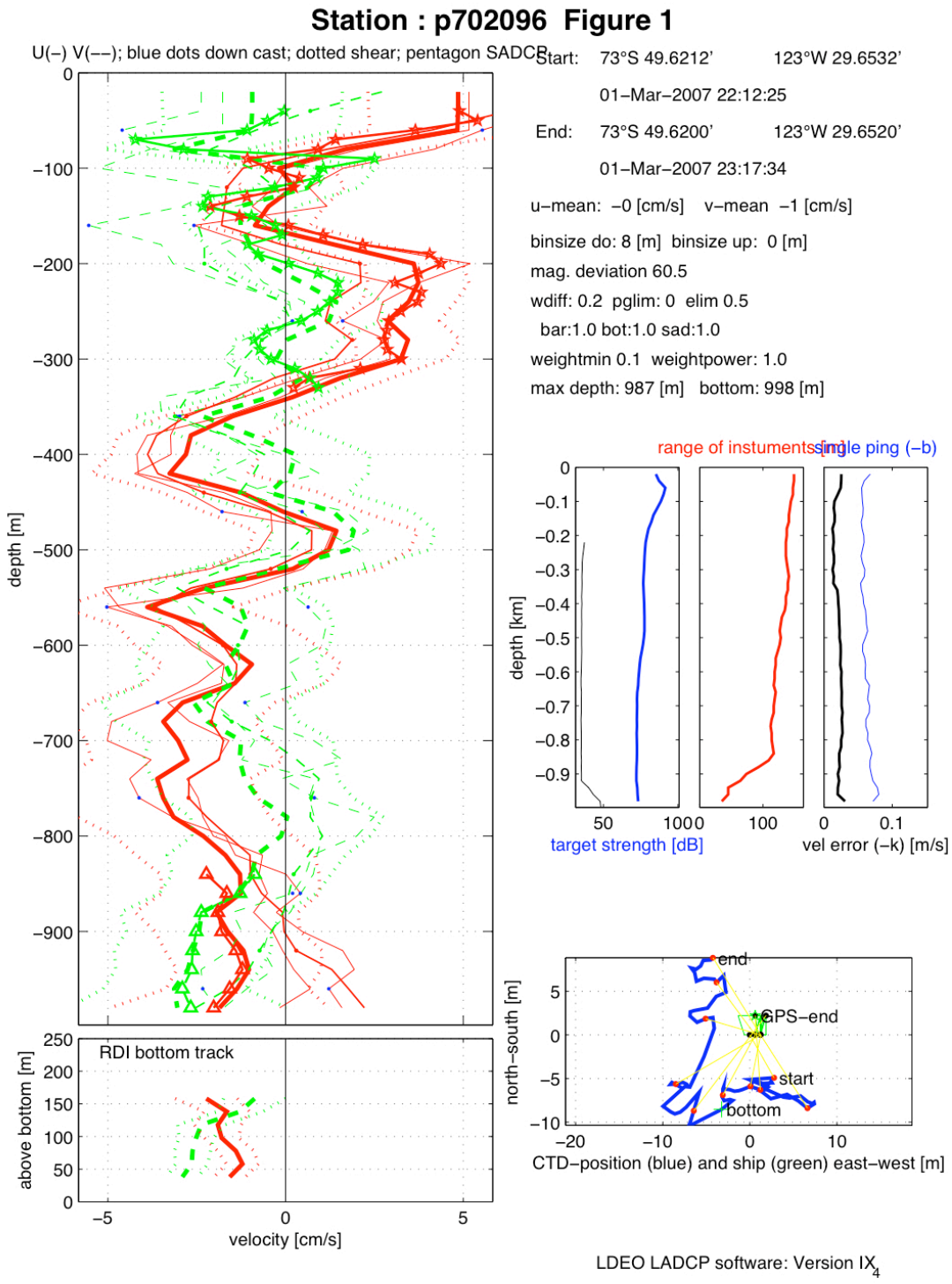


Figure 22 Sample LADCP data

Rechargeable battery -

The DeepSea Power and Light lead acid battery is a vast improvement over the expendable alkaline battery packs used on previous cruises. The battery performed flawlessly, and had plenty of power to keep up with the cast schedule. Routine maintenance consisted only of charging between casts and inspecting the gas bubble under the urethane pressure compensation boot on top of the battery, venting the bubble when it became too large. In fact, the bubble never grew to the extent that venting was needed during routine use. Only when the Baltic room heaters were inadvertently left on and the room became hot did the bubble require venting. The battery charger obtained from DeepSea Power and Light was used throughout to keep the battery charged. The charger is designed to provide the correct voltage and current to the battery at each stage of the charging cycle, and to maintain a "float" charge on the battery in between uses. The charger has no on-off switch, no voltmeter, and is not in a splash-proof enclosure. It is recommended that the charger be repackaged in an enclosure which can be securely bench mounted, protects it from wet hands, has an on-off switch and a connector or junction panel to connect the charger to the charging cable.

Two problems arose during the cruise.

1. Normally, the CTD acquisition software is configured to store GPS-generated latitude and longitude with each CTD scan. These positions are used in the processing stage to provide a geographic reference for the conversion from beam coordinates to earth-referenced velocities. While not required, the GPS data if used can significantly reduce the velocity errors. The lat lon fields in the CTD files for stations 1-43 however do not increment with each scan. Apparently, the instrument configuration file is overridden by a control in the SEASAVE Configure submenu. The instrument config files all had "add nmea data" checked, but in SEASAVE, the configure selection for handling NMEA data was set to "Store in header only". As a result, the ctd files have the position at the start of the cast in the header, and this position is repeated for each recorded scan rather than being incremented for each scan as expected from the instrument configuration file.

For a fix we will have to extract navigation info from the rvdas files after the fact. The ship was using DP for all but one or two stations during this period, so in the meantime, the processed ladcp data is probably ok as a first look. For stations 44 et seq. the SEASAVE configuration info has been set for add nmea to each scan.

2. The slave unit sn 754 developed problems on CTD 53, when the processing software reported that beam 1 was broken. The unit was left in place, since in principle it is possible to obtain a 3-beam solution to the transformation from beam to earth coordinates (the processing software does not currently do this). On CTD 75, the software reported the loss of beam 2. The unit was used on one more cast (76) to see if this was a temporary condition. It was not. The unit was removed after CTD 76 since no data recovery is possible with only 2 beams. The unit was opened and found to have leaked slightly through one of the transducer faces. Seawater dripped from the leaking transducer, through a hole in the transducer housing, causing corrosion on the transducer transmit/receive circuit board located under the copper shield in the transducer head. The damage was photographed, and the corrosion cleaned before reassembling the unit for shipping and repair.

For casts 77 through 189, the LADCP system was operated with just the downlooking unit. Data return was good throughout, with no noticeable degradation in system performance. This is in keeping with earlier observations by Thurnherr and others that two heads are not necessarily better than one, especially if the one head has good range. The custom high power unit appears to have sufficient range in the waters sampled to provide reasonable estimates of the velocity field.

## 6.2 Underwater Photography

(Greg Watson)

A camera and strobe provided by Vernon Asper were attached to the bottom of the CTD frame to take photos during CTD casts. The camera is a digital Nikon Coolpix 955 that was modified by Insite-Pacific and inserted in a waterproof housing with accompanying electronics in order to function remotely - and to be attached to an ROV. This being the first time the camera had been used in this capacity, and the limited documentation initially provided, resulted in a steep learning curve. Eventually manuals were acquired and camera operation improved over time.

We were able to take photos of the sea floor and in the water column, probably the first on the Amundsen Sea continental shelf. The strobe that was provided was not very strong, and the CTD could not intentionally be lowered very close to the sea floor, which negatively impacted picture quality. The design of the camera housing and the way we were using it required opening for programming and battery charging between casts. Repeated access to the inside of the housing was a weak point in the operation, if not the camera design, which eventually led to flooding.

Mounting a camera on the CTD frame is a potential way to obtain useful information about the sea floor and water column, without expenditure of additional over-the-side time. Everyone seemed to enjoy seeing the photos from each cast, as many interesting creatures were digitally captured. Future camera/CTD work should consider an instrument that could be triggered remotely, perhaps in lieu of a couple of rosette bottles, external power, data downloading and programming without the need to open the camera housing, and a more powerful strobe.

Sample photos taken during NBP07-02 are presented in the appendix.

## 6.3 Mooring Operations

### 6.3.1 Amundsen Continental Shelf ( Jacobs O-274)

Data collected during the cruise will be supplemented with time series of temperature, salinity and currents obtained from six moorings deployed nearly a year ago during POLARSTERN cruise XXIII-4 by messrs. Frank Nitsche and Raul Guerrero. Each mooring was simply constructed using a lightweight acoustic release (ORE CART), braided polypro line, plastic trawl floats, and one or two instruments for measuring temperature, pressure, salinity, and on one mooring, current velocities. The design was meant to address 3 primary criteria - ease of deployment, without the need for winches, cranes or capstans; ease of recovery, and low cost. Three types of moorings (or bottom landers, as they also came to be known) were deployed, depicted in the schematic below.

Five of the six moorings were recovered during NBP0702. Recovery was facilitated by fairly benign sea state during the recoveries, but a layer of new gray ice during the fourth recovery made it difficult to spot the small green trawl floats, which had come up under the translucent, fairly rigid ice cover. The acoustic releases also double as relocation transponders, a necessity when trying to recover small packages with no other relocation aids.

The moorings were positioned in front of the Getz (central and west), Dotson, and Pine Island glaciers, in depths between 800 and 900 m, and on the outer continental shelf near 106 W and 073 W (Bellingshausen Sea). Use of the lightweight and relatively inexpensive CART releases limited the deployment depths to less than 1000 m. Measurements were made every 12 minutes, with all instruments returning records which fully span the deployment. Minimal corrosion and wear of the hardware on most of the releases and post deployment examination of the release and instrument batteries indicate that the releases could remain submerged for two years and perhaps a bit more.

A rack-mounted deck command unit wired to the ship's 12kHz hull transducer was used to communicate with the release/transponders. This is a convenient setup, but is a bit hampered by the fact that the hull transducer is installed on the starboard side of the keel, resulting in a shadow zone to port. Additionally, the hull mounted transducer has a relatively narrow beam pattern compared to the hemispherical response pattern of the dunking transducer typically used with the deck unit. This limits the utility of the hull mounted transducer for ranging on the releases when they are close to and at the surface. The ship was maneuvered during triangulation and recovery so that the starboard side was always presented to the target. Even so, most recoveries suffered some difficulties with ranging and receiving status replies from transmitted commands. A brief description of the individual recoveries is given below.

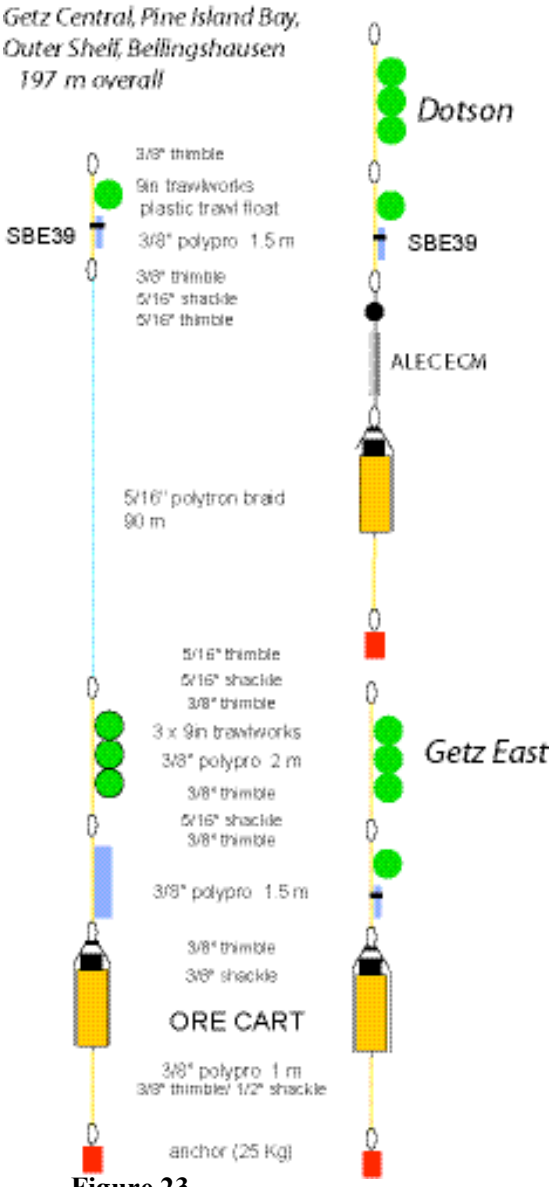


**Figure 23**

Table 1. Amundsen Mooring Characteristics

| Mooring ID | Lat (s) | Long (W) | Depth (depl) | Release | Instr/sn | Depl 2006 | station # PS69- | Rec 2007 | CTD |
|---|---|---|---|---|---|---|---|---|---|
| Getz Central | 73 49.01 | 116 59.91 | 806 | 31095 | 37/ 2504; 39/3269 | 7 Mar | 276-2 | 21 Feb | 51 |
| Getz East | 73 50.79 | 115 34.28 | 939 | 31117 | 39/3267 | 7 Mar | 278-1 | 22 Feb | 58 |
| Dotson | 74 03.49 | 112 25.07 | 859 | 31093 | 39 /3268; ECM 648 | 8 Mar | 279-2 | 23 Feb | 66 (10 mi) |
| Pine Island Bay | 74 36.51 | 103 52.36 | 850 | 31094 | 37/2505; 39/3264 | 14 Mar | 290-1 | 26 Feb | 83 |
| Outer Shelf | 71 08.21 | 105 39.97 | 540 | 31096 | 37/1262; 39/3266 | 18 Mar | 302-1 | not recovered | |
| Bellingshausen | 67 40.64 | 073 19.70 | 496 | 31097 | 37/1264; 39/3265 | 02 Apr | 333-1 | 21 Mar | 190 |

Recovery details (depths are as reported by multibeam center beam)

Getz Central - Depth at site = 780 m. ENABLE command sent, confirmation received first time. Ranging at 4 waypoints proceeded without difficulties. Position from triangulation determined to be within 100 m of recorded drop postion. Release command sent, confirmation received, but ranging indicated that mooring was not surfacing. Release command sent twice more (not – on the CART releases, the RELEASE command opens and closes the release cam, so one can rock the release cam by repeatedly sending the RELEASE command.). At 11 minutes after the first command had been sent, the bridge reported sighting the mooring at the surface. Note that at this first recovery, we did not make special efforts to position the ship starboard side to the mooring site.

Getz East – Depth at site = 904 m. ENABLE command sent, but no confirmation received. Repeated 3 times, no reply. No response to range pulses. Decided to send RELEASE command anyway, since previous mooring had surfaced very close to the drop location. Sent RELEASE command, received a confirmation. Sent ENABLE, received confirmation reply. Repeated ranging at 10 s intervals showed mooring rising until range reached 607 m, then range jumped to 1086 m, decreasing from there. At 11 minutes after the release command was sent, mooring spotted at surface approximately 500 m to port. We were expecting it to surface on the starboard side.

Dotson – Depth at site – 852 m ENABLE command sent and confirmation received normally. No triangulation done. Range at planned recovery site 857 and increasing due to 0.4 to 0.7 kt drift of ship. RELEASE command sent and confirmation received normally, but ranging indicated still at bottom. RELEASE command repeated 5 times after which ranging indicated ascent. Tracked by ranging on ascent until range= 602 m, approximately 18 minutes later.

Pine Island Bay – Depth at site 825 m. Site covered in new, gray ice, and surrounded by numerous bergy bits. ENABLE command sent, confirmation reply received first time, ranging proceeded without difficulty. RELEASE command sent 3 times before receiving confirmation. Ranging upon ascent gave normal results, with the mooring sighted on the surface 24 minutes after the confirmed release command was sent. Mooring just visible through translucent cover of new ice. Ice had to be broken with poles to recover mooring.

Outer Shelf – Depth at site = 544 m. Visibility poor, degrading to under 0.5 mile while on site. ENABLE command sent and confirmation received from a position approximately 400 m NW of deployment position. Subsequent ranging yielded normal results (horizontal range of first position was measured to be 626 m using the deck box horizontal range mode with a depth of 544 and sound speed of 1452 m/s). Obtained 3 good waypoints for triangulation. Set up for recovery about 200 m away from triangulated position. Send RELEASE command but received no reply. Repeated – no replies. Sent ENABLE command – no reply. Send DISABLE command, no reply, and unit still ranging. Moved to other points farther from site, repeatedly attempted to send commands (ENABLE, DISABLE, RELEASE) using portable deck unit nd dunking transducer deployed from bow, to no avail. Still ranging, so obtained 3 fixes in horizontal range mode to get triangulation using simple range circles. Results agreed well with first triangulation.

Decided to depart from site to return some days later to attempt a release or drag operation. The drag could not be carried out immediately because the stern A frame had not been rigged with the proper block for the 9/16" trawl wire. It was also hypothesized that the release may have locked up electronically, and that the normal 48 hour "jiggle" cycle might reset it. Messages were exchanged with ORE to explore this possibility. Greg MacEachern at ORE replied with the opinion that the trouble was due to multipath issues and suggested we try from farther away at lower power to minimize multipaths. Various scenarios for dragging were discussed, and preparations made for a lightweight dragging tackle comprising 12 home-made hooks embedded in braided 5/16" polypro line, weighted with chain, and towed from either the 5/16" wire on the starboard A frame, or the trawl wire over the stern A frame. A suitable block was rigged from the stern A frame in case conditions prevented towing over the starboard side. Returning to the area some days later (18 Mar) the site was found to be overtaken by ice and accessible only by breaking through some very difficult ice, certainly too heavy a cover to allow any sort of recovery effort. The mooring was left unrecovered, at the following triangulated position:

Latitude 71 deg 08.298' S Longitude 105 deg 39.960' W

Bellingshausen – Depth at site = 477 m. Conditions calm, no seas, ideal for recovery. No triangulation done. In order to test the ORE multipath hypothesis, the deck unit was set to low power. ENABLE command sent, no reply received. Power increase. Command repeated, power increased, until reply received at power setting normally used (3 ½ bars). RELEASE command sent, confirmation received, but ranging indicated that the mooring had not broken loose from the bottom. RELEASE command resent several times, and finally the ranging showed ascent. Mooring sighted from bridge, again on the port side when we had expected it to come up to starboard. Mooring recovered shortly thereafter.

Two releases showed considerable corrosion around the release lever arm and clevis, sn 31093 (Dotson) and 31097 (Bellingshausen). Both of these moorings required repeated sending of the RELEASE command to free them from the bottom. If this design is used in the future, more excess flotation should be used to ensure a positive release. The cause of the corrosion will have to be investigated further. One hypothesis is that the galvanized thimble used in the polypro line attaching the release to the anchor may have moved off the insulating bushing and come into contact with the stainless steel release lever and clevis. One can use plastic thimbles to eliminate this possibility.

**Figure 24** Corrosion on release lever and clevis of sn 31097 (left). An uncorroded release sn 31117 (right) shown for comparison.

NBP0702 SBE39 intercomparison

To facilitate preliminary comparisons of the moored temperature records, and to eliminate the possibility of outlier instruments, the five recovered SBE39 temperature-pressure recorders were placed in a plastic bucket and immersed in running seawater from the ship's uncontaminated seawater supply for approximately 14 hours. The recorders were arranged in a bundle held together with rubber bands. Seawater flowed into the bucket from a piece of tubing stuffed into the middle of the bundle. Sample rate was set to 5 minutes. The instrument clocks were not synchronized. The bucket was not insulated, and water was not circulated beyond what was induced by the flow emanating from the tubing. The table below summarizes the results. The differences among the sensors are likely to be within the uncertainty of the intercomparison. A careful post deployment calibration at Sea-Bird Electronics is planned.

| Instr sn | Mooring | Tmean $^{o}$C | stdev (n=160) |
|---|---|---|---|
| 3264 | Pine Island Bay | 2.0725 | 0.4251 |
| 3265 | Bellingshausen | 2.0518 | 0.4193 |
| 3267 | Getz East | 2.0489 | 0.4209 |
| 3268 | Dotson | 2.0613 | 0.4260 |
| 3269 | Getz Central | 2.0621 | 0.4254 |

### 6.3.2 Cape Adare

The first approximately 6 days of the cruise were allocated to the CALM program to recover one mooring near Cape Adare, occupy a short CTD section while the recovered mooring gear was serviced, and to deploy 2 new moorings in the vicinity. Of the 6 days allocated, it was anticipated that 2 days would be spent on site.

The mooring to be recovered had been deployed in 2004 during the second AnSlope cruise; instruments from that mooring were to be refurbished for use on the two new CALM moorings. Communications with the mooring were normal . The dual releases confirmed receipt of commands including the

commands to release the mooring, but ranging indicated that the mooring did not leave the bottom. Due to impending foul weather, it was decided to triangulate the mooring once more, then proceed to deploying one of the two planned new moorings, then return to the first mooring to attempt recovery by dragging for it. Triangulation was successful, and the second mooring was deployed without incident, but in increasingly bad weather. By the time the mooring had been deployed the sea state had deteriorated to the point that it was too acoustically noisy to range on the releases, and so there is no triangulated position for the new mooring. Conditions prevented further CTD work. A forecaster from called the vessel on the Iridium phone to warn of the approach of a strong storm, and suggested the ship leave the area to seek shelter. Having reached the end of the allocated 2 day on site period, we departed the area ahead of the storm, leaving the unrecovered mooring to a later dragging attempt scheduled for cruise NBP0801. The new mooring is shown schematically in Figure 25. The unrecovered mooring sits at 71° 27.5865'S 172° 18.0035'E.

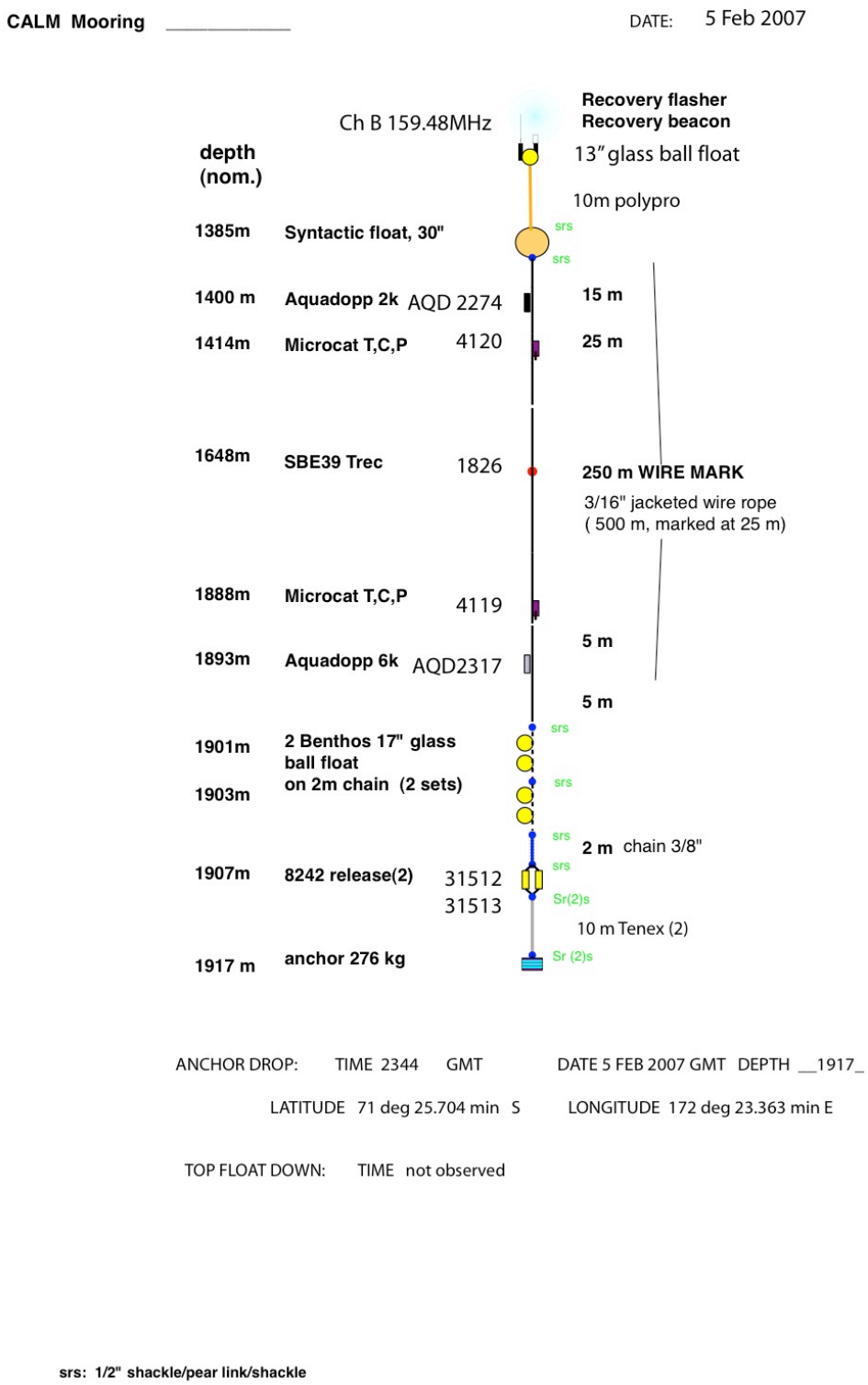


Figure 25 CALM Cape Adare Mooring

## 6.4 Seafloor Mapping

(Frank Nitsche, Kathleen Gavahan, Rose Vail)

### 6.4.1 Introduction

A large portion of the bathymetry of the continental margin around Antarctica is still unmapped, especially around the Amundsen Sea. Scientific questions concerning warm water entering the shelf and collecting in deep troughs on the inner shelf depend on the local and regional bathymetry. Therefore, we have been running the swath-mapping system throughout the whole cruise. The main mapping team consisted of Kathleen Gavahan (Raytheon), Rose Vail (Colorado College), and Frank Nitsche (LDEO) and was supported by several others who helped edit ping files.

### 6.4.2 System Description and Operation

The main system used on this cruise for seafloor mapping is the Simrad EM-120 swath-mapping system. The system operates at a 12 kHz main frequency and receives up to 191 beams from angles up to 65° to each side of the ship, providing a resolution of ~1.5° of the seafloor and a coverage of ~4 times the water depth. To adjust for changes in the sound velocity, CTD and XBT data are used to update to the local conditions throughout the cruise.

The raw data are recorded digitally and displayed in real-time. Once a day the raw data are processed and edited manually for outliers and false bottom returns of the swath data. The final data are stored in MBsystem format 57 and will be archived at the Antarctic Multibeam Synthesis Database (http://www.marine-geo.org/antarctic/).

In addition to the swath-mapping system we almost continuously ran a sub-bottom profiler to provide independent depth measurements and sub-bottom data used to determine sediment sample locations. In the beginning a Knudsen 320B echosounder with 3.5 kHz main operating frequencies was used. Starting on the transect south from Cape Adare in the Ross Sea (8. Feb. 2007) we used the Ocean Data Equipment Corporation Bathy 2000 echosounder and sub-bottom profiler. The Bathy 2000 transmits a chirp signal of 3.5 to 4 kHz. It determines the bottom and records the topmost few meters around the bottom detect. The data were archived digitally in the Bathy2000 variant of the SEGY-format.

### 6.4.3 System Performance and Problems

Throughout the cruise both systems, the EM-120 swath-bathymetry and the Bathy2000 echosounder, were working without major problems. They operated normally under most conditions, but both had problems with receiving good data in sea ice. The Bathy2000 was only disturbed by heavy pack ice but the EM-120 multibeam had problems with heavy pack ice and certain types of newly formed ice such as grease ice and nilas. The ice gets under the ship, blocking signals coming to and from the transducers, producing bad data even in easy and calm conditions.

The SeaSurveyAdvanced display software, which allows real-time display of new and pre-existing multibeam data, was an essential tool for route and station planning as well as for ship navigation. The additional helmsman display on the bridge allows the mates to steer a course designed to ensure maximum coverage by not duplicating pre-existing data from the NBP, BAS, and AWI. Occasionally there were problems with this software and/or the computer it runs on. The IT personnel minimized the interruptions by switching a hard drive. Due to the age of the system and the software itself, an upgrade or replacement in the near future is highly recommended.

### 6.4.4 Results: Swath-Bathymetry

During this cruise we collected and processed ~13,400km of multi-beam swathdata (880,000 pings, 168,000,000 beams (soundings) representing ~12 GigaBytes of data.

Most of the newly acquired bathymetry data cover previously uncharted areas, adding significantly to our understanding of the regional bathymetry. Highlights include the more accurate definition of the shelf break between 135°W and 119°W, the discovery of new small troughs in front of the Nickerson Ice Shelf (Fig. x-1), and an unusual bedrock ridge attached to the shelf break north of Siple Island (Fig. x-3).

### 6.4.5 Troughs in front of the Nickerson Ice Shelf

During this cruise we discovered two troughs just in front of the Nickerson Ice Shelf, an ice shelf located between the Ross and Amundsen Seas. These troughs are quite different from those mapped in the Ross or Amundsen Sea. The first trough (Figure 26a) was exceptionally steep (a range of depth from 160 to 1088 m) and narrow (a width of approximately 60 km). Parallel striations indicate a glacial origin and direction for a paleo ice-stream, The overall rough seafloor suggests that the trough was eroded into crystalline bedrock.

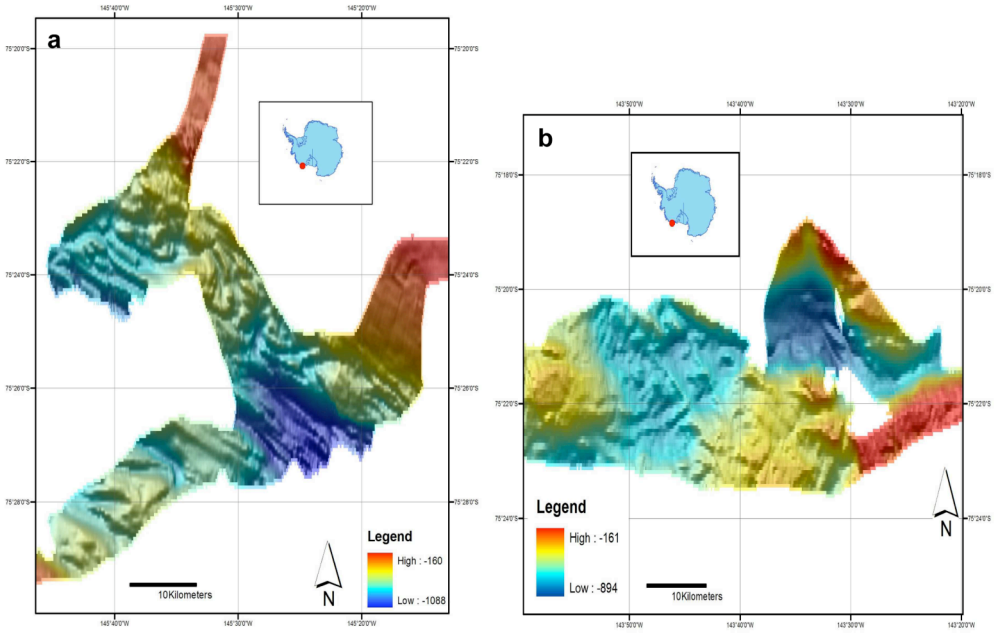


**Figure 26 Newly discovered troughs in front of the Nickerson Ice Shelf**

Just about two degrees east of the first Nickerson trough was another, smaller trough (Figure 26b). This trough differs from others through its lack of glacial morphological features, its concentrated depth and steepness, and its geometry. The meandering path indicates that melt water flow may have played a significant role in its formation rather then just glacial erosion.

### 6.4.6 Improved shelf break definition in the western Amundsen Sea

This cruise included a transect along the entire shelf break of the Amundsen Sea. As a result, we collected multibeam data for most of the shelf break, although difficult ice conditions limited the data quality in some section of the shelf break. However, we gathered enough good data to define the shelf break in the western Amundsen Sea (135°W – 120°W) where the shelf break had previously been located on only a

few crossings. Figure 27 shows the newly defined shelf break of this area. While we added to existing data as much as possible, more work is need, particularly in the far eastern Amundsen Sea.

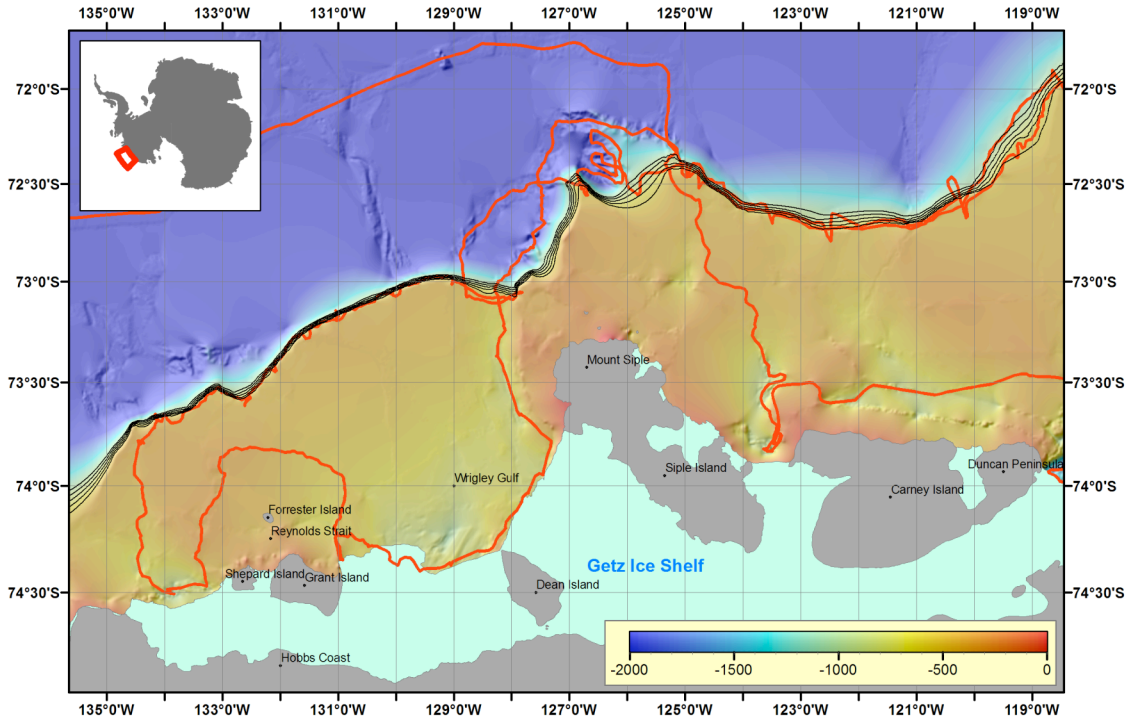


Figure 27 Bathymetry of the western Amundsen Sea with NBP0702 track line (red) and the shelf break indicated by the thin black contours representing 600 m, 700 m, 800 m, 900 m, and 1000 m seaward of the shelf break.

### 6.4.7 Ridge north of Siple Island

One of the surprises during NBP07-02 was the discovery of an odd-shaped ridge attached to the shelf break north of Siple Island. Instead of the normal slope a triangular feature extends more than 30 km from the continental shelf Figure 28). The flanks of the ridge are incised by steep canyons, over 2000 m deep.

Shiptime was devoted to map the outline of this feature, but dense ice cover limited our ability to map its extent to the southwest, and a possible smaller ridge and the shelf break in that region. The origin and age of this feature is unclear, but it is located north of the Mount Siple volcano and south of the Marie Byrd Seamounts. Hence a tectonic origin seems likely, since it seems too deep to be of glacial origin or shaped by ice the from the shelf.

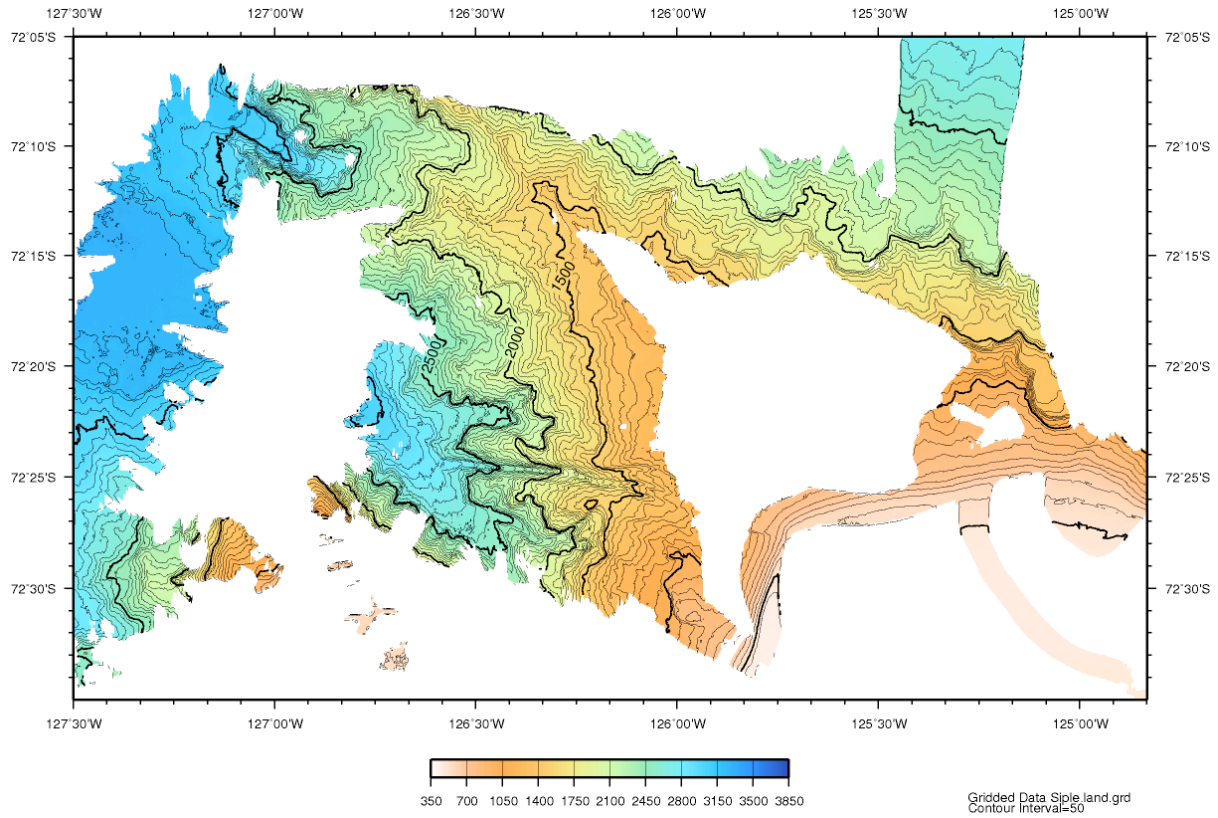


Figure 28 : Multibeam data with contours showing the newly mapped ridge northwest of the continental shelf break near Siple Island (~120°W).

### 6.4.8 Glacial morphologic features

The detailed bathymetry data also show many different types of sub-marine glacial morphologic features such as glacial lineations (Figure 26a-Nickerson), drumlin shaped bedrock features, drumlins, iceberg scour marks (Figure 29), and gullies on the upper slope. The lineations were usually observed in the area of troughs on the inner and mid shelf, whereas iceberg scour were usually observed in the shallower areas and on the outer shelf.

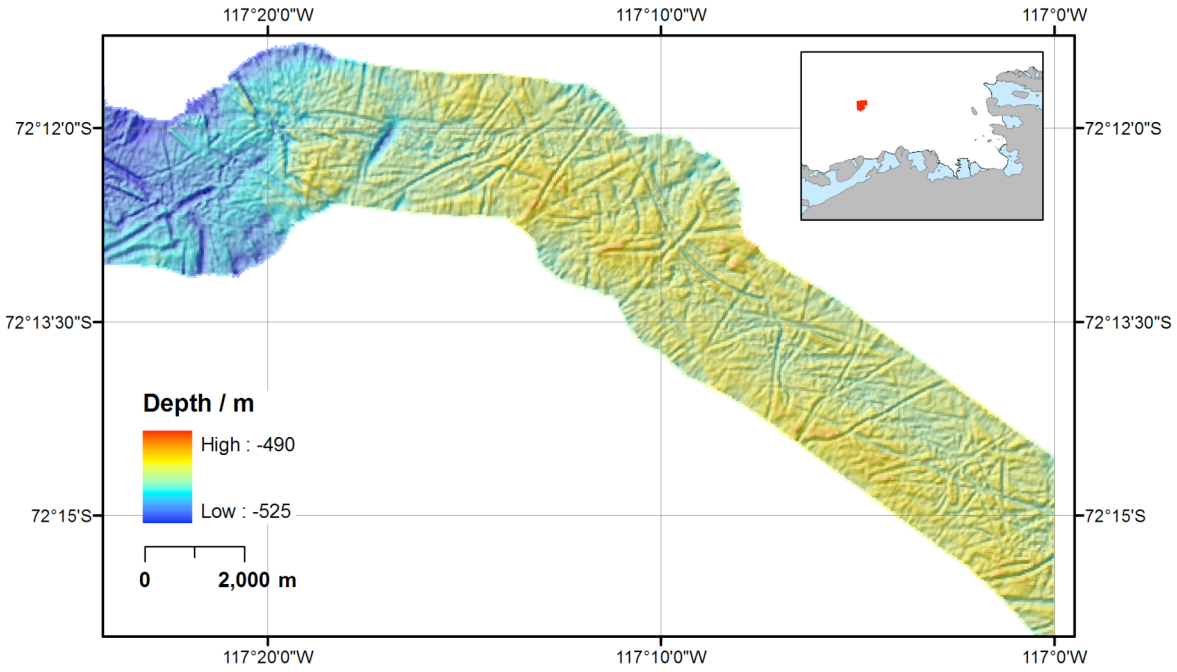


Figure 29 Apparent iceberg scours near the shelf break north of the Carney Island. Similar iceberg scours or furrows have been commonly mapped along near the shelf break and other shallow parts of the shelf.

### 6.4.9 Results: Sub-Bottom Profiling

During the cruise the Bathy2000 sub-bottom data were mostly used as guidance for sediment sampling and as an additional source for bathymetric depth information. We did not perform a systematic analysis of the sub-bottom data during the cruise, but they are digitally available and will aid the interpretation of morphological features identified in the swath-bathymetry mapping.

Typical features include sediment deposits in some troughs, usually thin (<10 m), but sometimes as e.g. in Pine Island Bay up to 20 m (Figure 30). Shallow areas, especially near the shelf edge are dominated by iceberg scours (Figure 31), and occasionally refilled by sediment.

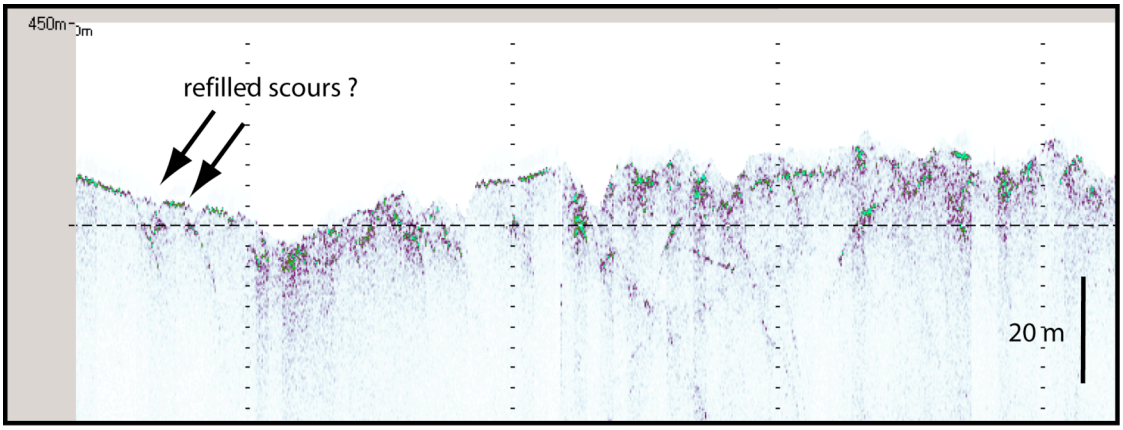


Figure 30 Icebergs scours near the shelf break of the Amundsen Sea. (W->E).

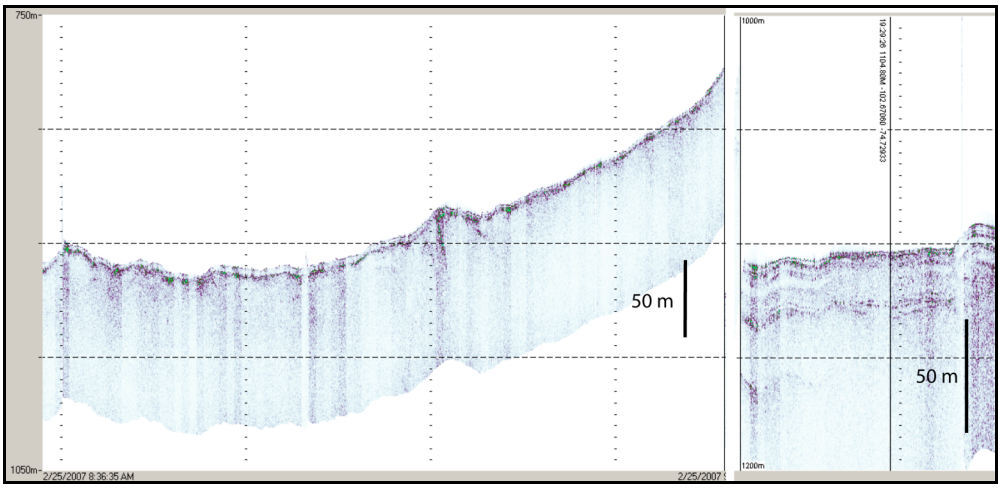


Figure 31 Examples of the sub-bottom data across troughs in Pine Island Bay that show a medium (5-10 m) and a thicker (~20 m) sediment cover.

## 6.5 Ice observations

Karl Newyear

### 6.5.1 Introduction

Throughout cruise NBP07-02 a team of 14 volunteers made 644 observations of local sea ice conditions over a period of 827 hours encompassing more than 7700 km of trackline. The protocol used was devised by the ASPeCt (Antarctic Sea Ice Processes and Climate) working group of the Scientific Committee of Antarctic Research (SCAR). This data set was supplemented by estimates of the number of icebergs. The data were recorded manually and transcribed into electronic format for inclusion in the cruise data set. The observations are necessarily subjective and reflections of each person's individual biases are inevitable but when taken as a whole the data set reveals some statistically valid trends.

### 6.5.2 Methods

Once per hour an observer made qualitative observations of sea ice, weather, and iceberg conditions from the bridge of the RVIB NATHANIEL B. PALMER (NBP) and recorded them manually on a log sheet. Observed variables included: location, time, ice areal coverage, type, thickness, floe size, topography, and snow cover for up to three ice types, character of open water, local numerical density of icebergs, sea surface temperature, air temperature, wind speed and direction, areal cloud coverage, visibility, and weather code. The weather codes were borrowed from NOAA's meteorological observation protocol and were intended to identify qualitative trends in local conditions such as type and rate of precipitation or fog formation. Observations extended to a radius of 1 km from the ship for sea ice and 6 nautical miles for icebergs. Observations were not made when the ship was stationary for CTD casts, Smith-MacIntyre sediment grabs, or other reasons.

Sea ice characterization is necessarily a subjective classification system. Two training sessions were held prior to the beginning of observations to introduce novices to the various types of sea ice and an on-line tutorial produced by ASPeCt was made available via the ship's computer network. In addition, experienced observers assisted as necessary until all volunteers became more comfortable in classifying

the ice. Thickness and floe size estimations were aided by hanging a "Norwegian buoy" boat bumper of approximately 0.5 meter diameter over the ship's starboard railing near waterline as a visual reference. Other reference scales included the 18-meter beam and 98-meter length of the vessel itself.

Ship's location, sea surface temperature, air temperature, and wind speed and direction were taken from the vessel's data acquisition system (DAS) which displays various "channels" of information via the NBP's closed-circuit TV system available throughout the ship. These quantitative variables were continuously recorded throughout the cruise and distributed in JGOFS format as part of the end-of-cruise data set. Their inclusion in the sea ice observations was merely for completeness of the ASPeCt protocol – all data is included elsewhere at higher temporal resolution.

Iceberg numerical density was estimated visually and verified or supplemented by a count using a repeater display running from the bridge navigation radar. This display was set for a radius of 6 miles from the ship which helped determine visual range because it was often difficult to tell if a particular iceberg near the horizon was within 6 miles or not. This range was chosen somewhat arbitrarily and did not ensure independent samples. That is, any given iceberg might have been counted in successive observations, depending on how far the ship had traveled in the meantime. The radar could not easily distinguish between bergs, bergy bits, growlers, and ground clutter but was unaffected by darkness.

### 6.5.3 Software/Transcription

The observation log sheets were transcribed into the ASPeCt-prescribed database, provided as part of the software package. This format is similar to a simple spreadsheet but with a more user-friendly appearance, internal consistency checking, and the ability to calculate some rudimentary statistics. The process of transcribing data allowed for editorial oversight and error-correction. However, like hanging chad from the 2000 presidential election, in some cases this required an educated guess as to what the observer intended to record. Difficulties encountered in this process are detailed below.

### 6.5.4 Limitations

Determining the characteristics of sea ice is necessarily subjective and prone to the biases of each observer, ship tracks skewing toward open water rather than heavy ice, difficulty of winter access to many regions, and darkness/visibility limitations. Part of the intent of the ASPeCt protocol is to compile a broad, statistically significant database to average out the data scatter. The Amundsen Sea is relatively infrequently visited compared to the Ross Sea or Western Antarctic Peninsula areas and there are no permanent terrestrial stations along this section of the coast to encourage frequent vessel traffic. Therefore the observations made during this cruise are especially important in filling in a data-sparse section of the Southern Ocean. However, they do not carry the same statistical weight of the cumulative observations made elsewhere such as the Australian Antarctic sector.

A well-recognized but inherent limitation of ice observations from surface vessels is that, when given a choice, regions of heavy pack ice are avoided. This sometimes requires rather large detours as illustrated in Figure 32 and skews the observations toward lower ice concentration.

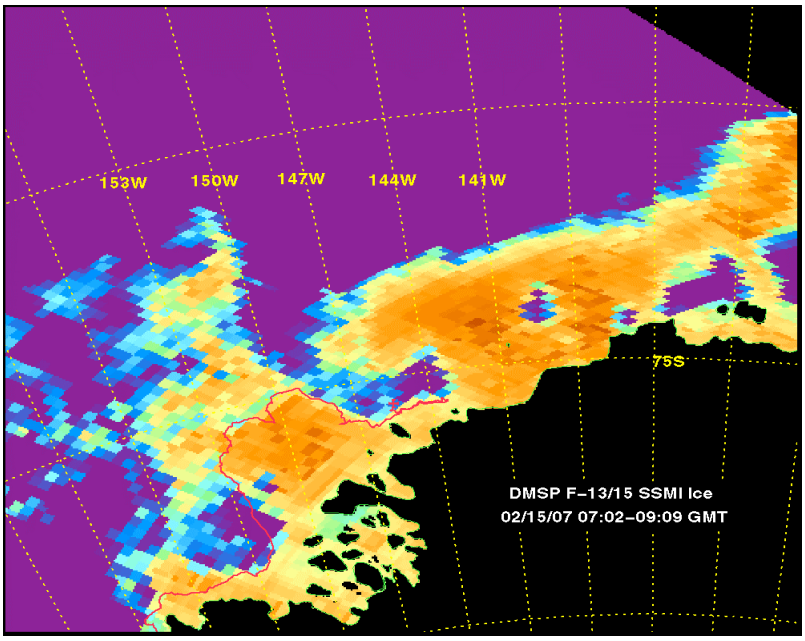


**Figure 32** Ship track (red line) and ice concentration from SSM/I sensor on DMPS/F-13 satellite.

During the height of summer high latitudes enjoy 24 hours of daylight, making ice and weather observations relatively easy. During the later part of the season, when cruise NBP07-02 occurred, we experienced several hours of nighttime darkness each day and observers sometimes noted in their comments the difficulties posed by darkness. The observable radius for sea ice was reduced from the 1 km prescribed by the ASPeCt protocol to the local area illuminated by the ship's exterior lighting which was only a few tens of meters. Iceberg observations were similarly hampered at night, and the locally lit area was a smaller percentage of the berg observation radius (6 miles) than the sea ice radius (1 km), but to some degree radar could be used to identify bergs even when darkness precluded direct observation.

This cruise did not assign specific individuals the primary task of making ice observations. Therefore, we relied upon a team of volunteers, most of whom made only 1 or 2 observations each day. This leads to some level of inconsistency in estimations of coverage and determination of ice types. Even experienced observers may disagree on the finer points of classifying sea ice; this issue is exacerbated by utilizing a team of relatively inexperienced personnel. With a larger statistical database, this issue could be minimized.

While transcribing data from handwritten log sheets into the database it was sometimes noted that observers recorded internally inconsistent data. For example, an ice classification of "first year sea ice (0.7-1.2 m thick)" might be followed with a thickness estimate of 150 cm. This required interpretation by the editor based on the previous or following entries on the log sheet or their own casual observation. Such problems could be alleviated through additional or refresher training after observers have become more familiar with the protocol.

The ASPeCt software performs some internal checks before allowing the data to be saved. This step helped prevent internally inconsistent entries as noted above, but also introduced its own biases by limiting the parameter values based on what the software authors decided were "realistic" values. This was most apparent during the present cruise for the variables of snow pack depth and brash thickness. We nearly uniformly observed heavy, thick snow cover on the sea ice which was "out of bounds" for the software. This required a downward estimate of total snow volume for the software to accept the entry. While it could be argued that the observers were consistently overestimating snow cover, the fact that

data entries by all observers were biased in the same direction suggests otherwise. Similarly, brash ice thickness was limited at the upper end by the software at 50 cm, and no snow cover was permitted on this ice type, both of which were likely inaccurate assessments for much of the observation period and locations. However, after data transcription was completed for this cruise it was discovered that the software's data validation checks could be turned off. Therefore this "flaw" is not as significant as originally thought and a final data analysis should include editing of the transcribed data to match the handwritten log sheets.

### 6.5.5 Results

At a first approximation, the ice type distribution in the Amundsen Sea during late summer was bimodal between thick first year floes (>100 cm) and brash/open water. Consistent with satellite imagery (Figure 33) we observed that the western portion of the study area was covered with close pack containing some small polynyas, the central Amundsen was largely ice-free, and the eastern portion was a mix of very thick ice in the north and lower ice concentration in the south. Icebergs were plentiful throughout the region but not evenly distributed and consisted of a mix of small irregularly shaped bergs and large tabulars. Observations ranged from zero within sight to literally hundreds. Some of the larger icebergs may be grounded, especially in the vicinity of Pine Island Bay, and might be locally important in modifying the water column thermohaline structure. On one memorable day we encountered a field of innumerable small (city-block sized) bergs near 71º10'S 109º05'W including some with stripes or inclusions of "green" ice. This assemblage of icebergs appeared to be relatively uniformly distributed to the horizon in all directions and there was little to no sea ice present.

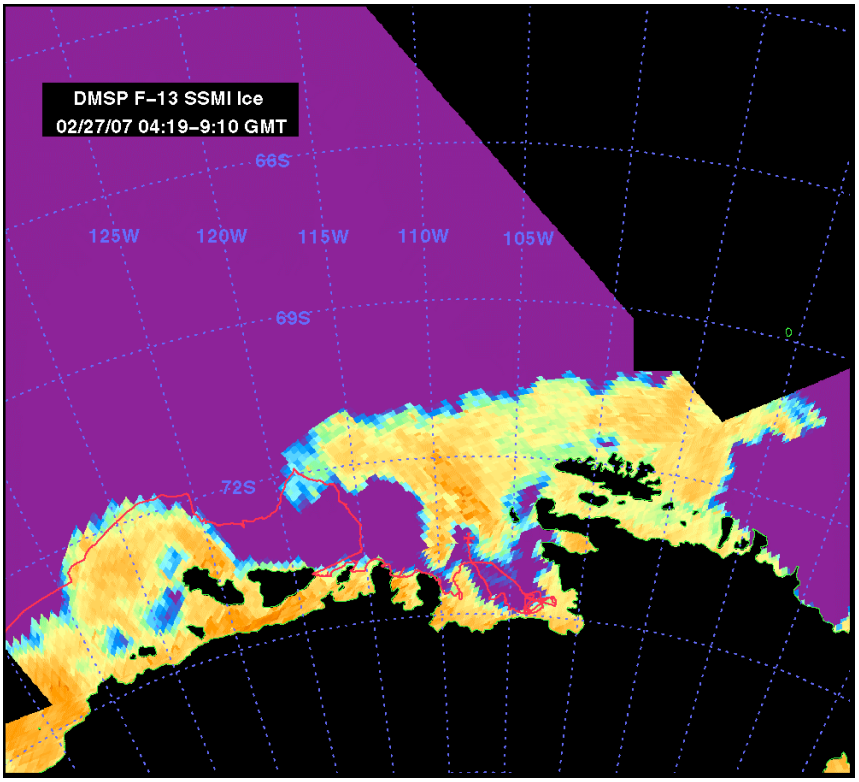

Figure 33 SSM/I image of general Amundsen Sea ice distribution near the mid-point of cruise NBP07-02

In association with thick and therefore relatively old ice we observed very deep snow cover on the floes as shown in Figure 34. In many (most?) cases the amount of snow was sufficient to submerge the upper surface of the sea ice which leads to a slush layer at the snow-ice interface. This effect is visually highlighted by the frequent occurrence of a distinctive algae layer at the waterline and upper surface of floes. With cold atmospheric conditions during the winter causing the slush to freeze, and additional snowfall, it's reasonable to expect that ice floes will grow from above.

The ice topography (i.e. degree of ridging and rafting) was not as pronounced as the ice thickness would suggest. Under realistic atmospheric forcing the maximum amount of undeformed sea ice thickness that can form in one year is approximately 150 cm, while we observed significant amounts of nearly level ice thicker than this value. This may be due to the high snowfall which, when blown by the wind, smooths over ridges and fills in low spots. This effect is amplified by isostatic depression of the ice near ridges where drifts preferentially form. We had no way of observing the underside of the ice to see if the keel depth/spatial frequency distribution was similar to that of ridges.

Figure 34 Typical ice floes in Amundsen Sea with thick snow cover causing submergence of upper surface and leading to layer of snow ice. Photo credit: Raul Guererro.

While mass appears to be added at the upper surface of the ice, we often saw that the submerged portions of floes were quite honeycombed and rotten. The recorded surface water temperature was somewhat variable and was sometimes several tenths of a degree above the freezing point even when ice was locally present. This meant that ice was likely melting from below for much of the late-summer observation period and even thick floes did not possess much mechanical integrity. Operationally, large floes were often not a significant navigational consideration for an icebreaker (with notable regional exceptions such as near Siple Island and Cape Flying Fish) but snow cover was occasionally problematic in "softening" the impact of the bow into ice floes.

The boundaries between pack ice and open water were quite distinct; there was a notable lack of any marginal ice zone characterized by large fields of shuga and pancake ice. Instead, brash ice was very prevalent not only near the ice edge but throughout the entire Amundsen Sea. This might be due to the

ice pack being worked by storms, or given the relatively benign weather conditions experienced during this cruise, the effect of differential iceberg movement relative to the pack ice. The latter is generally wind-driven while the former is responsive to deeper ocean currents and tides.

Despite the usefulness of remote sensing imagery, especially SSM/I microwave products, there were occasions in which we directly observed conditions that were significantly different from what they indicated. For example, Figure 35 shows that the ship traversed an area of apparently open water in the southeast Amundsen Sea on 23-25 February. However, the observation logs show at least 1-2 tenths of ice coverage throughout this period. A possible explanation is that the upper surface of the ice is flooded by seawater due to the heavy snowcover, and that the snowpack is invisible at the microwave band so that the satellite "sees" the saturated snow layer instead of the ice below.

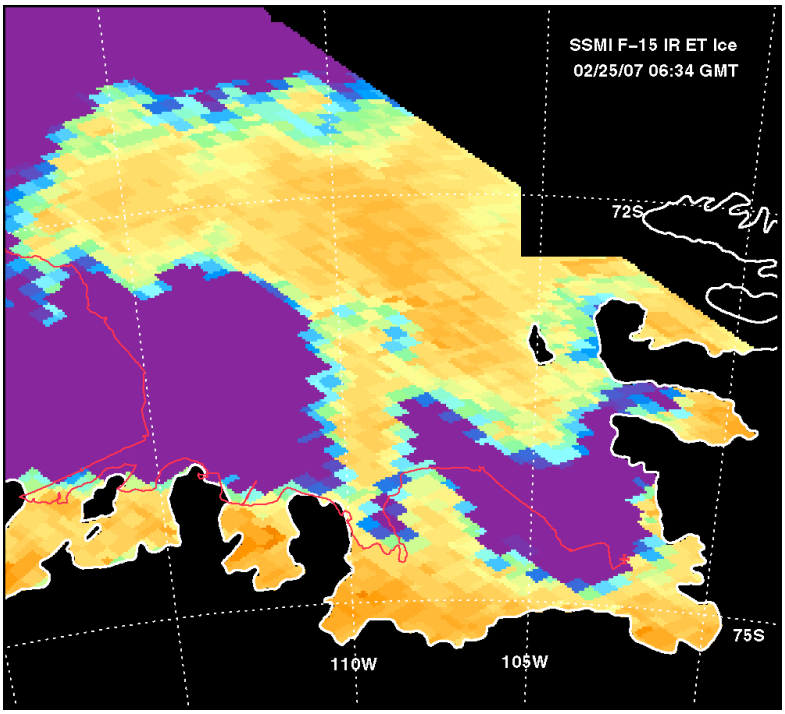


**Figure 35** SSM/I image suggesting open water in the southeast Amundsen Sea.

Conversely, we also experienced at least one case in which remote sensing imagery depicted the presence of ice where we saw none, as shown in Figure 36.

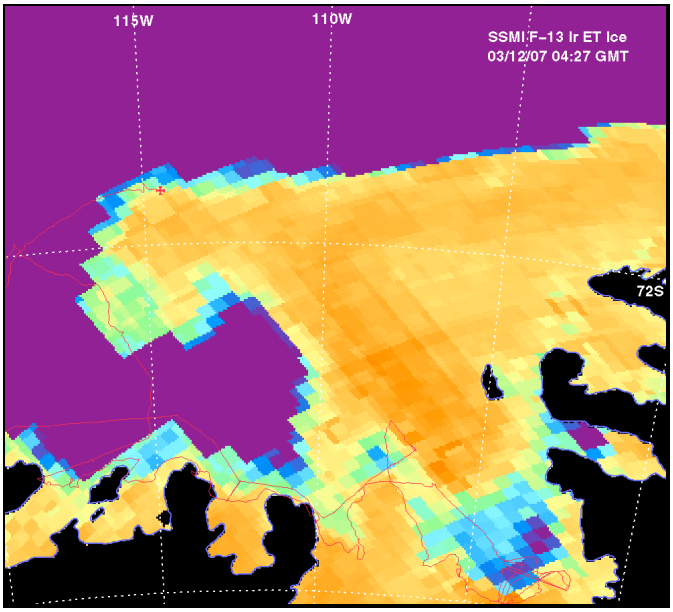


**Figure 36** Apparent ice cover in the eastern Amundsen Sea. Ship's track on 11-12 March suggests significant ice coverage while direct observations indicate zero ice presence.

One unsolved question is, given the large amount of thick first year ice observed at the end of the summer melt season, why isn't there more multi-year ice present from previous years? Perhaps the deployment of two ice-tracking buoys during this cruise will tell us how quickly individual floes are advected into locations where large-scale melting occurs and suggest a residence time for ice in the Amundsen Sea.

### 6.5.6 Conclusions

Sea ice observations, while not a primary goal for this cruise, are a valuable addition to the data set and help to set the oceanographic observations into context and even help explain the convoluted ship track which may not be captured in any other way. The addition of an iceberg count, not formally part of the ASPeCt protocol, helps to characterize the environment we were working in throughout NBP07-02. The Amundsen Sea ice pack is characterized by a bimodal distribution of types with the near-absence of a conventional marginal ice zone. We consistently observed a high percentage of thick first year (>100 cm thick) floes interspersed with brash ice and a thick snow cover throughout the study area. The Amundsen Sea is populated by many small icebergs, and several large-scale coastal or open-ocean polynyas where ice is absent or present in only small amounts. Even at the end of the summer melt season we observed a regionally dense ice cover but toward the end of the cruise began to see new ice forms such as cemented pancakes, nilas, and occasional frost flowers.

Notes

The ice observations recorded during cruise NBP07-02 and transcribed into electronic format will be submitted to the ASPeCt data office at the Antarctic Cooperative Research Centre, University of Tasmania. For further information on the observation program please contact:

Dr. Anthony Worby

Antarctic Cooperative Research Centre

University of Tasmania

PO Box 252-7001

Hobart, Tasmania, 7001

Australia

a.worby@utas.edu.au

fax: +61-3-6226-7650

http://antcrc.utas.edu/aspect

Acknowledgements

Many thanks to the dedicated ice observers from this cruise including: George Aukon, Jennifer Ayers, Jesse Christensen, Ali Criscitiello, Richard Cullather, Kathleen Gavahan, Lily Glass, Katie Leonard, Amy Leventer, Stephanie McClellan, Rachael Mueller, Bettina Sohst, Rose Vail, Greg Watson, and Karl Newyear.

Raul Guererro took the photo used as Figure 3 and has granted permission for its use in this report.

The RPSC Electronics Technicians, consisting of Victor Shen, George Aukon, and Greg Watson operated the ship's TeraScan system and produced many images such as the ones used as figures 1, 2, 4, and 5 in this report. Credit for specific images in unknown, so thanks is due to the entire group.

Thanks also to Tony Worby of the Australian Antarctic Division and the ASPeCt working group of SCAR for devising the sea ice observation protocol and freely distributing it for use on ships operating throughout the Antarctic.

References

Worby, A. and I. Allison (1999), A Technique for Making Ship-board Observations of Antarctic Sea Ice Thickness and Characteristics, *ASPeCt Report 14*, Cooperative Research Centre for Antarctica and the Southern Ocean, Hobart, Tasmania, Australia

## 6.6 Meteorology

R. Cullather

Figure 37 Mackerel sky near Wright Island, 20 February 2007. ( photo by R Cullather)

### 6.6.1 Instruments

Air temperature, relative humidity, atmospheric pressure, true wind direction and speed, and the downwelling shortwave and longwave radiative fluxes are measured with various onboard instruments and have been recorded at one minute intervals of the NBP0702 cruise under the JGOFS archival system, along with specific navigational and oceanographic variables. The acronym JGOFS stands for Joint Global Ocean Flux Study, a biology project for whose data reporting method has endured. Navigational variables within the archive are instantaneous, while the meteorological sensor readings are averaged over the one minute interval. The Palmer's combination temperature and humidity sensor is an RM Young Model 41372LC with an accuracy of ±0.3°C and ±3.0% and is located behind the pilot house at 15.0m above the waterline. Atmospheric pressure is measured with an RM Young Model 6102 electronic barometer with an accuracy of 0.5hPa, and is located on the ship's mast at 30.0m above the waterline. Two RM Young anemometers, model 05106, are also located on the ship's mast 30.5m above the waterline and have an accuracy of ±0.3 m $s^{-1}$ and ±3 degrees in direction. The maximum wind speed of

the port and starboard anemometers is used in the JGOF data stream. Downward radiative fluxes are measured by an Eppley Precision IR Radiometer/Purgeometer (PIR) and an Eppley Precision Spectral Pyranometer (PSP), which are also located on the ship's mast. The PIR measures terrestrial wavelengths between 4 and 50μm with a voltage /flux relation that is linear to 1.0 percent, while the PSP measures the solar flux between 0.3 and 3μm with a voltage/flux relation that is linear to 0.5 percent. The ship's C.O. maintains a separate set of instruments, including a pilot house hygrometer and a third anemometer that is centrally located on the mast. Observations from these instruments are not recorded by the JGOF system. Katherine Leonard maintained a snow particle counter during NBP0702 that was located on the ice tower above the pilot house, and is described in more detail elsewhere. It is important to recognize that the particle counter does not distinguish between snow that is falling out of the sky and blowing snow that has been initially deposited and then recaptured by the wind from a nearby ice or land surface. Apart from these direct observations, several remote sensing products were available, including DMSP microwave sea ice cover, visible and infrared imagery from NOAA polar orbiters, and a high latitude synoptic analysis of sea level pressure from the University of Wisconsin at Madison (**Figure 38**). Less frequently, high resolution MODIS visible imagery and AMSR-E sea ice cover plots were also available.

The 2006/07 Antarctic field season occurred during a mild negative or "warm" phase of the Southern Oscillation, an interannual atmospheric phenomenon that is typically initiated in the tropical Pacific by El Niño. In the middle and high latitudes, the Southern Oscillation is characterized by a wave-train of alternating pressure anomalies that stretch from the western Pacific down to the Antarctic Peninsula region and beyond. Anomalous high pressure and blocking in the far South Pacific are associated with the Southern Oscillation. The Antarctic Oscillation (AAO), another climate index, is a measure of the meridional pressure gradient between southern middle and high latitudes. In recent years, the November-December-January AAO index has behaved in a manner similar to that of the Southern Oscillation.

### 6.6.2 Notable Synoptic Events

The NBP0702 cruise was characterized by long periods of stable weather with some cyclonic activity. The barometer remained above 990hPa for about a third of the cruise ( **Figure 39**). The first storm occurred during mooring recovery and deployment efforts off of Cape Adare in the western Ross Sea on 4-6 February. At 00:00 4-Feb GMT, the Wisconsin synoptic analysis indicated a 972hPa low pressure exiting on the eastern side of the Ross Ice Shelf, with a second 968hPa low located just north of Dumont d'Urville. Over the next two days this second storm filled slightly to 972hPa and tracked slowly eastward. The slow movement of this storm allowed for it to afflict the northwestern Ross Sea over an extended period of time. From 12:00GMT on the 5th until 01:00GMT on the 6th, the weather glass dropped 9hPa down to 976hPa, with hourly wind speeds of up to 26 m $s^{-1}$. On the 6th, the Palmer retreated south while the system began to accelerate eastward, eventually reaching Marguerite Bay on 11-Feb.

As the Palmer was reaching the end of the Ross Ice Shelf transect on 12-Feb, another system moved down from the southern Tasman Sea to stall and dissipate along the Saunders Coast. This lowered the pressure reading from 993hPa on 9-Feb to 969hPa on 11-Feb. Air temperatures dropped to –15°C on the 9th but warmed as the ship advanced beyond the location of cyclolysis.

After a brief transit and stations along the Amundsen Sea shelf break, the Palmer turned towards higher latitudes on 19-Feb. This coincided with an intense storm moving to the southeast and parking in Pine Island Bay. The prior trajectory of this storm is not clearly defined in the Wisconsin analysis. Winds greater than 20m $s^{-1}$ from the southeast were briefly encountered on 20-Feb, and the barometer continued to march down to less than 965 hPa on 22-Feb before recovering.

After an extended period of relatively calm weather in the Amundsen, a large cyclone moved westward over the central Southern Ocean to about 90°W on 16-Mar. At this point the analysis suggests a retrograde motion to the SSW into the Bellingshausen and eastern Amundsen Sea, with a central pressure of 948hPa in the analysis of 18-Mar. This was an expansive storm which affected conditions from Alexander I Island to the Amundsen Sea. While high wind speeds were not observed onboard in the heavy ice pack, the introduction of southerlies on the western side of the storm dropped the mercury to a cruise-record low of –24°C on 17-Mar. The observed minimum pressure onboard was 951hPa on 18-Mar.

There is the sense that four synoptic storms over the period of the cruise is a relatively small number for this location, which would be consistent with typical blocking conditions of the Southern Oscillation. In general, the high pressure located to the west of Patagonia remained in place for most of the cruise with few exceptions, the most notable associated with the advance of the cyclone that was encountered on 17-Mar and 18-Mar. Depending on the location and the orientation of this blocking high, a low pressure trough was preferentially located in the eastern Bellingshausen Sea and extending to the Peninsula, while a high pressure ridge was located in the central Amundsen Sea.

### 6.6.3 The Diurnal Cycle

Over the course of the cruise, the solar transit time decreased from 24 hours at the beginning of the cruise to about 13 near the end. As a result, the average daily downward solar flux trended downward from about 82W $m^{-2}$ to 46 W $m^{-2}$, however the variability that is associated with cloudiness dominated the time series. Figure 40 shows the diurnal cycle for selected days. As may be seen, some of the larger values occurred later in the cruise, in fair weather. Shown in **Figure 39**, the air temperature responds more directly to synoptic conditions, while the diurnal cycle is not readily apparent. This is consistent with the low sun angle in high latitudes and in maritime conditions. A perception that was made during the cruise was that it persistently snowed after sundown, particularly out near the shelf break. This notion is more commonly referred to as the Higdon Hypothesis. A preliminary analysis indicates that this perception was not represented by the particle counter (Figure 41). It would be interesting to compare the particle counter values with the weather conditions recorded in the sea ice observations log. The spatial distribution of the particle counter values is shown in Figure 42.

### 6.6.4 Wind Features

A few characteristics of the wind field are highlighted. At close proximity to the Ross Ice Shelf, the prevailing wind direction is from the south and is associated with katabatic drainage farther inland. On the eastern edge of the shelf, wind drainage from Marie Byrd Land adds an easterly component. This basic wind field may be modulated by the presence of geographic features, such as is shown for Roosevelt Island in Figure 43. In general, the air flow off the ice shelf combines with the easterlies from Marie Byrd Land and channels around the island in a manner such that the effects of the island are felt much farther to the west of the island's location. A preliminary analysis was also conducted of the wind field between the Ross Ice Shelf and a nascent iceberg. While the wind direction remained from the south near the mouth of the opening, the wind field became easterly at the end of the chasm, suggesting the presence of a barrier wind field. Finally, the wind field associated with the CTD "yo-yo" experiment is shown in Figure 44. It may be seen that the wind field varied by only a small amount during the course of the experiment, suggesting that the oscillating trajectory results from oceanographic and/or iceberg processes.

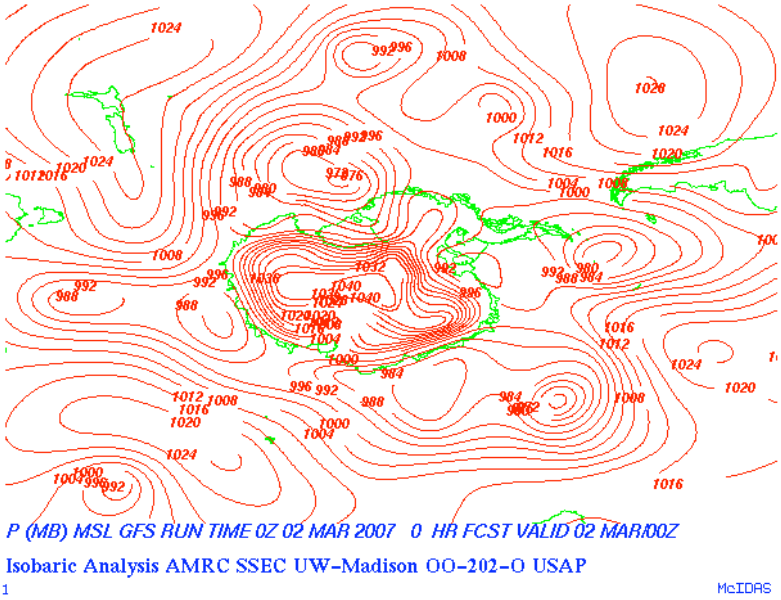


Figure 38 Synoptic analysis from University of Wisconsin at Madison. This analysis shows the characteristic 1026hPa high pressure to the west of Patagonia, a ridge along the Amundsen coast, and cyclones over the eastern Ross Sea and Peninsula.

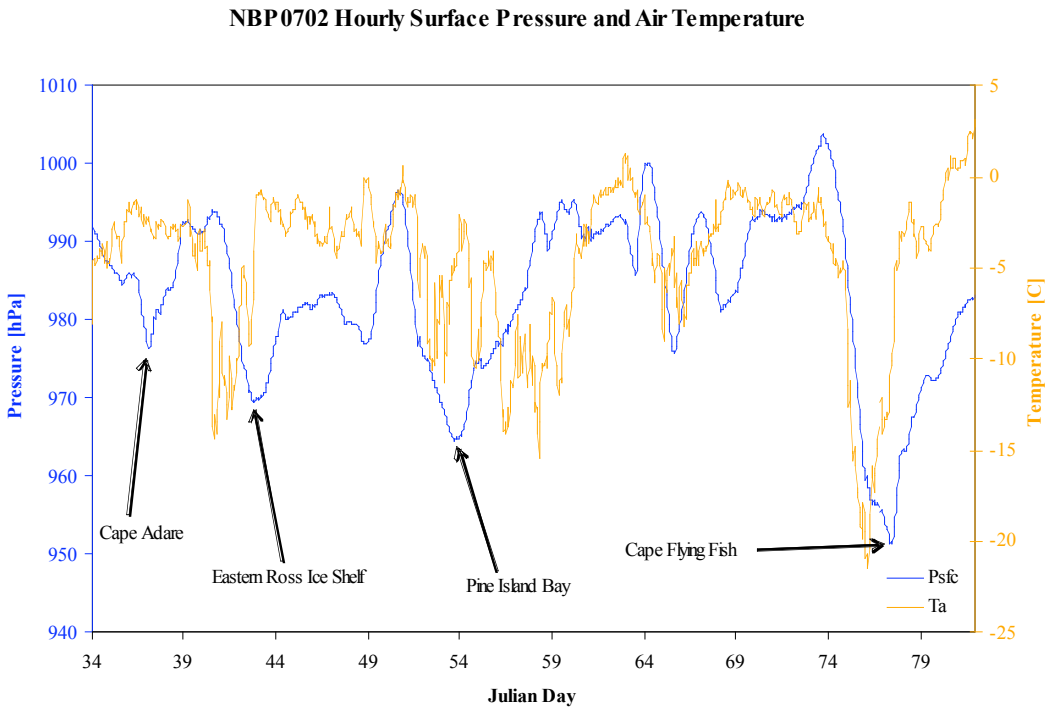


Figure 39 Hourly surface pressure and air temperature from NBP0702.

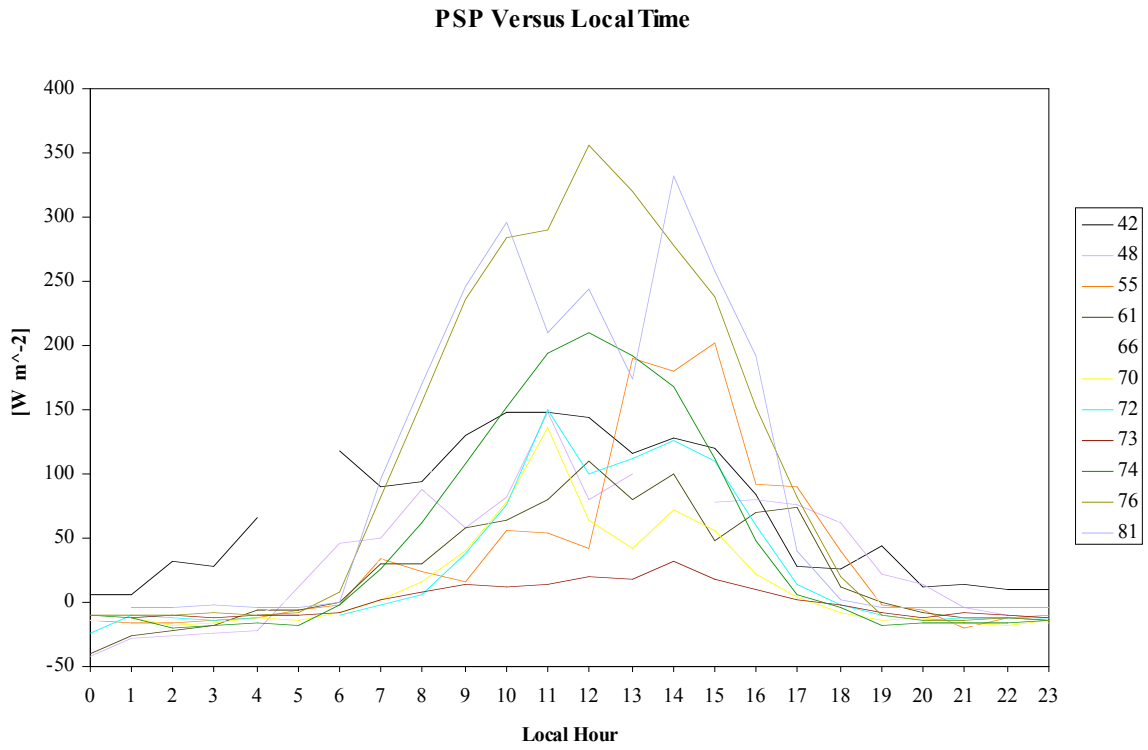


Figure 40 Diurnal cycle of downward solar radiative flux for selected Julian days.

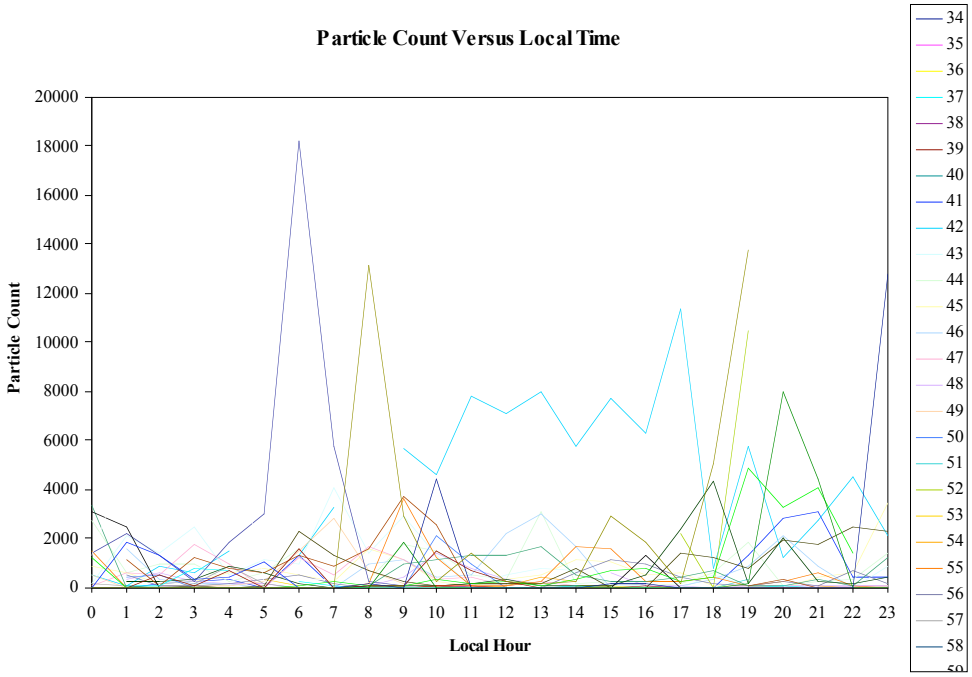


**Figure 41** Diurnal cycle of particle count for Julian days during NBP0702.

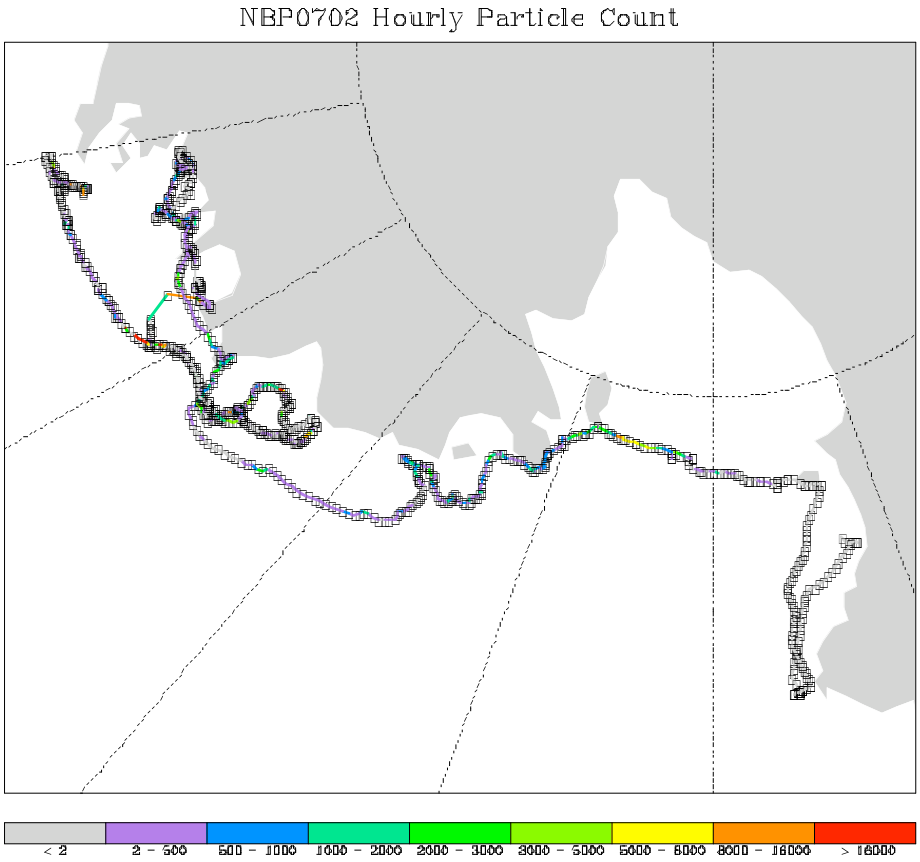


**Figure 42** Hourly particle count as shown for cruise trajectory.

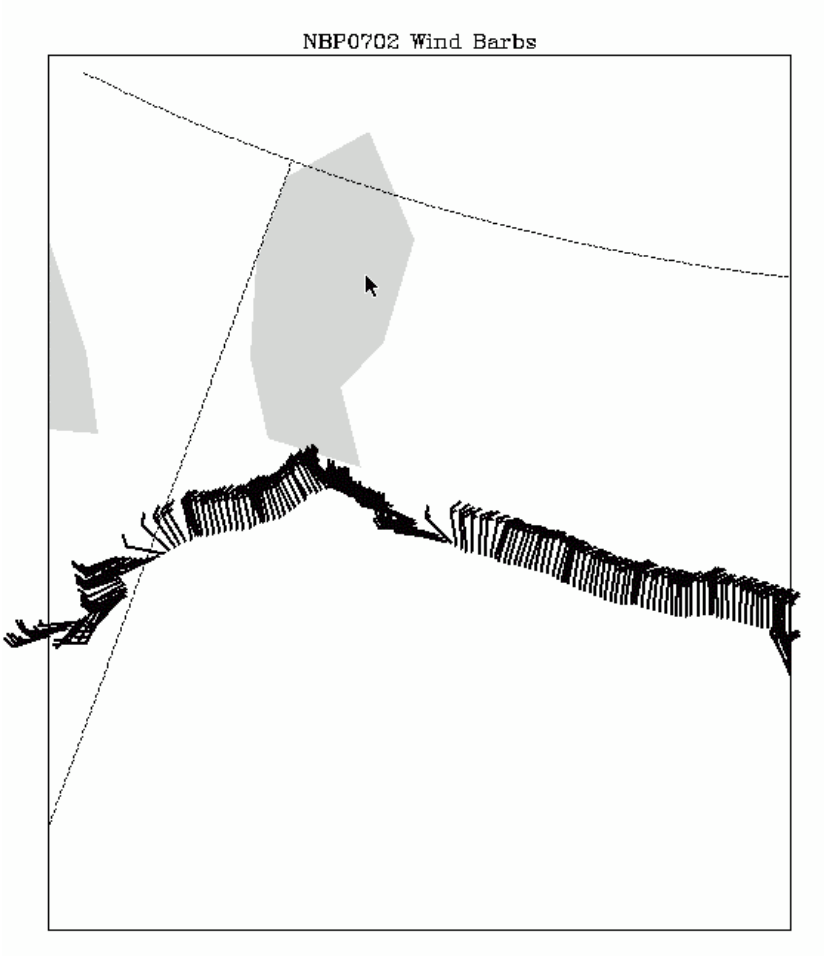


Figure 43 Ten-minute wind barbs in vicinity of Roosevelt Island.

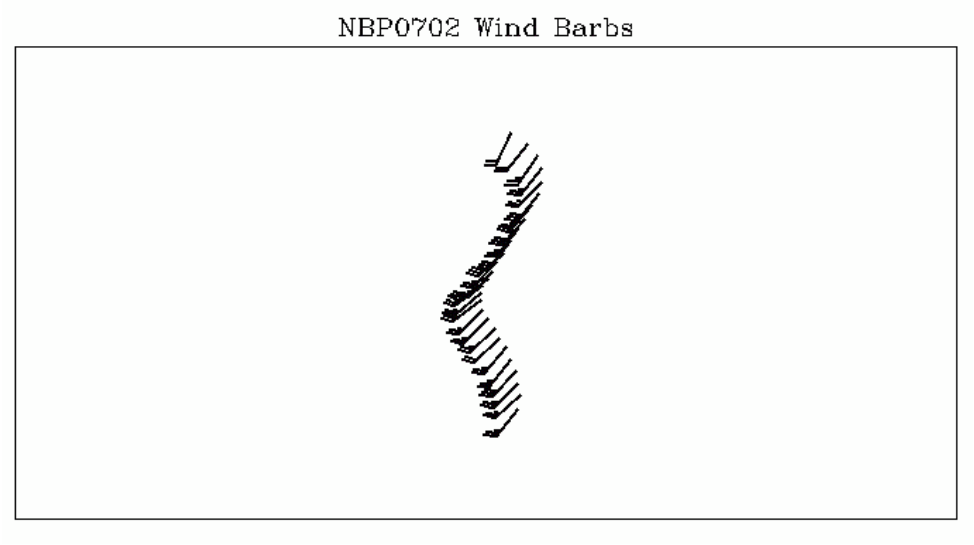


Figure 44. Thirty-minute wind barbs during the CTD polynya experiment. The barbs are shown on a Cartesian projection and bounded by 105.5°W(left), 105.1°W(right),71.0°S (top), and 71.2°S (bottom).

## 6.7 Phytoplankton sampling

(Amy Leventer and Stephanie McClellan)

The primary objective of the phytoplankton sampling program was to evaluate the distribution of diatom species and major phytoplankton groups along the transit from McMurdo Station to Punta Arenas Chile. The transit allowed access to a relatively under-sampled and under-studied region; consequently the data will be of interest in terms of addressing differences in phytoplankton assemblages that have been observed between the Ross Sea and Antarctic Peninsula. In addition, the phytoplankton data were collected in conjunction with a suite of physical and chemical oceanographic measurements that are critical to understanding observed algal distribution patterns. Specifically, at the time of each sampling, the following parameters were recorded based on surface data acquired through the uncontaminated seawater line: sea surface temperature (external), salinity, % transmittance, fluorometer voltage, and $pCO_2$. A note concerning sea ice conditions was made as well. In the longer term, these phytoplankton data will help with interpretation of the floral record in marine sediment cores that have been recovered from around the Antarctic margin on previous cruises. It is important to note however that these samples represent late summer conditions; sampling in other seasons is key to developing a complete understanding of the relationship between primary productivity in surface waters and its fossil record at the sea floor.

Surface water samples for quantitative diatom analysis were collected from the uncontaminated seawater system of the *NB Palmer* (intake depth ~5-7 meters water depth) approximately every 4-6 hours during NBP0702. Surface water samples for plankton work also were collected from the Niskin bottle tripped at the shallowest depth at every CTD station (Figure 45). Generally this was the sea surface, but under rougher sea state conditions, the uppermost bottle was tripped at a depth between 5 to 10 meters below the surface. The benefit of taking samples from the CTD casts was the additional physical and chemical oceanographic data tied to each sample. Water column profiles of temperature and salinity allowed for an evaluation of mixed layer depth; nutrient and pigment data will provide additional insight into controls on the phytoplankton community. In total, 275 underway and CTD samples were collected. At each site, a 500 ml volume of water was collected in a polypropylene bottle, immediately preserved with an acidified Lugol's solution (1000 ml deionized water + 100 g KI + 50 g crystalline iodine + 100 ml glacial acetic acid), and stored at +4°C until filtered over a 0.4 micron gridded Millipore cellulose acetate filter, and mounted in immersion oil for light microscopy. Storage time for samples ranged from one day to 2 weeks. Qualitative analysis of samples collected so far document the variable diatom assemblage composition as well as changing dominance of major planktonic groups, as diatoms, prymnesiophytes and silicoflagellates. Quantitative diatom counts and morphologic analyses will be completed on these samples once back in the US.

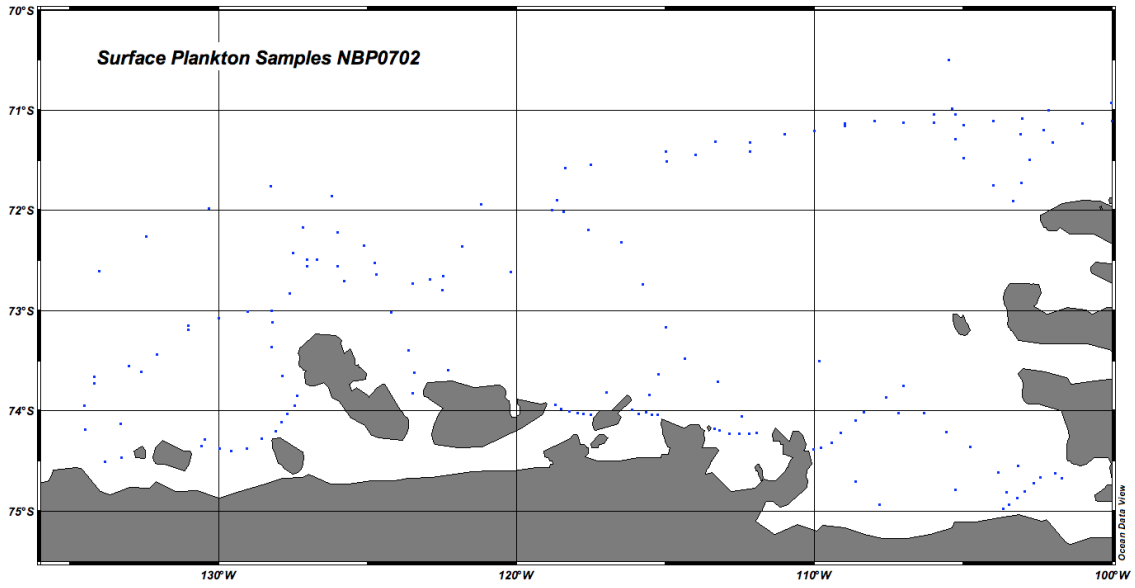


Figure 45 Distribution of surface plankton sampling

### 6.7.1 Discussion

As stated, the major goal of the phytoplankton sampling program was to evaluate the distribution of different groups of phytoplankton and different species of diatoms in surface waters of the Antarctic continental margin and to assess the relationship of these patterns to the physical and chemical oceanography of the study area. Since quantitative assessment of phytoplankton populations requires high magnification observation (1000x) which is very difficult on a moving ship, only qualitative assessment of all the slides was done on board. For this report, we focus on the samples collected between 135°W and 110°W, the region including the Getz and Dotson Ice Shelves. This region was selected based on the strong gradients easily observed in our preliminary view of the slides. This preliminary regional study also serves as an example of the type of work that will be completed on the entire data set over the next year. The phytoplankton data (Figure 46) are presented in conjunction with surface measurements of temperature, salinity, fluorometer voltage, and $pCO_2$ (**Error! Reference source not found.**), and nitrate and silicate concentration (Figure ). General observations, organized spatially from west to east, are described below with the caveat that more detailed quantitative work is needed to verify these data. Unanswered *questions* are presented as well; continued discussion among cruise participants will help address these queries.

1. The lowest fluorometer and highest $CO_2$ values were observed from 135°W to 125°W indicating low primary productivity along the western margin of the Getz Ice Shelf (Getz 1, 2, and 3) and extending offshore. Nitrate concentrations are relatively high, reflecting a low level of nutrient utilization *(but the silicate concentrations are not so high….)*. These observations are supported by examination of the phytoplankton under the microscope; the population is quite sparse. South of 73°S, the assemblage is dominated by the silicoflagellate *Dichtyocha speculum* and the diatoms *Fragilariopsis curta* and *Fragilariopsis cylindrus*. Little is known concerning silicoflagellate distribution in the Southern Ocean; in fact, its abundance in many of the NBP0702 samples was a surprise. The two species of *Fragilariopsis* are both common members of the sea ice algal community and are common in waters that have been seeded by melting sea ice. Heavy sea ice cover and decreased light levels most likely are responsible for

the observed minimally productive sea ice assemblage. Moving offshore, north of 73°S, diatom abundance increases, as does the contribution of *Fragilariopsis kerguelensis*, commonly associated with the Antarctic circumpolar current.

2. Surface waters in front of Getz 3, while generally similar to those to the west, demonstrate greater spatial variability in the distribution of diatom species. Several of the samples had a much greater absolute and relative abundance of long chains of *Chaetoceros* sp. and *Thalassiosira* sp. Until these can be identified to the species level, it is difficult to explain their patchy occurrence in this region, but the patchiness likely reflects differences in oceanographic conditions over a small spatial scale. It is unlikely that these populations were advected from offshore, since populations to the north are dominated by *F. curta* and *F. cylindrus*.

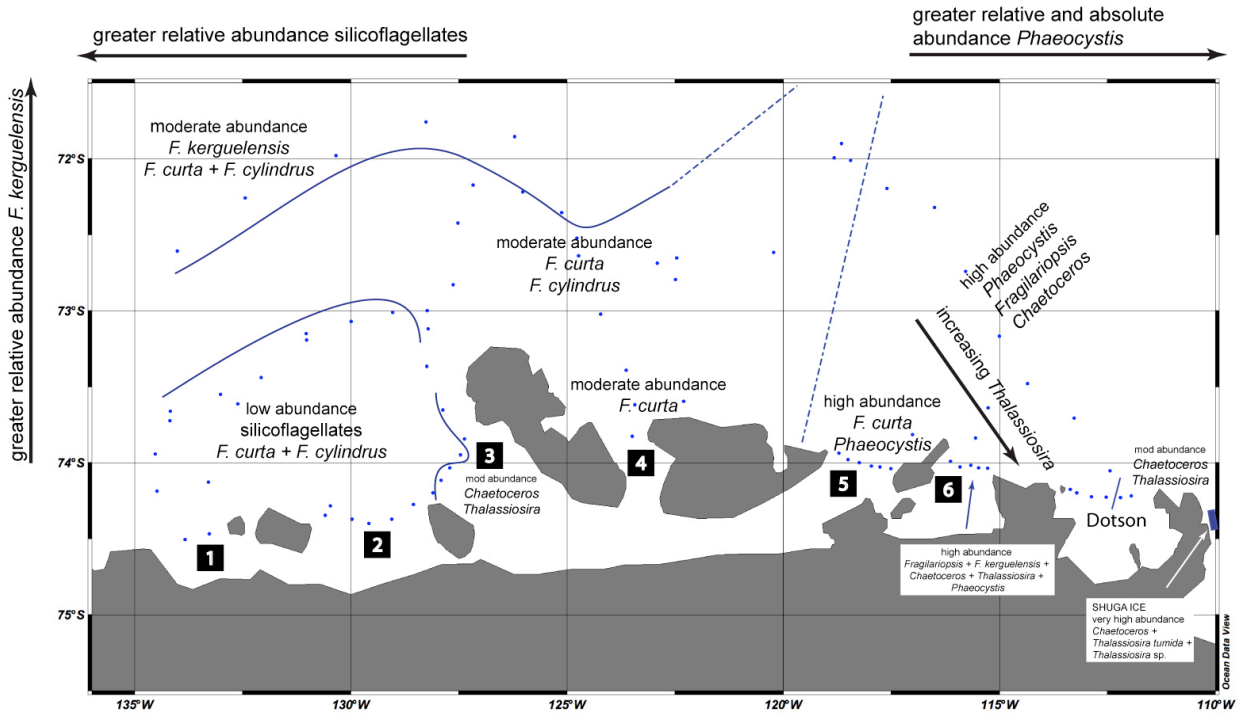


Figure 46 Summary of phytoplankton distribution in region of the Getz and Dotson ice shelves.

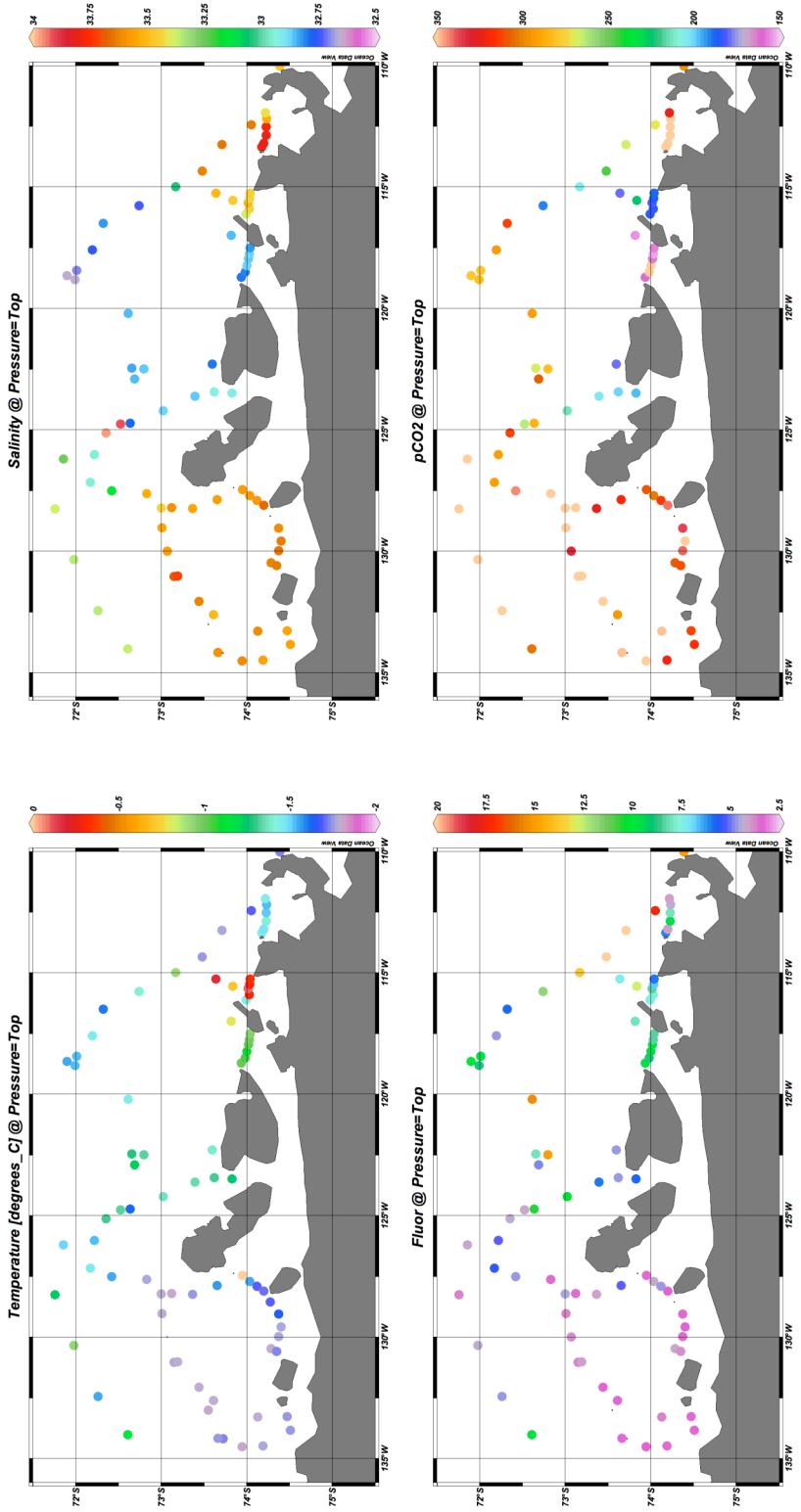
Salinity @ Pressure=Top
pCO2 @ Pressure=Top
Temperature [degrees_C] @ Pressure=Top
Fluor @ Pressure=Top
Ocean Data View
72°S
73°S
74°S
75°S
110°W
115°W
120°W
125°W
130°W
135°W

**Figure 47**

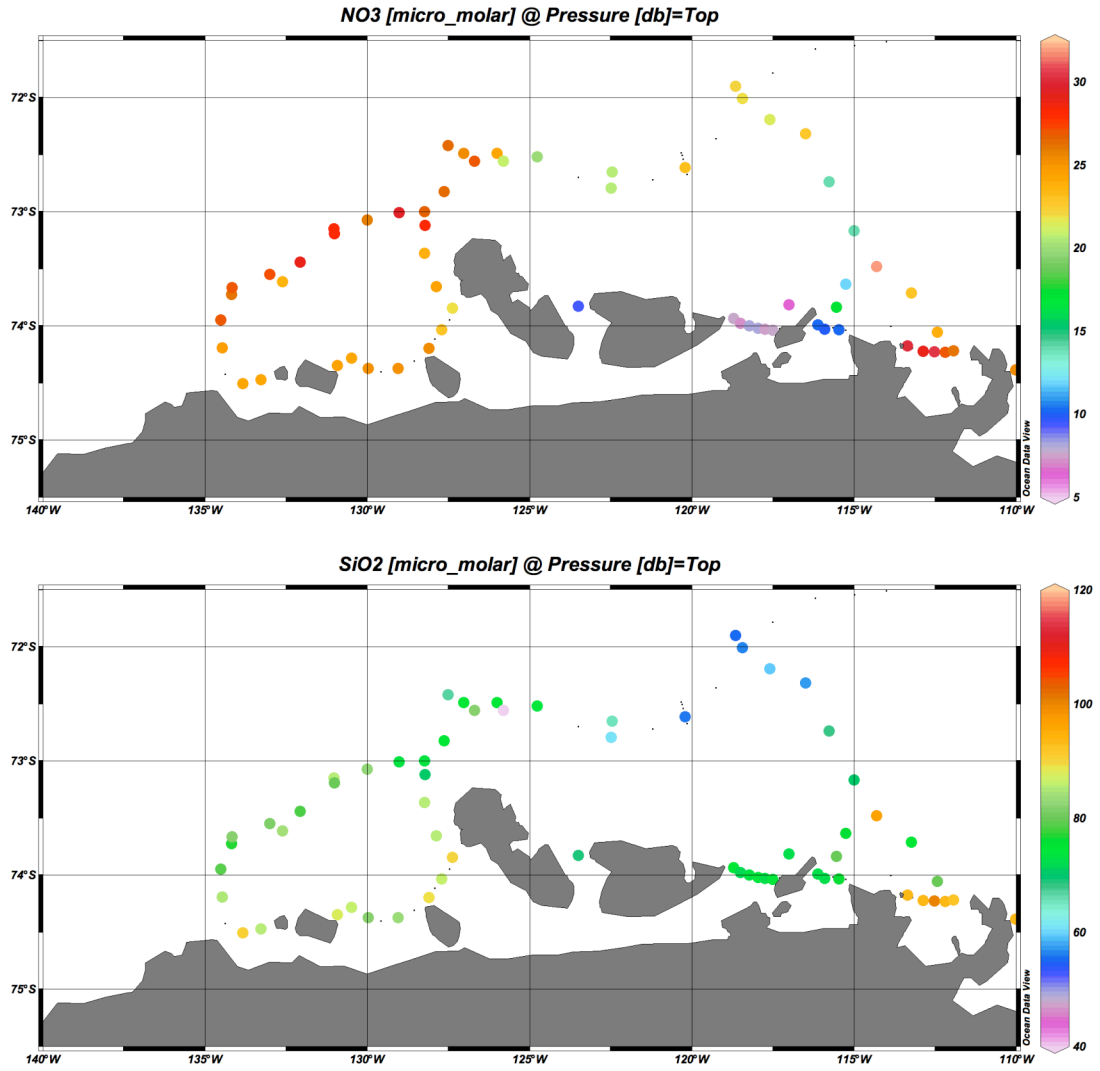


**Figure 49**

3. The samples in front of Getz 4 and 5 are dominated completely by the diatom *F. curta*, as are the samples that lie farther seaward. Silicoflagellate abundance is greatly diminished as compared to samples to the west. Low surface salinities, resulting in a strong and relatively shallow pycnocline between 30–50 m, suggest the presence of meltwater, though it is not possible to determine if this is sourced from melting glacial ice or sea ice. The high abundance of the sea ice indicator *F. curta* suggests a sea ice source, but oxygen isotopic analyses of the water will address this question more definitively. Productivity increases to the east and may result from the presence of *Phaeocystis* in samples east of ~119°E. Increased primary productivity is marked by an increase in fluorometer values and a decrease in $pCO_2$. Lowest nitrate concentrations are observed along the front of the Getz 5 Ice Shelf front, reflecting the increased level of *Phaeocystis*-based productivity as compared to Getz 4. The relatively moderate drawdown of silicate supports this interpretation, as diatom abundance seems to be equivalent in the two regions.

4. *Phaeocystis* abundance continues to increase in an eastward direction, though the phytoplankton assemblage in front of the Getz 6 Ice Shelf is quite diverse and productive, with significant concentrations of *F. curta* and *Thalassiosira* spp. and lesser concentrations of *F. kerguelensis* and *Chaetoceros* spp. The presence of *F. kerguelensis*, an Antarctic circumpolar current indicator, suggests some onshore transport. The pycnocline is relatively weak, perhaps allowing *Phaeocystis* to thrive, since it is reported to do well under weaker and more variable light conditions than diatoms. The high primary productivity, with a high abundance of *Phaeocystis*, is reflected by the low $pCO_2$ and nitrate concentrations, and moderate silicate drawdown. Surface water temperatures reach a maximum here (*what does this suggest?*).

5. *Phaeocystis* abundance appears to be greatest in front of the Dotson Ice Shelf, again perhaps reflecting the weak pycnocline. Like Getz 6, the overall diatom assemblage is diverse, with significant concentrations of *Thalassiosira* spp., *Chaetoceros* spp. and minor contributions of *Fragilariopsis* spp. Nitrate and silicate concentrations reach their maxima in front of the Dotson Ice Shelf; $pCO_2$ is similarly high. Given the apparently high primary productivity in this region, the high nutrient and $pCO_2$ may result from upwelling of older deep water.

### 6.7.2 Sea Ice Sampling

The sea ice serves as a habitat for sea ice algae, primarily diatoms. Its role in biological cycles in the Southern Ocean ranges from seeding the adjacent water column as it melts, resulting in ice edge phytoplankton blooms, to serving as a food source for krill during the polar winter. During NBP0702, discolored sea ice was observed often, with the discoloration noted at the interface between the sea ice and the overlying deep snow cover (a surface flooded by seawater), within the bottom 10-20 cm of the ice (observed in floes overturned during ice breaking), as strands attached to the underside of the ice (also observed in overturned floes), and within broad bands of shuga. Although a comprehensive sea ice sampling program to evaluate algal concentration and distribution within sea ice was not an objective of this project, a sea ice core was acquired with a Kovacs corer at each of the two sites where a drifter was deployed. In the field, each core was sliced into 10 cm sections and each section was placed in a plastic zip-lock bag. The samples were melted at ~2°C in the dark, and then treated in the same manner as the phytoplankton samples. In addition, on February 23rd, we encountered aligned bands of shuga ice adjacent to first year ice east of Bear Peninsula (Figure 48.). This ice was sampled by simply lowering a bucket from the ship. The material was preserved, melted and filtered, as described above.

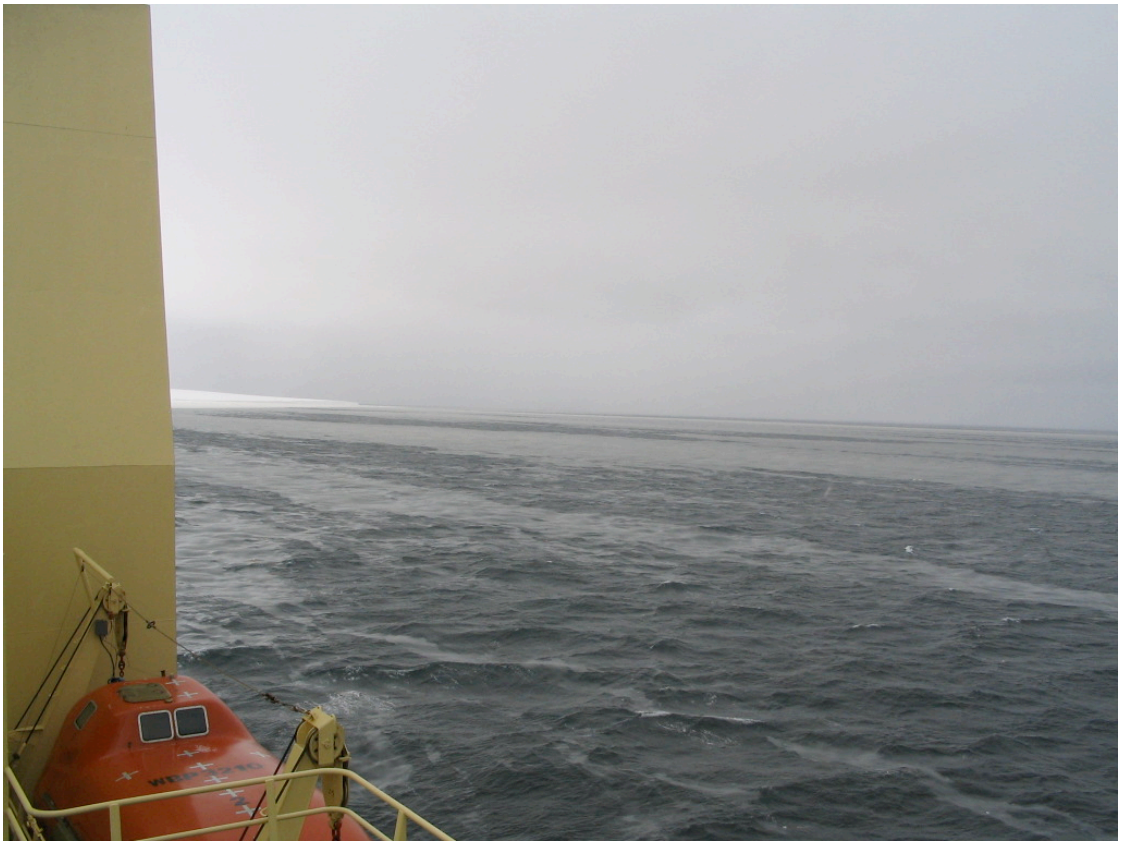

Figure 48 Shuga ice east of Bear Peninsula

Given the few samples obtained, information regarding gained regarding the distribution of algae versus depth in the sea ice will be limited. And although this kind of data is available from the region based on previous cruises, we took advantage of the opportunity to add to a spatially and temporally limited data base. The shuga sampling was of greater interest, given the small number of reports of algal concentration and composition within shuga ice. The frazil ice found in the observed shuga could have been generated by either wind turbulence or the rising of ice platelets as supercooled water rose from beneath a nearby ice shelf. Given the Langmuir-type circulation appearance of the sub-parallel bands of shuga, it is more likely that wind turbulence was responsible. Observations of the concentration of suspended material within frazil ice, including algal cells, have been made by many researchers. Concentration may occur via ice nucleation on suspended particles and/or scavenging by ice crystals as they move through the water column. Initial microscopic observation of the filtered material and comparison to adjacent waters without shuga indicates that the ice we encountered contained an algal cell concentration many times higher than the surrounding waters. In addition, two groups of diatoms dominated the shuga, long chains of a small *Chaetoceros*, many of which were forming spores, and relatively large centric diatoms. Many of the centrics were *Thalassiosira tumida*, of interest in view of El-Sayed's 1968 observation of a large *T. tumida* bloom in the Weddell Sea, in a region he described as comprised of alternating bands of clear water and patches of phytoplankton concentrated in slush ice. Although *T. tumida* is ubiquitous in Southern Ocean waters, it is rarely observed as a dominant component of the phytoplankton community. The only other location where significant relative abundance of *T. tumida* was observed on this cruise was just north of the Drygalski Ice Tongue, but that observation was not in association with shuga. Quantitative analysis and more detailed taxonomic work will be completed on these samples to provide a better understanding of the mechanism for shuga ice formation and the concentration of algal cells.

## 6.8 Pigment Analyses

( Leventer and McClellan)

Samples for pigment analysis were collected at every CTD station (see Appendix 1). These 350 samples will be used to evaluate the concentration and composition of the phytoplankton community. In addition, the pigment data will be compared to the phytoplankton cell count data to re-evaluate the use of pigment data to estimate the variable contribution of different phytoplankton groups to the total community. At each station, from one to three water samples were taken from depths less than 100 m and filtered through Whatman GF/F glass microfibre filters, wrapped in aluminum foil, placed in cryovials, and then stored at -80°C for later analysis by Walker Smith at Virginia Institute of Marine Science. The volume of water filtered ranged from 500 to 4000 ml; in general water was filtered until the filters appeared colored.

## 6.9 Underway $Co_2$ Sampling

(Leventer)

Samples for Total $CO_2$ and nutrients were taken every 12 hours (midnight and noon local time (Appendix 2). The carbon dioxide samples will be analyzed at Lamont Doherty Earth Observatory in conjunction with the ongoing $pCO_2$ surface observation project. The nutrient samples were processed on board ship for silicate, phosphate nitrate, nitrite and ammonia. Nutrient analysis and data interpretation are discussed in the nutrient section of this report.

## 6.10 Surface Sediment Sampling – Smith-Mcintyre Grab And "Mini-Core"

(Leventer, Nitsche, et al.)

Surface sediment samples (Figure 49 and Appendix) were collected with two objectives in mind. First, quantitative diatom analysis will be completed on all the surface sediment samples as a comparison to the surface water diatom assemblage data that is being generated based on water samples obtained from the uncontaminated seawater system. These complementary data sets will be used to develop a better understanding of the relationship between the living and fossil diatom assemblages, and the processes that alter the living diatom assemblage as it settles to the sea floor. Second, sample material collected by the Smith-McIntyre grab (SMG) will be curated at the Antarctic Marine Geology Research Facility (AMGRF) at Florida State University and available to interested researchers. Smear slides from the "mini-core" will be stored at the AMGRF.

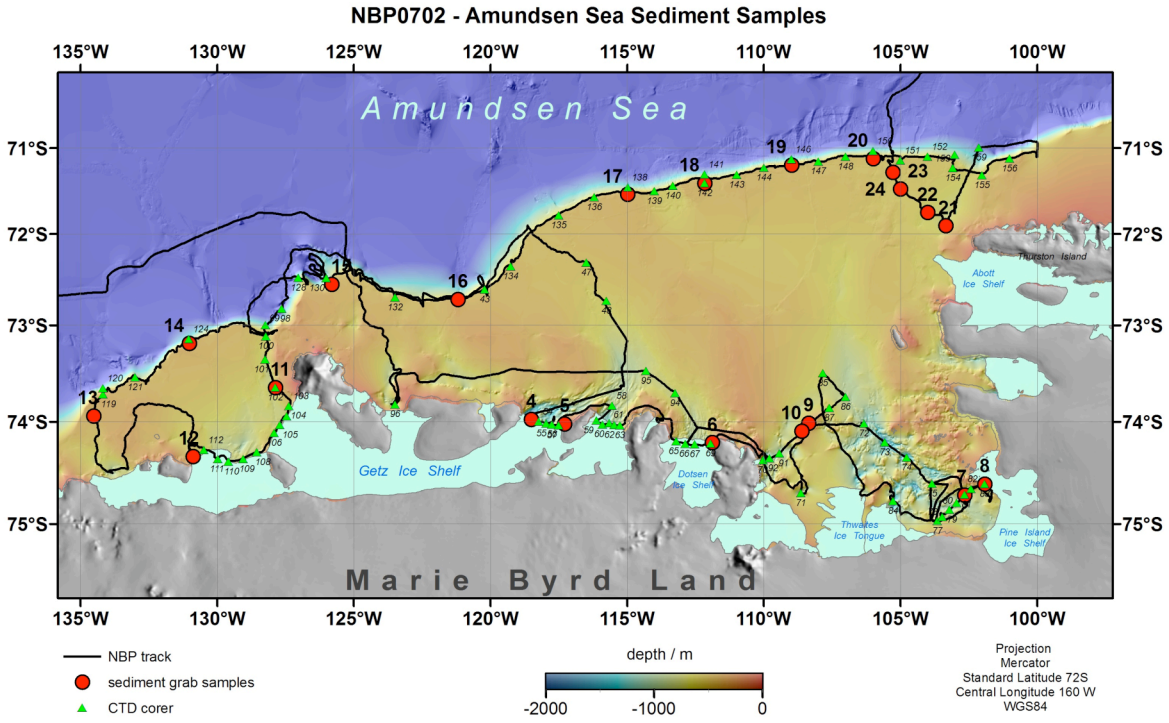


**Figure 49** Sediment sample locations

Sampling of sea floor surface sediments was accomplished using two different bottom sampling systems, a Smith-McIntyre Grab sampler, deployed at a limited number of stations, and a "mini-core" made by Stian Alesandrini, deployed beneath the CTD rosette and used as a bottom sensor. The advantage of the "mini-core" is that its deployment beneath the CTD permits recovery of surface sediment without taking time for a second deployment at the same station. Its very limited depth of recovery, only 1-3 cm, makes these samples useful for those researchers studying surface sediment properties. However, the limited sample volume limits its potential to be used by more than a few researchers. In contrast, the SMG collects about the top 10-15 centimeters of the sediment column and a much greater volume of sediment. The SMG worked perfectly during the cruise, however given the lack of a tension reading on the lower waterfall winch, wire payout was stopped when the winch operator noted the "block drop." This was more difficult to observe in deeper water (>1000 m); use of a pinger on deeper SMG deployments is recommended. This was not done on NBP0702 since only one backup pinger was available; it was held in reserve for use with the CTD rosette.

The SMG samples were photographed and described upon recovery. Then the sediment was sampled both as bagged material into whirlpaks, and in short (12 -13 centimeter) "subcores." Whenever possible, two surface (0-1 cm) samples were collected into a small whirlpak and a 125-ml nalgene bottle. Two larger samples were collected from ~0-5 cm depth, and then two more samples were collected from the surface to bottom of the grab. Living carbonates from the surface were removed and curated in 125 ml nalgene bottles. Larger (> 2 cm) gravel was picked out and stored in whirlpak bags.

### 6.10.1 Mini-Core Description

(Stian Alesandrini):

At the request of the scientists, the Marine Technicians designed and built a “mini-core” for obtaining small mud samples from the bottom during CTD casts. After several iterations, it was found that a square barrel allowed for the easiest construction of functional core catchers, resulting in a highly successful bottom sampling program.

In the final design, approximately one inch square tube stock was used for the barrel with a length of about 12 inches. One and an eighth inch square tube stock about an inch long with an end covered with a bit of steel plate was used as the core top. This cap was connected to the core body with a quick release pin that passes through a set of holes drilled for this purpose. This cap functioned as a one way valve when the core pierced the mud. As the cap is slightly bigger than the core barrel, there is room for water to escape as the core penetrates the sea floor. The gap is too small and is oriented in the wrong direction for flushing to occur while the core is retrieved.

The most difficult portion of the design was making the core catchers. The design that worked best was one using a double core catcher. Each core catcher was made of a strip of curved flat plastic taken from the rim of a standard core cap. The width of the strip was measured to fit exactly inside the core barrel. The core catchers were placed with the convex portion of the curve facing towards the opening and pop riveted into place. The core catchers were placed just far enough apart to prevent them from interfering with one another. To create the tightest seal the two catchers were mounted on different sides of the square barrel, 90° apart.

Initially, the core was weighted with two 6 pound dive weights secured with hose clamps. These were later replaced with a section of 3-1/2 inch steel pipe encircling the top of the core barrel and welded into place with pieces of plate steel that also served to seal the bottom of the pipe section. The pipe section thus formed a cup which was filled with lead to equal the previous total weight of the core. The lead was then melted to form a permanent weight integrated with the rest of the core.

A two pound nose weight was fashioned out of an old square dive weight. The middle of the weight was cut away to allow for the core barrel and holes were drilled to allow the attachment of the weight to the rest of the core. The nose weight functioned in exactly the same manner as those used with full size cores.

The mini core was suspended from the bottom of the CTD rosette, acting as the weight for the bottom contact switch. This setup worked very well when the ship was holding station but was less successful when the ship was drifting at a speed > ~0.5 knot over ground during the CTD cast.

## 6.11 Sea-ice buoy deployments

Michael Schroeder, AWI

In the framework of the "WCRP/SCAR International Program of Antarctic Buoys" (IPAB), the Alfred-Wegener-Institute has regularly deployed drifting buoys on sea ice floes since 1986. Every three hours, the buoys measure air temperature, air pressure and position, data that is transmitted to AWI and the Global Telecommunication System via ARGOS satellites. The buoy drifts can be followed at http://www.ipab.aq and

http://zzz.awi-bremerhaven.de:8002/servlet/Init . These datasets allow improved weather analyses, forecasts, and numerical models for the Southern Ocean and its ice cover. With the help of drifting buoys, sea ice models can be validated and their rheology improved.

During NBP07-02 we deployed two sea ice buoys at 73°42.5'S, 107°10.9'W (ID 9357, 27.02.2007) and

at 73°47.6'S, 134°24.2'W (ID 9368, 06.03.2007). Katie Leonard measured some characteristic values for the snow cover by means of snow pits. These buoys complement earlier Amundsen Sea deployments in 2000 and 2003 (Assmann, K, Hellmer, H, and Jacobs, S, 2005, Amundsen Sea ice production and transport. J. Geophys. Res. 110, C12013, doi:10.1029/2004JC002797). In addition, they will provide information of potential interest to upcoming cruises, e.g., a late winter sea ice drift experiment scheduled on NBP07-09.

Over the last 3/2 weeks, the sea ice buoys deployed on this cruise have moved ~ 20/30 miles to the NNW/NNE, somewhat at odds with the longer-term drift shown by most models for this sector.

First ice buoy: Buoy ID: 9357

27.02.07 18:43 GMT

Position: 73 degr. 42.536 min. South, 107 degr. 10.996 min. West

Floe size: 9 nm * 3 nm, 1.2 m -2.0 m thick with 0.2 m – 0.3 m snow (mean values from two snow pits and three ice cores)

First year ice

~ 206 m from the floe edge

water depth: ~ 800 m

air temperature: -8.9 degr. Celsius

wind: 7 m/s from 68 degr. (northeast)

snow pit 1:

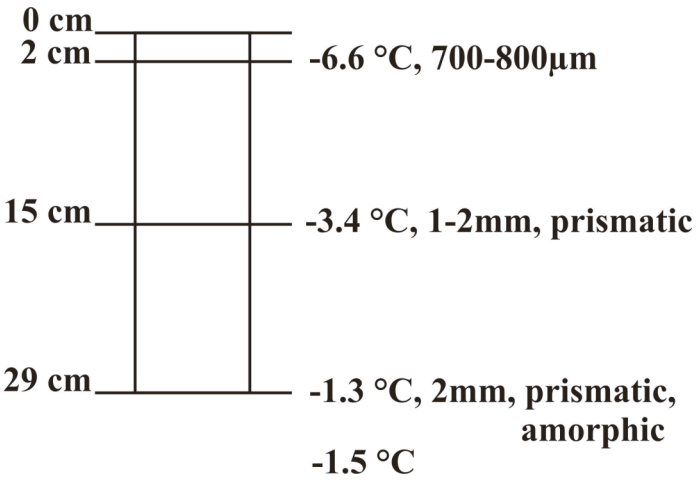

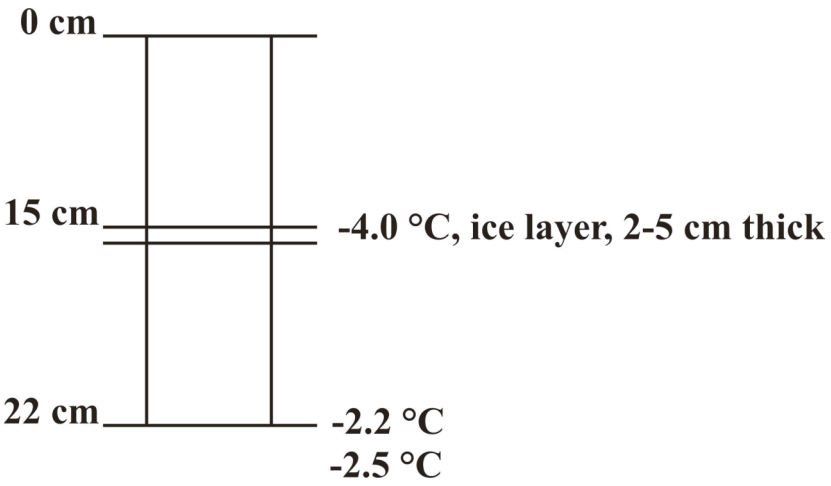


Second ice buoy: Buoy ID: 9368
06.03.07 17:45 GMT
Position: 73 degr. 47.695 min. South, 134 degr. 24.211 min. West
Floe size: 1.8 nm * 1.8 nm, 1.5 m thick with 0.4 m – 0.65 m snow
(mean values from one snow pit and two ice cores)
First year ice
~ 208 m from the floe edge
water depth: ~ 450 m
air temperature: -7.2 degr. Celsius
wind: 11.8 m/s from 205 degr. (southwest)

snow pit 1:

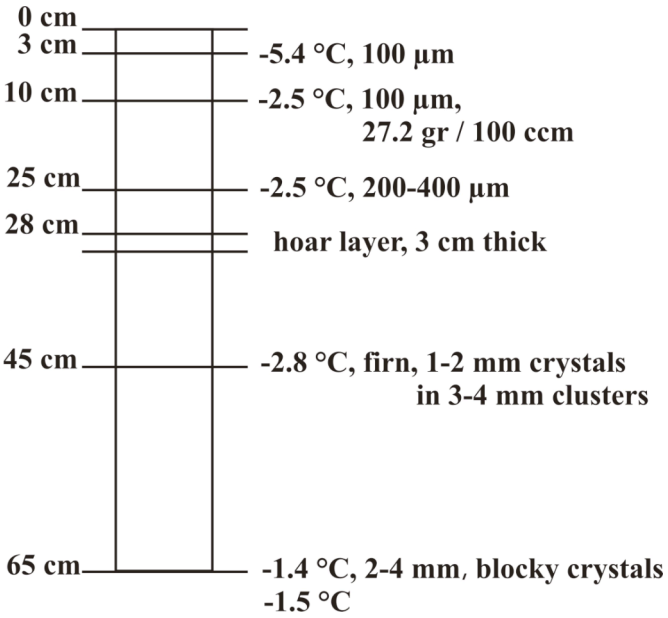

## 6.12 Underway Snow Measurements

(K. Leonard)

Snow drifting off a north-facing promontory of the Getz ice shelf, with Carney Island partly obscured by snow in the background to the west of the ship.

From 03 Feb –21 Mar a photoelectric snow particle counter (SPC) was mounted on the NBP's ice tower, ~90 feet above waterline, and recorded particles larger than 30 microns passing through a light beam. One objective was to measure snow flux off the edges of ice shelves during the ship's passage and while in close proximity (0.1 – 0.2 nm) from the ice fronts during CTD stations. The transport of snow off of ice shelves by the wind is a poorly quantified and previously unmeasured (we think) term in mass balance studies. Drifting snow is also important to sea ice formation and other Antarctic processes. Snow blown off of ice shelves and icebergs was observed to be a nucleation site for frazil and grease ice, and shuga appeared to be forming beneath plumes of blowing snow. While previous studies found low snow-depths (averaging 0.2m) over sea ice in the Amundsen Sea, snowfall appears to be high in this region, and the underway sea ice observations as well as snowpits dug on two sea ice floes suggest that number should be adjusted upward. Additional uses for the data include the recording of precipitation frequency, and answering such R. Cullather questions as whether it snows more at night.

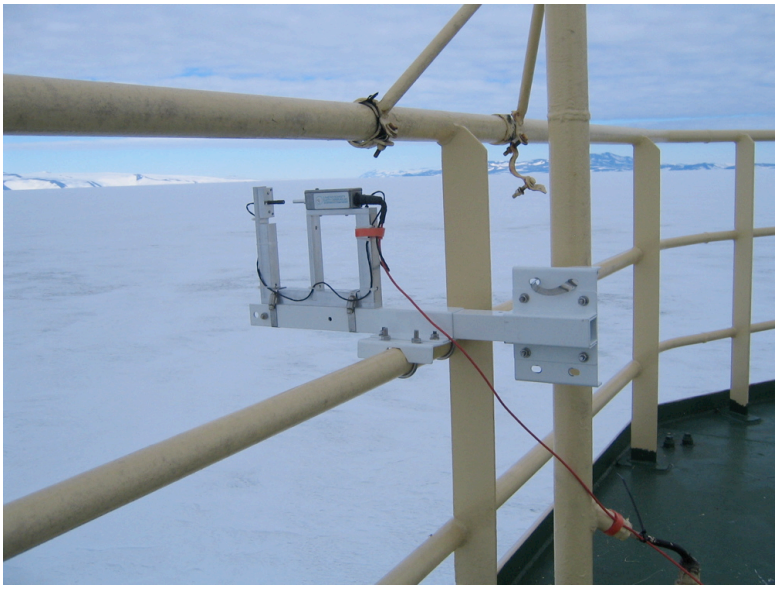

The SPC mounted on top of the NBP ice tower in McMurdo Sound

The SPC (shown above) was built at York University, Canada, following the design of Brown and Pomeroy and is on loan from Peter Taylor. The instrument consists of a laser diode and a detector, separated by 2cm. The beam of near infrared light is restricted on the detector end of the aperture by a 300 micron pinhole. The volume of air in which the frequency of passing snowflakes is measured is thus a cylinder 0.3mm wide and 20mm long, or approximately 19mm3. This will be scaled for comparison with the number of particles per unit volume predicted by numerical models of snowdrift.

Measurements were logged at ten second intervals for the duration of the cruise. The data was recorded by a Campbell CR10X datalogger located inside the ice tower, and powered by a portable 12V power supply which ran on ship's power. The recorded measurements included a one-second sample of snowflakes passing through the beam, the average number of snowflakes during the ten second interval, the maximum number of snowflakes per second and the time of that maximum, and the total number of snowflakes that passed through the beam during the ten seconds between data records. Additionally, the temperature measured by the CR10X's internal thermister was recorded every ten seconds (in this case, the inside temperature in the ice tower), as was the voltage received by the datalogger.

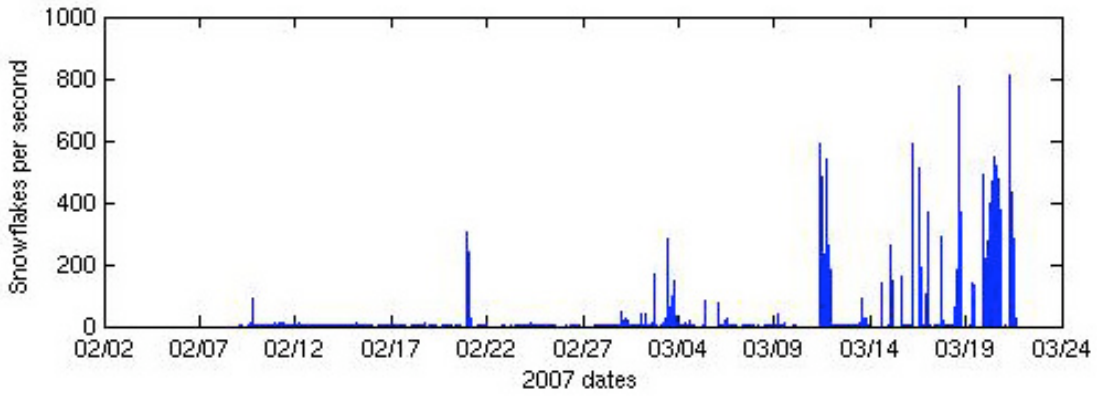


The record shown in the above plot appears to be heavily biased towards high values following the icing over of the SPC (and all other exposed metal surfaces on the ship) during heavy fog on the 11th of March. Prior to that date, peaks in the snow count were associated with the ship's presence beside ice shelves, while precipitation appeared not to produce large spikes in snow count. An instance of rime deposition on the ship in cold temperatures early in the morning on the 5th of March did not appear to affect the record.

Other challenges included difficulties with the 12V power supply in late February leading to loss of data recording for short intervals over the course of several days. The power supply was replaced, and no further power-related issues were observed.

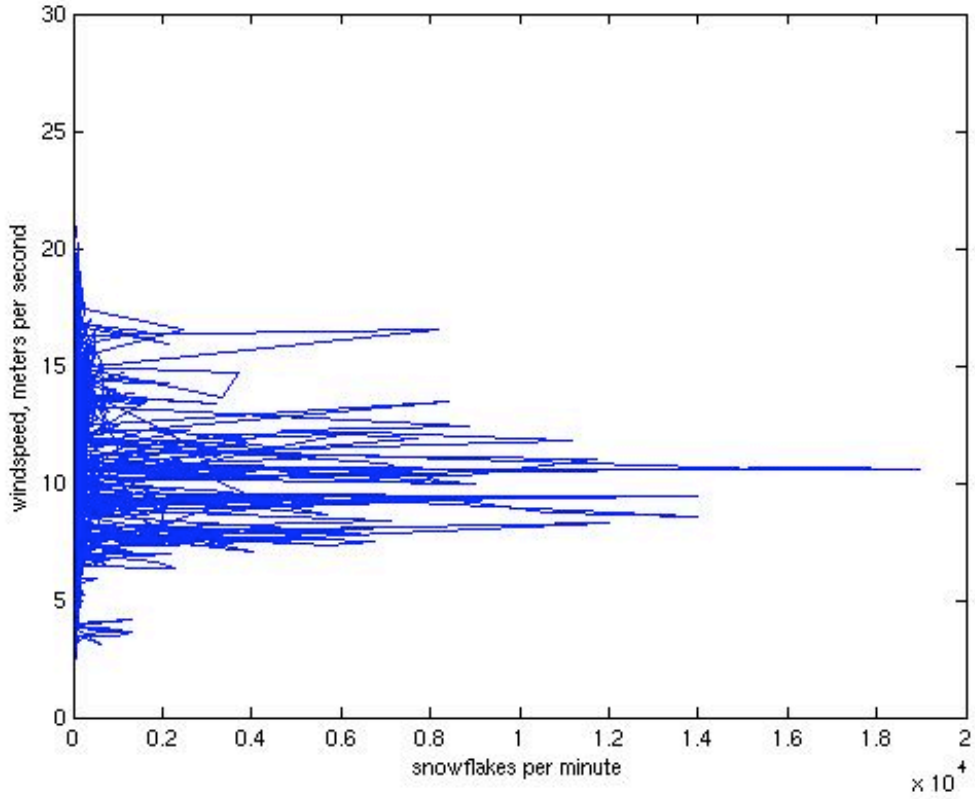


The relation between windspeed and snow counts is complicated by the ship's heading. Snowflakes should only pass through the SPC's beam when there is a cross-ship component to the wind direction. The figure above shows the recorded number of snowflakes per minute as a function of "true" windspeed which has been corrected to take into account the ship's speed and heading. An initial glance at the record might suggest that precipitation was poorly recorded, as there is little record of snow passing through the beam at windspeeds lower than 5 meters per second. However, this is a ship speed issue: the relative wind was parallel to the SPC's beam when the ship's speed outpaced the windspeed.

The SPC was used and calibrated in field studies at McMurdo Station, the embarkation point for the NBP07-02 cruise, earlier in the 2006-2007 season as part of a different project. The measurements discussed here demonstrate that ship-based measurement of snow fluxes off of ice shelves are possible and practicable, but the results of this investigation of snow transport will depend heavily on modeling that would be improved by further verification. An experiment that was discussed but did not occur was to drive the ship through the same plume of snow at multiple distances from the ice front, to determine whether the expected decline in snow counts with distance from the ice was in fact measured. Additional sensors and better measurements of the distance to the ice shelves, as well as better records of ice front morphology would also be desirable components of any future ship-based ice shelf snow-drift measurements.

## 6.13 Tide modeling

NBP0702 ROMS modeling Summary (R. Mueller)

### Introduction

Tides are known, in some regions, to be the dominant source of mixing and turbulence affecting these processes. In the Pine Island Bay (PIB) region, other mixing processes are currently thought to dominate since existing barotropic tide models suggest that tidal currents are small. (The ESR/OSU circum-Antarctic tide model, CATS02.01, predicts mean tidal current speed ($U_{av}$) of <2 cm/s in PIB, and typically ~5 cm/s along the shelf break north of PIB.) However, the accuracy of tide model predictions is greatly affected by the quality of the bathymetry used in the model, and existing CATS model is based on extremely inaccurate bathymetry. For the Amundsen Sea, the bathymetry grid for the 10-km resolution CATS02.01 model predates much of the recent depth sounding in this area, whereas a new grid compiled by Frank Nitsche (LDEO) includes multibeam data collected from several recent cruises. Comparisons of the two grids (Figure 50, 53, 54) show that the shelf break (roughly the 500 m isobath) in CATS02.01 is ~$2^o$ (~200 km) south of the new shelf break. In general, the new bathymetry shows the presence of deeper troughs leading to the ice shelves of PIB and more shallow regions along the shelf break at around 71°S, when compared to CATS02.01. These differences are important for two reasons:

The quality of the bathymetric grid is the single most important factor determining the accuracy of tide (and other ocean) models; and

More accurate tide prediction will change our understanding of the degree to which tides can contribute to mixing of CDW as it crosses the continental shelf through troughs, and in contact with the ice shelf cavities.

A new version of the CATS model is in development but is not yet available. Therefore, to help provide this cruise with updated tide information (based on the new bathymetry) and for my own learning experience, I used my free time during this cruise to develop a better understanding of the regional tidal currents through the use of 2D ROMS model simulations that incorporated the improved bathymetry into a 5 km resolution grid. I describe these efforts below, but note that development of a reliable tide model must await post-cruise efforts beginning with revisions to CATS model bathymetry.

### Model accuracy

Comparisons between the CATS 02.01 model tidal speeds and the observed speeds (from LADCP) for a few of the stations (Table 1) show that the measurements are 3-7 times larger than the CATS02.01 predictions. This difference is not surprising given that the CATS bathymetry in this region is 250-500 m deeper than Frank Nitsche's latest bathymetry. In other regions of the Antarctic shelf, where CATS incorporates more accurate bathymetry, CATS02.01 has yielded much better predictions of tidal velocities. We anticipate that the CATS model will greatly improve velocity predictions in this region once it is run with the new bathymetry. In the absence of an updated CATS model for this region, a tidally forced 2D ROMS model was run for a more accurate source of tide velocity predictions.

### Tidal mixing within the ice shelf cavity

As the *N.B. Palmer* neared Pine Island Bay, I attempted to merge Frank Nitsche's bedrock bathymetry with the BEDMAP ice shelf thickness grid to produce a grid that incorporated both updated bathymetry and a newer estimate of ice shelf cavity thickness. The intention was to generate a ROMS model prediction that could provide some insight for where CDW could be concentrated and/or the PIB derived Ice Shelf Water transported away from the ice shelf. Unfortunately, combining the datasets resulted in a grid that had inaccurate ice shelf extents and fixing the grid would have taken more time than could be afforded for generating useful information for this cruise. We will return to this problem after the cruise.

Tidal mixing across the ice shelf break

I created a model grid with the improved bedrock bathymetry but ignoring the presence of the ice shelves. Since the area of interest (the shelf break) was far north of the ice shelves, I hypothesized that shelf-break tides would be reasonably well represented despite this simplification.

To begin with, I incorporated Dr. Nitsche's improved bathymetry into a 5 km resolution grid with land masks in the southwest and southeast regions that were estimated to be covered with ice. The model was forced by tides along the north, west and east boundaries with the CATS02.01 tide model output. The model was forced with the four most energetic constituents ($K_1$, $O_1$, $P_1$, $S_2$) plus $M_2$; other constituents available in CATS02.01 would have a negligible affect on the results. The model ran for thirty two model days and showed equilibration with a couple of spring/neap (fortnightly) modulations. Because both the forcing model (CATS) and the ROMS model are based on depth-integrated equations of motion, we used volume transport rather than currents along the open boundaries, *i.e.*, CATS currents along the open boundaries were scaled by the ratio of ROMS-to-CATS water depths. This procedure for open-boundary forcing improves model performance but cannot eliminate the error caused by poor bathymetry in the forcing model.

Preliminary results are shown by "v" component of velocity (**Figure 53**) during the time of maximum kinetic energy in the second, estimated spring tidal cycle (approximately model run day 28). To determine the accuracy of this prediction, tide velocities were estimated from the LADCP measurements by averaging the v-component of velocity from 50 m from the surface to 50 from the bottom. The results of this estimate are shown in figure 5. Although these values give a crude estimate of tidal velocities, I should make clear that the calculation does not take into consideration the spring/neap cycle, and the stations were taken at different points in the fundamental (primarily diurnal) cycle.

**Figure 53** and **Figure 54** show that the magnitudes of velocities between 100°W and 107°W compare reasonably well with observations while those that are west of 112°W do not. Around 118°W, the magnitude of velocity is around 0.9 m/s (off scale), although the observed magnitude is much smaller, around 0.15 m/s. While the time of this observation is somewhere between the fortnightly cycle (hence the maximum tidal velocities will most likely exceeds 0.15 m/s) the estimate of 0.9 m/s still seems too large.

A possible explanation for this difference is suggested by **Figure 52**, which shows that the difference between the CATS 02.01 model and the ROMS model run bathymetries is around half of the CATS02.01 bathymetry depth, or of order 250-500 m. This difference in depth along the western boundary introduces a discontinuity that is great enough to introduce errors with the tidal forcing along this boundary. Once the CATS 02.01 model is upgraded to incorporate the newest bathymetry, we expect that the velocities in this region won't be as large, although they may still be larger than surrounding areas. Furthermore, we expect that the improved bathymetry will greatly enhance the accuracy of tidal predictions in this region

Summary

Tide predictions were made for the shelf-break region north of Pine Island Bay. Although these results are preliminary, the predictions for the eastern side of the shelf approximate LADCP estimates while those close to the western boundary seem overly influenced by a discontinuity between the grid used to force tides and that used for the ROMS model run.

Based on model/data comparisons elsewhere around the Antarctic, the CATS model (based on depth-integrated equations of motion) performs well when local bathymetry is well known. The Amundsen Sea is a relatively poorly mapped sector of the Antarctic, and we anticipate that incorporating the new Amundsen Sea bathymetry grid into CATS will significantly improve the accuracy of model predictions.

The improved CATS model can then be used to force regional 3-D ROMS solutions for investigations of Amundsen Sea shelf-break currents, tidal stirring in the troughs and over the banks of the continental shelf, within Pine Island Bay and under the ice shelves. Laurie Padman is currently working on a new CATS model simulation that will provide improved model predictions based on an upgraded bathymetry and increased resolution compared with CATS02.01. Model performance will be optimized by incorporating an Amundsen Sea grid that supplements the latest bathymetry with input from NBP07-02. The new CATS model will be run by summer 2007, and will be released immediately for use in post-cruise data analysis.

Figures and Tables

| Longitude | Latitude | LADCP velocity (m/s) | CATS model range (m/s) |
|---|---|---|---|
| -123.5 | -72.7 | 0.08 | -0.02 – 0.025 |
| -117.5 | -71.8 | -0.13 | -0.04 – 0.04 |
| -108 | -71.2 | 0.15 | -0.02 – 0.03 |

Table 3: Tide velocity estimates for the time of CTD deployment in which LADCP data was collected. LADCP velocity refers to average velocity from 50 m. to 50 m. above the bottom. The CATS model range reflects maximum velocity estimates over a spring and neap cycle (centered around time of CTD sample). The timing of LADCP measurements are estimated to be about half way between the spring and neap cycle.

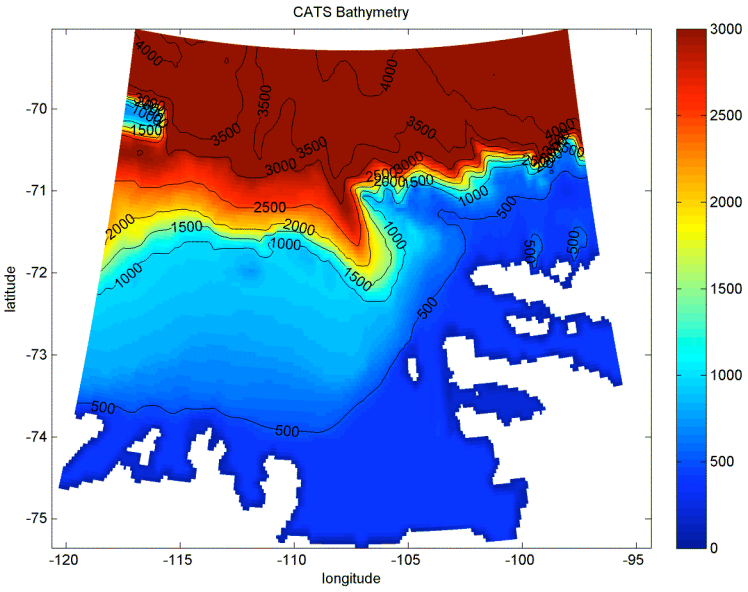


**Figure 50:** Grid bathymetry for the CATS 02.01 model.

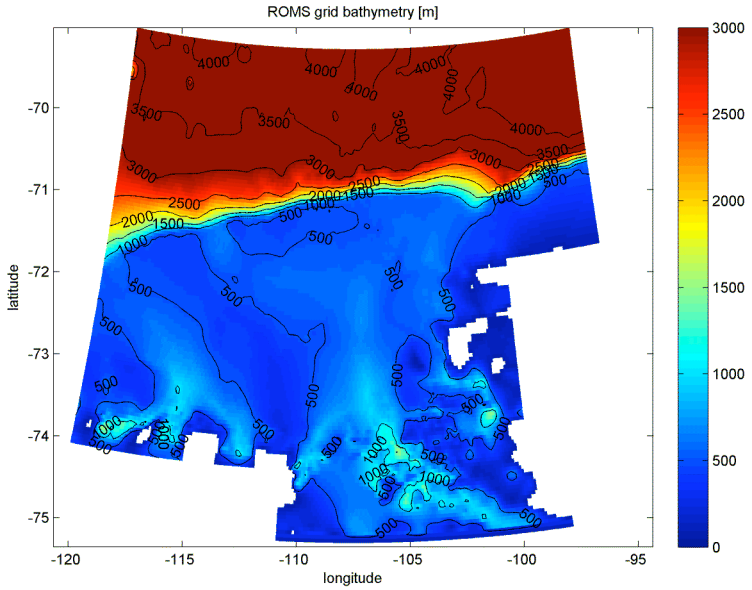


Figure 51: Grid bathymetry used for the ROMS model run and provided by Frank Nitsche.

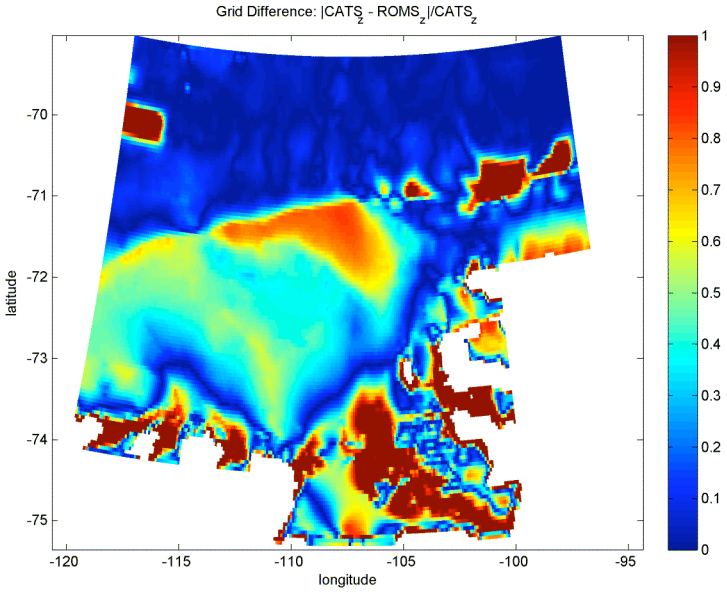


Figure 52: Regions of small (zero) to large (one) differences between grids. Any values greater than one reflect regions where the CATS grid is shallow and the new grid is deep.

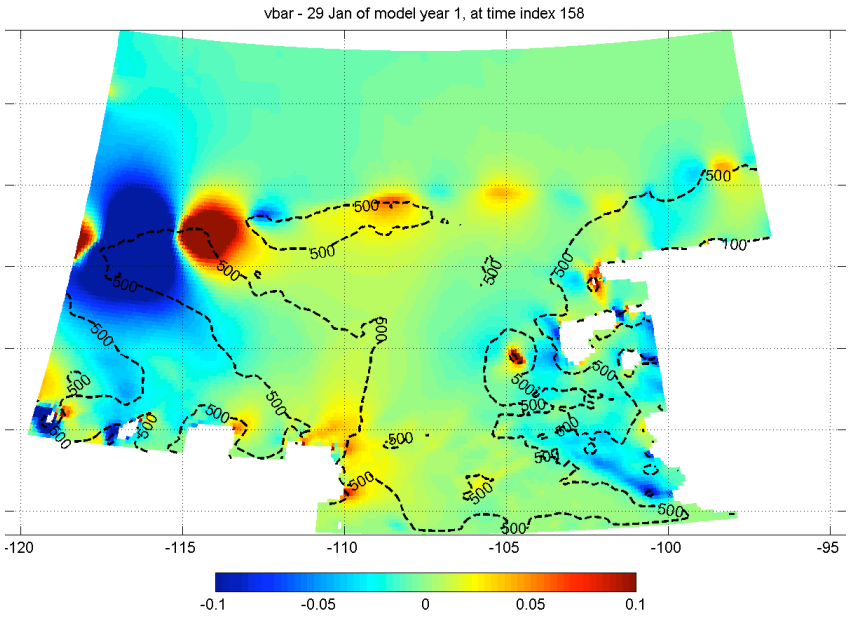


Figure 53: ROMS model output for the v component of velocity between model run days 27 and 28, which corresponds to the maximum of the spring neap cycle. White regions indicate the model land mask. The 500m isobath is shown by the dotted line.

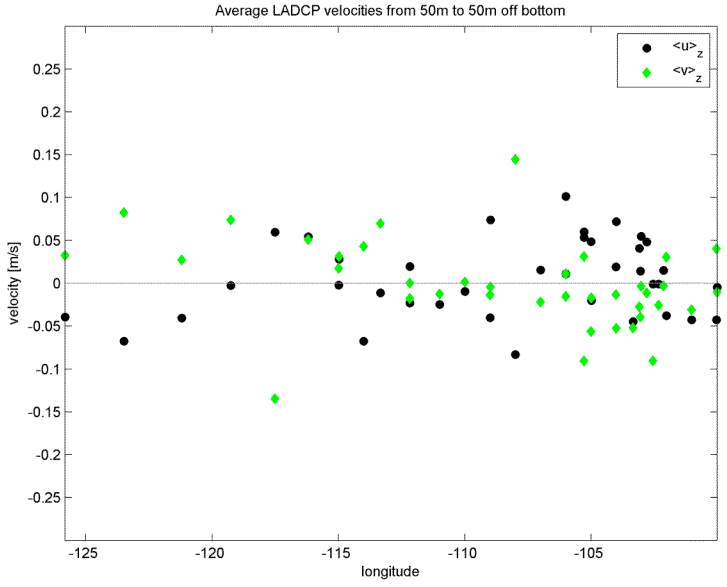


Figure 54: Averaged u- and v-velocity over depth of CTD station, excluding the upper and lower 50m. The station latitudes are all around the shelf break region, reflecting a series of stations aimed at resolving the shelf break flow along the indicated longitudes.

## 6.14 Outreach

(R. Mueller)

### NBP0702 OUTREACH SUMMARY

The NBP0702 cruise united scientists and technicians from disparate backgrounds to collaborate in physical, chemical and biological oceanography as well as climate modeling and geophysics. This diverse research environment provided a great opportunity for public outreach. To this end, two blog sites and a website were maintained during the cruise: Richard Cullather wrote a weekly report on shipboard activities for the Lamont-Doherty Oceans and Climate Physics Division (nbp-07-02.blogspot.com); Chris Little, on a roughly daily basis, attempted to relay, in a non-technical way, personal reflections on daily scientific pursuits as well as non-science activities (nbp0702.blogspot.com); and Rachael Mueller sent science and cruise briefs to an Earth & Space Research (ESR) hosted website that was maintained and supported by Susan Howard and Laurie Padman (http://www.esr.org/wais07_index.html).

These efforts affectively engaged a broad range of individuals in the cruise activities and Antarctic research. The most rewarding response for Rachael was the excitement of 4-6 year olds whose questions and interest were related through their parents. Meanwhile, Chris Little engaged in a e-dialogue with a group of 7 and 8 year old students at an elementary school in Philadelphia; upon his return, he plans to visit them to show pictures from the trip and answer more of their questions.

Website Overview

The ESR hosted website was designed to be not only a vehicle for Rachael Mueller's cruise blog, but also an archive of the cruise background. The site provides an updated map of cruise track and CTD locations, daily situation reports, weekly science summaries from the Chief Scientist, links to near-real time and daily archived sea-ice images, weather reports for Antarctic bases, and links to other blogs and Antarctic photo galleries. The site will be maintained past the end of the cruise as a science resource.

Many people deserve recognition for their contributions to this site. Susan Howard put many hours into creating the site, and maintaining it on a daily basis. While simple blogging from the ship is now possible without mainland support, the extended nature of the ESR cruise web site required Susan's constant attention. Both Stan Jacobs and Laurie Padman offered feedback and suggestions for many of the postings. Amy Leventer, Brice Loose, Katie Leonard, Chris Little, Michael Schroeder, and Bruce Huber were also generous with their time and comments. Karl Newyear orchestrated the ship-side technical support for the website, which was carried out by Robert Acha and Jennifer Ayers. The crew of the *N. B. Palmer*—particularly Capt. Mike Watson, Rachelle Pagtalunan, John Higdon, and Sebastian Paoni—helped to make the ship and transit information more accurate.

Unfortunately, this website didn't capture all the details of science onboard and missed relating the research of Frank Nitsche, Michael Schroeder, Raul Guerrero and Richard Cullather, whose expertise will have to be captured in future iterations.

Web posting summary

Website Introduction

A broad overview of the motivations of this trip, including an introduction to ice sheets.

January 26th: Preparing to depart

Experience of traveling to New Zealand to begin cruise.

January 31st: We made it to McMurdo!

Operation logistics for Antarctic research given through description of flight to McMurdo.

February 4th: First few days on NBP

Introduction to life on board the Nathaniel B. Palmer with a description of wildlife and scenery.

February 5th: Science Intro

An overview of CTD sampling and terminology

February 6th: Sampling begins

Mooring deployment and details of ship activities in heavy seas.

February 11th: Observations and instabilities

Introduced the concepts of instabilities and mixing through a description of Kelvin-Helmoltz billows observed in clouds and the experience of watching the CTD profiles as they unveil the characteristics of the water column.

February 14th: Cape Adare and Amundsen Sea science overview

Description of Cape Adare science objectives as well as details on the Amundsen Sea objectives introduced by an account of recovering a mooring.

February 17th: Penguins, snow and the challenges of observations

Conveyed the complexity of scientific observations and remote sensing through a discussion of penguins, sea ice and snow.

February 20th: Weather and sea ice conditions

Used a discussion of our weather and sea ice conditions to describe some of the regional characteristics that distinguish the Amundsen Sea area. In so doing, this posting also tried to relate some of the challenges of Antarctic observations.

February 24th: Ocean variability, observations and Coriolis

Introduced the Coriolis Force and imparted a sense of variability in the oceans through a discussion of CTD efforts.

February 26th: Sea ice types

Description of sea ice types motivated by mooring recovery

February 27th: Ice buoy deployment

Made use of the activities on an ice floe to describe ice buoys, the graduate studies of Katie Leonard and Brice Loose, and the research goals of Amy Leventer.

March 7th: Aurora Australis and morale upkeep

A description of the sunrise, the 2nd buoy deployment, an Aurora Australis sighting and the camaraderie of watchmates. (somewhat of a break from science writing).

March 11th: Patchiness in ocean biology.

Gave a brief overview of activities and used a change in wildlife observations to emphasize the patchiness in ocean biology.

March 15th: Modeling ocean and ice shelf interactions

A description of the complexity in modeling ocean-ice shelf interactions related through my discussions and interactions with Chris Little.

March 18th: Yo-yo station and sun halo

An overview of ice halos weaved into a description of watch activities during the yo-yo station.

Goodbye!

End of cruise reflections.

# 7 Appendices